

Vol. 9, no. 3, 2025

eISSN 2541-9129

PEER-REVIEWED SCIENTIFIC AND PRACTICAL JOURNAL

Safety of Technogenic and Natural Systems

Technosphere Safety

Machine Building

Chemical Technologies,
Materials Sciences,
Metallurgy



www.bps-journal.ru
DOI 10.23947/2541-9129



Safety of Technogenic and Natural Systems

Bezopasnost' Tekhnogennykh i Prirodnnykh Sistem

Peer-Reviewed Scientific and Practical Journal

eISSN 2541-9129

Published Since 2017

Periodicity – 4 issues per year

DOI: 10.23947/2541-9129

Founder and Publisher — Don State Technical University (DSTU), Rostov-on-Don, Russian Federation

The journal is created in order to highlight the results of research and real achievements on topical issues of Mechanical Engineering, Technosphere Safety, Modern Metallurgy and Materials Science. The journal highlights the problems of the development of fundamental research and engineering developments in a number of important areas of technical sciences. One of the main activities of the journal is integration into the international information space.

The journal is included in the List of the leading peer-reviewed scientific publications (Higher Attestation Commission under the Ministry of Science and Higher Education of the Russian Federation), where basic scientific results of dissertations for the degrees of Doctor and Candidate of Science in scientific specialties and their respective branches of science should be published.

The Journal Publishes Articles in the Following Fields of Science:

- Labor protection in construction (Engineering Sciences)
- Ground Transport and Technological Means and Complexes (Engineering Sciences)
- Machines, Aggregates and Technological Processes (Engineering Sciences)
- Metallurgical Science and Heat Treatment of Metals and Alloys (Engineering Sciences)
- Powder Metallurgy and Composite Materials (Engineering Sciences)
- Materials Science (Engineering Sciences)
- Fire Safety (Engineering Sciences)
- Environmental Safety (Engineering Sciences)
- Occupational Safety (Engineering Sciences)

Registration: Mass Media Registration Certificate ЭЛ № ФС 77 – 66531 Dated July, 21, 2016, Issued by the Federal Service for Supervision of Communications, Information Technology and Mass Media

Indexing and Archiving: RISC, CyberLeninka, CrossRef, DOAJ, Index Copernicus, Internet Archive

Website: <https://bps-journal.ru>

Address of the Editorial Office: 1, Gagarin Sq. Rostov-on-Don, 344003, Russian Federation

E-mail: vestnik@donstu.ru

Telephone: +7 (863) 2–738–372

Date of Publication No.2,2025: 30.08.2025





Безопасность техногенных и природных систем

Safety of Technogenic and Natural Systems

Рецензируемый научно-практический журнал

eISSN 2541-9129

Издается с 2017 года

Периодичность – 4 выпуска в год

DOI: 10.23947/2541-9129

Учредитель и издатель — Федеральное государственное бюджетное образовательное учреждение высшего образования «Донской государственный технический университет» (ДГТУ), г. Ростов-на-Дону

Создан в целях освещения результатов исследований и реальных достижений по актуальным вопросам машиностроения, техносферной безопасности, современной металлургии и материаловедения. В журнале освещаются проблемы развития фундаментальных исследований и инженерных разработок в ряде важнейших областей технических наук. Одним из главных направлений деятельности журнала является интеграция в международное информационное пространство.

Журнал включен в перечень рецензируемых научных изданий, в котором должны быть опубликованы основные научные результаты диссертаций на соискание ученой степени кандидата наук, на соискание ученой степени доктора наук (Перечень ВАК) по следующим научным специальностям:

- 2.1.16 – Охрана труда в строительстве (технические науки)
- 2.5.11 – Наземные транспортно-технологические средства и комплексы (технические науки)
- 2.5.21 – Машины, агрегаты и технологические процессы (технические науки)
- 2.6.1 – Металловедение и термическая обработка металлов и сплавов (технические науки)
- 2.6.5 – Порошковая металлургия и композиционные материалы (технические науки)
- 2.6.17 – Металловедение (технические науки)
- 2.10.1 – Пожарная безопасность (технические науки)
- 2.10.2 – Экологическая безопасность (технические науки)
- 2.10.3 – Безопасность труда (технические науки)

<i>Регистрация:</i>	Свидетельство о регистрации средства массовой информации ЭЛ № ФС 77 – 66531 от 21 июля 2016 г., выдано Федеральной службой по надзору в сфере связи, информационных технологий и массовых коммуникаций
<i>Индексация и архивация:</i>	РИНЦ, CyberLeninka, CrossRef, DOAJ, Index Copernicus, Internet Archive
<i>Сайт:</i>	https://bps-journal.ru
<i>Адрес редакции:</i>	344003, Российская Федерация, г. Ростов-на-Дону, пл. Гагарина, 1
<i>E-mail:</i>	vestnik@donstu.ru
<i>Телефон:</i>	+7 (863) 2–738–372
<i>Дата выхода №2, 2025 в свет:</i>	30.08.2025



Editorial Board

Editor-in-Chief

Besarion Ch. Meskhi, Dr.Sci. (Eng.), Professor, Don State Technical University (Rostov-on-Don, Russian Federation)

Deputy Chief Editors

Anatoliy A. Korotkiy, Dr.Sci. (Eng.), Professor, Don State Technical University (Rostov-on-Don, Russian Federation)

Valery N. Azarov, Dr.Sci. (Eng.), Professor, Volgograd State Technical University (Volgograd, Russian Federation)

Executive Editor

Manana G. Komakhidze, Cand.Sci. (Chemistry), Don State Technical University (Rostov-on-Don, Russian Federation)

Executive Secretaries

Grigoriy Sh. Khazanovich, Dr.Sci. (Eng.), Professor, Don State Technical University (Rostov-on-Don, Russian Federation)

Nadezhda A. Shevchenko, Don State Technical University (Rostov-on-Don, Russian Federation)

Aleksandr A. Poroshin, Dr.Sci. (Eng.), All-Russian Research Institute for Fire Protection of the Ministry of the Russian Federation for Civil Defence, Emergencies and Elimination of Consequences of Natural Disasters (Balashikha, Russian Federation)

Aleksandr N. Chukarin, Dr.Sci. (Eng.), Professor, Rostov State Transport University (Rostov-on-Don, Russian Federation)

Aleksandr P. Amosov, Dr.Sci. (Phys.-Math.), Professor, Samara State Technical University (Samara, Russian Federation)

Aleksandr P. Tyurin, Dr.Sci. (Eng.), Associate Professor, Kalashnikov Izhevsk State Technical University (Izhevsk, Russian Federation)

Aleksandr V. Lagerev, Dr.Sci. (Eng.), Professor, Ivan Petrovsky Bryansk State University (Bryansk, Russian Federation)

Aleksey S. Nosenko, Dr.Sci. (Eng.), Professor, Shakhty Road Institute (branch) SRSPU (NPI) named after. M.I. Platova (Shakhty, Russian Federation)

Boris V. Sevastyanov, Dr.Sci. (Eng.), Cand. Sci. (Pedagog.), Professor, Kalashnikov Izhevsk State Technical University (Izhevsk, Russian Federation)

Ekaterina V. Ageeva, Dr.Sci. (Eng.), Associate Professor, Southwest State University (Kursk, Russian Federation)

Eleonora Yu. Voronova, Dr.Sci. (Eng.), Associate Professor, Shakhty Road Institute (branch) SRSPU (NPI) named after. M.I. Platov (Shakhty, Russian Federation)

Evgeniy V. Ageev, Dr.Sci. (Eng.), Professor, Southwest State University (Kursk, Russian Federation)

Fanil Sh. Hafizov, Dr.Sci. (Eng.) Professor, Ufa State Petroleum Technological University (Ufa, Russian Federation)

Grigoriy Sh. Khazanovich, Dr.Sci. (Eng.), professor, Don State Technical University (Rostov-on-Don, Russian Federation)

Igor A. Lagerev, Dr.Sci. (Eng.), Associate Professor, Ivan Petrovsky Bryansk State University (Bryansk, Russian Federation)

Ildar F. Hafizov, Dr.Sci. (Eng.), Associate Professor, Ufa State Petroleum Technological University (Ufa, Russian Federation)

Konstantin P. Manzhula, Dr.Sci. (Eng.), Professor, Peter the Great St. Petersburg Polytechnic University (Saint Petersburg, Russian Federation)

Mikhail S. Pleshko, Dr.Sci. (Eng.), Associate Professor, National University of Science and Technology (MISiS) (Moscow, Russian Federation)

Nadezhda V. Menzelintseva, Dr.Sci. (Eng.), Professor, Volgograd State Technical University (Volgograd, Russian Federation)

Nail Kh. Abdrakhmanov, Dr.Sci. (Eng.), Professor, Ufa State Petroleum Technological University (Ufa, Russian Federation)

Natalya I. Baurova, Dr.Sci. (Eng.), Professor, Moscow Automobile and Road Construction State Technical University (Moscow, Russian Federation)

Oksana S. Gurova, Dr.Sci. (Eng.), Associate Professor, Don State Technical University (Rostov-on-Don, Russian Federation)

Sergey L. Pushenko, Dr.Sci. (Eng.), Professor, Don State Technical University (Rostov-on-Don, Russian Federation)

Sergey N. Egorov, Dr.Sci. (Eng.), South-Russian State Polytechnic University (NPI) named after MI Platov (Novocherkassk, Russian Federation)

Vadim I. Bepalov, Dr.Sci. (Eng.), Professor, Don State Technical University (Rostov-on-Don, Russian Federation)

Viktor N. Pustovoit, Dr.Sci. (Eng.), Professor, Don State Technical University (Rostov-on-Don, Russian Federation)

Viktor O. Gutarevich, Dr.Sci. (Eng.), Associate Professor, Donetsk National Technical University (Donetsk, Donetsk People's Republic)

Vladimir L. Gaponov, Dr.Sci. (Eng.), Professor, Don State Technical University (Rostov-on-Don, Russian Federation)

Vladimir V. Moskvichev, Dr.Sci. (Eng.), Professor, Krasnoyarsk Branch of the Federal Research Center for Information and Computational Technologies (Krasnoyarsk, Russian Federation)

Vladimir Yu. Dorofeev, Dr.Sci. (Eng.), Professor, South-Russian State Polytechnic University (NPI) named after MI Platov (Novocherkassk, Russian Federation)

Vladislav B. Deev, Dr.Sci. (Eng.), Professor, National University of Science and Technology (MISiS) (Moscow, Russian Federation)

Vsevolod A. Minko, Dr.Sci. (Eng.), Professor, Belgorod State Technological University named after V.G. Shukhov (Belgorod, Russian Federation)

Vyacheslav G. Kopchenkov, Dr.Sci. (Eng.), Professor, North-Caucasus Federal University (Stavropol, Russian Federation)

Yuriy I. Bulygin, Dr.Sci. (Eng.), Professor, Don State Technical University (Rostov-on-Don, Russian Federation)

Zhanna V. Ereemeva, Dr.Sci. (Eng.), Professor, National University of Science and Technology (MISiS) (Moscow, Russian Federation)

Редакционная коллегия

Главный редактор

Месхи Бесарион Чохоевич, доктор технических наук, профессор, Донской государственной технической университет (Ростов-на-Дону, Российская Федерация)

Заместители главного редактора

Короткий Анатолий Аркадьевич, доктор технических наук, профессор, Донской государственной технической университет (Ростов-на-Дону, Российская Федерация)

Азаров Валерий Николаевич, доктор технических наук, профессор, Волгоградский государственный технический университет (Волгоград, Российская Федерация)

Выпускающий редактор

Комахидзе Манана Гивиевна, кандидат химических наук, Донской государственной технической университет (Ростов-на-Дону, Российская Федерация)

Ответственные секретари

Хазанович Григорий Шнеерович, доктор технических наук, профессор, Донской государственной технической университет (Ростов-на-Дону, Российская Федерация)

Шевченко Надежда Анатольевна, Донской государственной технической университет (Ростов-на-Дону, Российская Федерация)

Абдрахманов Наиль Хадитович, доктор технических наук, профессор, Уфимский государственный нефтяной технический университет (Уфа, Российская Федерация)

Агеева Екатерина Владимировна, доктор технических наук, доцент, Юго-Западный государственный университет (Курск, Российская Федерация)

Агеев Евгений Викторович, доктор технических наук, профессор, Юго-Западный государственный университет (Курск, Российская Федерация)

Амосов Александр Петрович, доктор физико-математических наук, профессор, Самарский государственный технический университет (Самара, Российская Федерация)

Баурова Наталья Ивановна, доктор технических наук, профессор, Московский автомобильно-дорожный государственный технический университет (Москва, Российская Федерация)

Беспалов Вадим Игоревич, доктор технических наук, профессор, Донской государственной технической университет (Ростов-на-Дону, Российская Федерация)

Булыгин Юрий Игоревич, доктор технических наук, профессор, Донской государственной технической университет (Ростов-на-Дону, Российская Федерация)

Воронова Элеонора Юрьевна, доктор технических наук, доцент, Шахтинский автодорожный институт (филиал) ЮРГПУ (НПИ) (Шахты, Российская Федерация)

Гапонов Владимир Лаврентьевич, доктор технических наук, профессор, Донской государственной технической университет (Ростов-на-Дону, Российская Федерация)

Гурова Оксана Сергеевна, доктор технических наук, доцент, Донской государственной технической университет (Ростов-на-Дону, Российская Федерация)

Гутаревич Виктор Олегович, доктор технических наук, доцент, Донецкий национальный технический университет (Донецк, Донецкая Народная Республика)

Деев Владислав Борисович, доктор технических наук, профессор, Национальный исследовательский технологический университет «МИСиС» (Москва, Российская Федерация)

Дорофеев Владимир Юрьевич, доктор технических наук, профессор, Южно-Российский государственный технический университет (НПИ) имени М. И. Платова (Новочеркасск, Российская Федерация)

Егоров Сергей Николаевич, доктор технических наук, профессор, Южно-Российский государственный технический университет (НПИ) имени М. И. Платова (Новочеркасск, Российская Федерация)

Еремеева Жанна Владимировна, доктор технических наук, профессор, Национальный исследовательский технологический университет «МИСиС» (Москва, Российская Федерация)

Копченко Вячеслав Григорьевич, доктор технических наук, профессор, Северо-Кавказский федеральный университет (Ставрополь, Российская Федерация)

Лагерева Александр Валерьевич, доктор технических наук, профессор, Брянский государственный университет имени академика И.Г. Петровского (Брянск, Российская Федерация)

Лагерева Игорь Александрович, доктор технических наук, доцент, Брянский государственный университет имени академика И.Г. Петровского (Брянск, Российская Федерация)

Манжула Константин Павлович, доктор технических наук, профессор, Санкт-Петербургский политехнический университет Петра Великого (Санкт-Петербургский, Российская Федерация)

Мензелинцева Надежда Васильевна, доктор технических наук, профессор, Волгоградский государственный технический университет (Волгоград, Российская Федерация)

Минко Всеволод Афанасьевич, доктор технических наук, профессор, Белгородский государственный технологический университет имени В.Г. Шухова (Белгород, Российская Федерация)

Москвичев Владимир Викторович, доктор технических наук, профессор, Красноярский филиал Федерального исследовательского центра «Информационных и вычислительных технологий» (Красноярск, Российская Федерация)

Носенко Алексей Станиславович, доктор технических наук, профессор, Шахтинский автодорожный институт (филиал) ЮРГПУ (НПИ) (Шахты, Российская Федерация)

Плешко Михаил Степанович, доктор технических наук, доцент, Национальный исследовательский технологический университет МИСиС (Москва, Российская Федерация)

Пустовойт Виктор Николаевич, доктор технических наук, профессор, Донской государственной технической университет (Ростов-на-Дону, Российская Федерация)

Пушенко Сергей Леонардович, доктор технических наук, профессор, Донской государственной технической университет (Ростов-на-Дону, Российская Федерация)

Порошин Александр Алексеевич, доктор технических наук, Всероссийский ордена «Знак Почета» научно-исследовательский институт противопожарной обороны МЧС России (Балашиха, Российская Федерация)

Севастьянов Борис Владимирович, доктор технических наук, кандидат педагогических наук, профессор, Ижевский государственный технический университет имени М.Т. Калашникова (Ижевск, Российская Федерация)

Тюрин Александр Павлович, доктор технических наук, доцент, Ижевский государственный технический университет имени М.Т. Калашникова (Ижевск, Российская Федерация)

Хазанович Григорий Шнеерович, доктор технических наук, профессор, Донской государственной технической университет (Ростов-на-Дону, Российская Федерация)

Хафизов Ильдар Фанисович, доктор технических наук, доцент, Уфимский государственный нефтяной технический университет (Уфа, Российская Федерация)

Хафизов Фаниль Шамильевич, доктор технических наук, профессор, Уфимский государственный нефтяной технический университет (Уфа, Российская Федерация)

Чукарин Александр Николаевич, доктор технических наук, профессор, Ростовский государственный университет путей сообщения (Ростов-на-Дону, Российская Федерация)

Contents

TECHNOSPHERE SAFETY

- Development of a Computational Complex for Fire Hazard Assessment of Production Facilities, Taking into Account Their Characteristics** 185
Andrey A. Kondashov
- Investigation of the Sorption of Heavy Metals by Terrestrial Ecosystems in Areas of the City of Chita with Various Anthropogenic Loads** 196
Tatyana V. Turusheva, Vyacheslav E. Esipov
- The Use of Coal Mine Methane as a Natural Gas Motor Fuel for Commercial Motor Transport in Donbass Cities** 208
Nikita V. Savenkov, Ekaterina L. Golovatenko

CHEMICAL TECHNOLOGIES, MATERIALS SCIENCES, METALLURGY

- Surface Morphology Identification of Steel Natural Ferrite-Martensitic Composite Using ImageJ Software** 221
Valentina V. Duka, Lyudmila P. Aref'eva
- Influence of the Production Method and the Structure of Chromium-Nickel Corrosion Resistant Steels on the Kinetics of the Formation of the Outer Cage of Spherical Joints**..... 230
Nikolai A. Konko, Badrudin G. Gasanov
- Influence of the Magnetic Field on the Behavior of Cracks in Steel after Heat Treatment to a High-Strength State** 242
Viktor N. Pustovoit, Yuri V. Dolgachev
- Fine Steel Structure after Microarc Molybdenum Steel Saturation** 250
Makar S. Stepanov, Yurii M. Dombrovskii

Содержание

ТЕХНОСФЕРНАЯ БЕЗОПАСНОСТЬ

- Разработка вычислительного комплекса для оценки пожарной опасности производственных объектов с учетом их характеристик**..... 185
А.А. Кондашов
- Исследование сорбции тяжелых металлов наземными экосистемами на участках города Чита с различной антропогенной нагрузкой** 196
Т.В. Турушева, В.Е. Есинов
- Применение шахтного метана в качестве газомоторного топлива для коммерческого автомобильного транспорта городов Донбасса** 208
Н.В. Савенков, Е.Л. Головатенко

ХИМИЧЕСКИЕ ТЕХНОЛОГИИ, НАУКИ О МАТЕРИАЛАХ, МЕТАЛЛУРГИЯ

- Идентификация морфологии поверхности стального естественного феррито-мартенситного композита с использованием программного обеспечения ImageJ**..... 221
В.В. Дука, Л.П. Арефьева
- Влияние способа получения и структуры хромоникелевых коррозионностойких сталей на кинетику формирования наружной облоймы сферических шарниров**..... 230
Н.А. Конько, Б.Г. Гасанов
- Влияние магнитного поля на особенности поведения трещин в стали после термической обработки на высокопрочное состояние** 242
В.Н. Пустовойт, Ю.В. Долгачев
- Тонкая структура стали после микродугового молибденирования**..... 250
М.С. Степанов, Ю.М. Домбровский

TECHNOSPHERE SAFETY

ТЕХНОСФЕРНАЯ БЕЗОПАСНОСТЬ



UDC 614.84

Original Empirical Research

<https://doi.org/10.23947/2541-9129-2025-9-3-185-195>

Development of a Computational Complex for Fire Hazard Assessment of Production Facilities, Taking into Account Their Characteristics

Andrey A. Kondashov 

All-Russian Research Institute of Fire Protection of the Ministry of the Russian Federation for Civil Defense, Emergencies and Elimination of Consequences of Natural Disasters, Balashikha, Russian Federation

✉ akond2008@mail.ru



EDN: SBQHNQ

Abstract

Introduction. Every year in the Russian Federation, approximately five thousand fires occur at production facilities, causing damage estimated in billions of rubles. To reduce the number of fires and minimize damage, work is underway to improve the methodology for calculating the number and equipment of fire protection units created to extinguish fires and conduct emergency rescue operations in organizations. This methodology was approved by Order of the Ministry of Emergency Situations of Russia dated October 15, 2021 No. 700 (hereinafter referred to as the Methodology). In the scientific literature on the analysis of fire hazards in industrial facilities in various sectors of the economy, there is a lack of a comprehensive indicator for fire hazard assessment of enterprises, which would take into account their technical and economic characteristics and industry affiliation. The aim of this study is to develop a dimensionless computing system describing the state of fire hazard of industrial facilities, taking into account their characteristic features. The developed complex was used in the formation of approaches to substantiate the number and technical equipment of facility-based fire protection units.

Materials and Methods. The analysis of statistical data on the number of fires, number of deaths and injuries, as well as the material damage caused by fires at production facilities in various economic sectors, was carried out using information from the Federal State Information System “Federal Database ‘Fires’”. To determine technical, economic and operational characteristics of enterprises with facility-based fire protection units, a survey was conducted using a questionnaire that collected information from 726 production facilities. Technical and economic characteristics of these facilities were studied, including: the area of land and buildings, number of employees, the mass of fire-hazardous, fire-explosive and explosive technological environments, the area of buildings and structures classified into certain categories of explosion and fire hazard, the number of fires at the enterprise, etc.

Results. A dimensionless U_{no} computing system has been developed that characterizes the fire hazard level of industrial facilities. The distribution of values of the U_{no} complex for production facilities where fire protection units have been established has been constructed, and the parameters of the resulting distribution have been determined. The criteria for classifying a production facility according to its fire hazard level have been established. The values of the fire hazard indicator for economic sectors have been calculated. Ferrous metallurgy ($U_{no} = 0.77$), mechanical engineering and metalworking (0.73), non-ferrous metallurgy (0.70) and fuel industry (0.68) fell into the category of high fire hazard. The paper provides an example of calculating the fire hazard level for an electric power company.

Discussion. When determining the number and location of fire protection units, as well as the number of personnel and technical equipment, it is important to consider the level of fire risk in the production facility. An analysis of the distribution of values of the U_{no} complex showed that it followed a normal distribution with an average value of $m = 0.47$ and a standard deviation of $\sigma = 0.19$. This meant that industries such as ferrous metallurgy and mechanical engineering had a higher level of fire risk compared to the electric power industry, which was classified as medium. The proposed method allows for an effective assessment of fire risk across different sectors of the economy.

Conclusion. The results obtained were used to develop a new version of the Methodology for calculating the number and technical equipment of fire protection units, created to extinguish fires and carry out emergency rescue operations in organizations. This methodology was approved by Order No. 700¹ of the Ministry of Emergency Situations of Russia dated October 15, 2021. The use of the developed complex will allow for a more accurate consideration of the specific characteristics of the production facility when determining fire protection resources.

Keywords: fire hazard, production facility, branch of the economy, fire department facility, complex indicator

Acknowledgements. The authors would like to thank the Editorial board and reviewers for their attentive attitude to the article and the comments indicated, which allowed us to improve its quality.

For Citation. Kondashov AA. Development of a Computational Complex for Fire Hazard Assessment of Production Facilities, Taking into Account Their Characteristics. *Safety of Technogenic and Natural Systems*. 2025;9(3):185–195. <https://doi.org/10.23947/2541-9129-2025-9-3-185-195>

Оригинальное эмпирическое исследование

Разработка вычислительного комплекса для оценки пожарной опасности производственных объектов с учетом их характеристик

А.А. Кондашов 

Всероссийский ордена «Знак Почета» научно-исследовательский институт противопожарной обороны», г. Балашиха, Российская Федерация

✉ akond2008@mail.ru

Аннотация

Введение. Ежегодно в Российской Федерации на производственных объектах происходит около 5 тыс. пожаров, ущерб от которых исчисляется миллиардами рублей. В целях снижения количества пожаров и минимизации ущерба в настоящее время ведется работа по совершенствованию методики расчета численности и технической оснащенности подразделений пожарной охраны, создаваемых для тушения пожаров и проведения аварийно-спасательных работ в организациях, утвержденной приказом МЧС России от 15 октября 2021 г. № 700 (далее — Методика). В научной литературе, посвященной анализу пожарной опасности производственных объектов различных отраслей экономики, отсутствует комплексный показатель для оценки пожарной опасности предприятий, который бы учитывал их технико-экономические характеристики с учетом отраслевой принадлежности. Цель настоящего исследования состоит в разработке безразмерного вычислительного комплекса, описывающего состояние пожарной опасности производственных объектов, принимающего во внимание их характерные особенности. Разработанный комплекс использован при формировании подходов к обоснованию численности и технической оснащенности объектовых подразделений пожарной охраны.

Методы и материалы. Проведен анализ статистических данных по количеству пожаров, числу погибших и травмированных, а также материальному ущербу от пожаров на производственных объектах по отраслям экономики с использованием информации из федеральной государственной информационной системы «Федеральный банк данных «Пожары». Для определения технико-экономических и оперативных характеристик предприятий, на которых созданы объектовые подразделения пожарной охраны, был проведен анкетный опрос, по результатам которого собраны сведения о 726 производственных объектах. Исследованы технико-экономические характеристики данных объектов: площади территории и застройки, численность персонала, массы обращающихся пожароопасных, пожаровзрывоопасных и взрывоопасных технологических сред, площади зданий и сооружений, отнесенных к определенным категориям взрывопожароопасности, количество пожаров на предприятии и др.

Результаты исследования. Разработан безразмерный вычислительный комплекс $U_{по}$, характеризующий уровень пожарной опасности производственных объектов. Построено распределение значений комплекса $U_{по}$ для производственных объектов, на которых созданы подразделения пожарной охраны, и определены параметры полученного распределения. Определены критерии отнесения производственного объекта к определенной категории пожарной опасности. Рассчитаны значения показателя пожарной опасности для отраслей экономики. В категорию высокой пожарной опасности попадает черная металлургия ($U_{по} = 0,77$), машиностроение и металлообработка (0,73), цветная металлургия (0,70) и топливная промышленность (0,68). Приведен пример расчета уровня пожарной опасности для предприятия электроэнергетики.

¹ On Approval of Methods for Calculating the Number and Equipment of Fire Protection Units. Order of the Ministry of Emergency Situations of Russia No. 700 dated October 15, 2021. Ministry of the Russian Federation for Civil Defense, Emergency Situations and Elimination of Consequences of Natural Disasters. (In Russ.) URL: <https://mchs.gov.ru/dokumenty/7454> (accessed: 11.05.2025).

Обсуждение. При нормировании количества и дислокации объектовых подразделений пожарной охраны, при определении численности их личного состава и технической оснащенности необходимо учитывать уровень пожарной опасности производственного объекта. Анализ распределения значений комплекса $U_{по}$ показал, что он распределен нормально со средним значением $m = 0,47$ и стандартным отклонением $\sigma = 0,19$. В результате, такие отрасли, как черная металлургия и машиностроение, отнесены к категории высокой пожарной опасности, в то время как электроэнергетика классифицирована как средняя. Таким образом, предложенный метод позволяет эффективно оценивать пожарную опасность в различных секторах экономики.

Заключение. Полученные результаты использованы для подготовки новой редакции Методики расчета численности и технической оснащенности подразделений пожарной охраны, создаваемых для тушения пожаров и проведения аварийно-спасательных работ в организациях, утвержденной приказом МЧС России от 15 октября 2021 г. № 700. Использование разработанного комплекса позволит более точно учитывать особенности производственного объекта при определении ресурсов пожарной охраны.

Ключевые слова: пожарная опасность, производственный объект, отрасль экономики, объектовое подразделение пожарной охраны, комплексный показатель

Благодарности. Автор выражает благодарность редакции и рецензентам за внимательное отношение к статье и указанные замечания, которые позволили повысить ее качество.

Для цитирования: Кондашов А.А. Разработка вычислительного комплекса для оценки пожарной опасности производственных объектов с учетом их характеристик. *Безопасность техногенных и природных систем.* 2025;9(3):185–195. <https://doi.org/10.23947/2541-9129-2025-9-3-185-195>

Introduction. Every year, direct material damage from fires at production facilities reaches several billion rubles, emphasizing the urgency of this issue. Fires at production sites can quickly spread over a large area due to the presence of flammable and combustible substances and materials, leading not only to significant financial losses for businesses, but also severe social consequences such as job loss, disruption of production processes, and the need for personnel evacuation. Furthermore, these fires can have severe environmental consequences, resulting in smoke and pollution of the lower atmosphere.

The study of fire hazards in various production facilities has been a subject of many studies. However, the problem of insufficient understanding of specific risks in different industries remains unsolved. This emphasizes the need for a more systematic approach to fire risk assessment. The increased danger at chemical industry facilities is due to the presence of flammable and explosive substances. A fire at these facilities can lead to severe social and economic consequences [1].

The fire and explosion hazards of metallurgical enterprises also raise legitimate concerns, since a lot of combustible dust is generated during their operations [2]. This occurs as a result of various technological processes [3]. Violations of safety regulations can directly lead to fires and explosions at such enterprises [4]. Work [5] highlights that enterprises in the forestry, woodworking, and pulp and paper industries have some of the highest fire risks. The main causes of fires include violations of electrical equipment installation and operation rules (30.5%), and careless handling of fire (20.2%) [6].

The fire hazard at power plants is caused by the handling of combustible materials, such as oils and insulating materials, as well as ignition sources related to electricity. This can lead to fires if the procedures for operating electrical equipment are not followed [7]. In the oil refining and petrochemical industries, fires often occur due to wear and tear of production equipment, violation of technological regulations [8], non-compliance with fire safety requirements [9], as well as deficiencies in the installation process [10]. The increasing complexity of production processes in this industry entails an increase in the number of flammable gases and volatile flammable liquids, which creates a real threat of large-scale fires [11]. Thus, the assessment of the fire safety of substances used at the facilities of the oil and gas complex becomes a key element in the fire safety system [12].

The occurrence of fires at mining enterprises is often associated with violations of safety regulations, malfunctions of equipment and infrastructure facilities, as well as unfavorable environmental conditions [13]. In mechanical engineering and metalworking enterprises, increased fire risk is associated with the presence of a large number of flammable materials and products [14].

Despite the extensive research on fire hazards in various industries, there is still no unified approach that can adequately assess fire hazards in different production conditions, considering their specific characteristics. The current study aims to develop a comprehensive indicator that would describe the state of fire hazard at a given production facility. This indicator will serve as a basis for substantiating the number and location of fire protection units, their staff and technical equipment.

The aim of the this research is to develop a methodology for determining fire hazard, which in turn should improve risk management practices and increase safety at production facilities. In order to achieve this, we have set out several specific objectives: to analyze existing fire hazard assessment methods, identify shortcomings in current approaches, and propose new solutions that contribute to improving the overall safety. Thus, the relevance of the research lies not only in its scientific and practical significance, but also in its ability to create the basis for further improvements in the field of fire safety.

Materials and Methods. To calculate the values of fire hazard indicators for different industries, an analysis of statistical data on fires at production facilities from 2020 to 2022 was conducted using information from the Federal State Information System “Federal Database “Fires”². The number of enterprises in each economic sector was determined based on data provided by the Federal State Statistics Service³.

A questionnaire-based survey was conducted to determine the technical and economic characteristics of enterprises operating fire protection units. As a result, data on 726 production facilities was collected [15]. The data was analyzed, and the average values for each indicator were determined for the entire set of companies and for individual sectors.

When developing dimensionless computing complex U_{no} , which characterized the fire hazard of an enterprise, the technical and economic indicators of the enterprise were normalized to the corresponding average values and multiplied by weighting factors that determined the contribution of a specific indicator. The values of fire situation indicators for economic sectors were normalized to the average values for the entire economy.

The values of dimensionless computing complex U_{no} for all production facilities with fire protection units have been calculated and the distribution of U_{no} values has been constructed. Average value m and standard deviation σ of the obtained distribution were determined, on the basis of which the boundaries of ranges of U_{no} values corresponding to different levels of fire hazard of the production facility were calculated.

Analysis of statistical data on fires in various sectors of the economy revealed the following picture. The average number of fires per 100 enterprises in all sectors of the economy was 0.75 fires per 100 enterprises. This indicator reached its maximum value at coal industry enterprises — 9.38 fires per 100 enterprises. The construction industry had the lowest number of fires — 0.14 fires per 100 enterprises (Fig. 1).

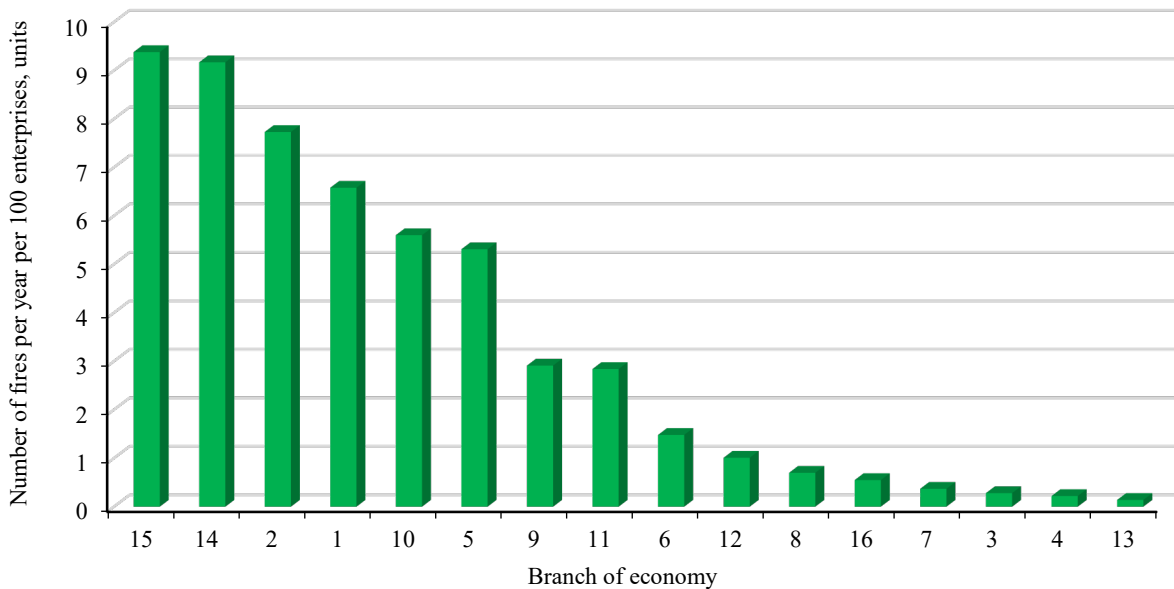


Fig. 1. Number of fires per 100 enterprises by economic sector: 1 — electric power industry; 2 — ferrous metallurgy; 3 — chemical and petrochemical industry; 4 — mechanical engineering and metalworking; 5 — forestry, woodworking and pulp and paper industry; 6 — building materials industry; 7 — light industry; 8 — food industry; 9 — agriculture; 10 — fuel industry; 11 — non-ferrous metallurgy; 12 — transport; 13 — construction; 14 — shipbuilding and ship repair; 15 — coal industry; 16 — other industries

² On the Formation of Electronic Databases for Accounting for Fires and Their Consequences. Order of the Ministry of Emergency Situations of Russia No. 625 dated December 24, 2018. GARANT. (In Russ.) URL: <https://base.garant.ru/72138544/> (accessed: 11.05.2025).

³ Russian Statistical Yearbook. 2022. Federal State Statistics Service: Moscow: 2022. 696 p. (In Russ.) URL: https://rosstat.gov.ru/storage/mediabank/Ejegodnik_2022.pdf (accessed: 11.05.2025)

On average, 53 people were killed or injured per 1,000 fires at production facilities. The lowest number of victims of fires was registered at electric power enterprises — 12 people per 1,000 fires. This indicator reached the highest value in the fuel industry — 452 people per 1,000 fires (Fig. 2)

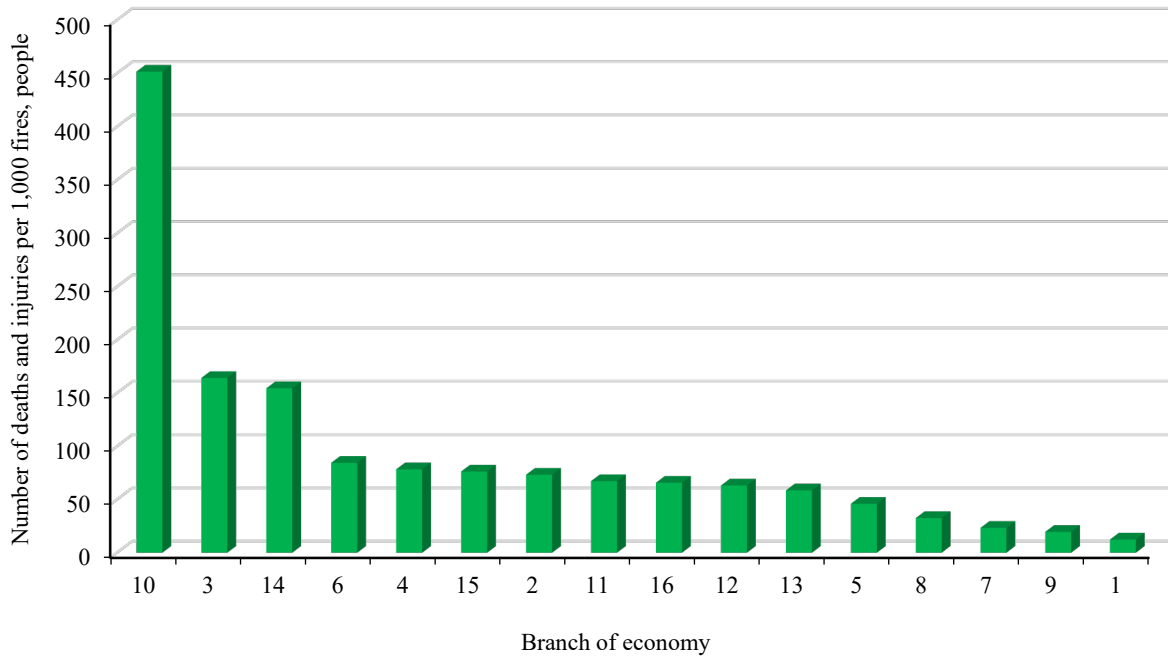


Fig. 2. Number of victims (deaths and injuries) in fires per 1,000 fires by economic sector. Economic sectors are listed in the caption to Figure 1

The average amount of damage caused by a single fire ranged from 16 million rubles for enterprises in the machine-building and metalworking industries to 60 thousand rubles for enterprises in the shipbuilding and ship repair industries. The average damage from a single fire in the entire economy was 904 thousand rubles.

The analysis of technical and economic characteristics of enterprises with fire protection units revealed the following patterns. The average area of enterprises varied from 3.7 hectares for light industry to 1.81 thousand hectares for transport enterprises. The average value for all enterprises with fire protection units was 238 hectares.

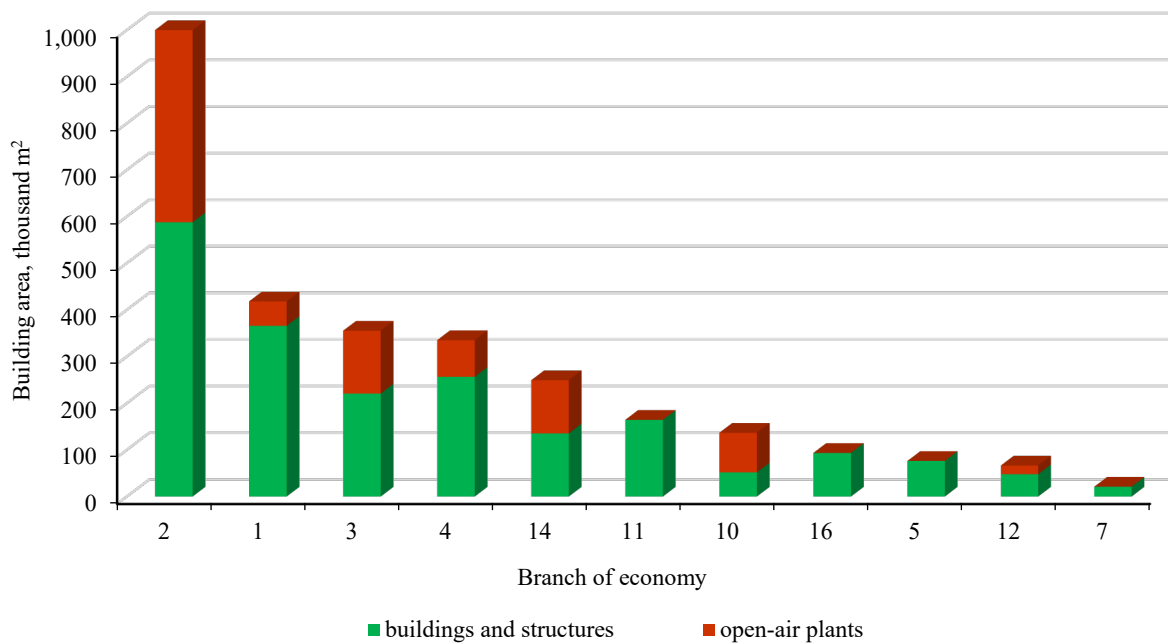


Fig. 3. Area covered by buildings, structures and open-air plants by sectors of the economy. Economic sectors are listed in the caption to Figure 1

Figure 3 provides the distribution of economic sectors by the area covered by buildings, structures and open-air plants. The largest average building area in machine-building enterprises was 587.8 thousand m² (buildings and structures) and 413.6 thousand m² (open-air plants). Light industry enterprises had the smallest building area with buildings and structures — 21.1 thousand m², and open-air plants at transport enterprises — 18.7 thousand m². The average building area for all enterprises was 155 thousand m² (buildings and structures) and 94 thousand m² (open-air plants).

The number of employees at ferrous metallurgy enterprises reached the highest values, with an average of 14,400 people. Of these, 5,700 worked in the most active shift. Light industry enterprises had the lowest number of employees, with an average of 208 and 154 people, respectively. Overall, the average number of employees across all enterprises was 1,567 and 678 in the busiest shift, respectively.

The largest amount of fire-hazardous and explosive substances circulating in open-air plants was observed at electric power enterprises, averaging 177 thousand tons. The smallest amount of these substances was at machine-building and metalworking enterprises with an average of 90 tons. The average value of this indicator for all enterprises was 98 thousand tons.

The average area of buildings and structures classified as having a V degree of fire resistance for all enterprises was 5 thousand m². This indicator reached its highest value at enterprises in the electric power industry — on average 10.1 thousand m², and at enterprises of non-ferrous metallurgy — 138 m².

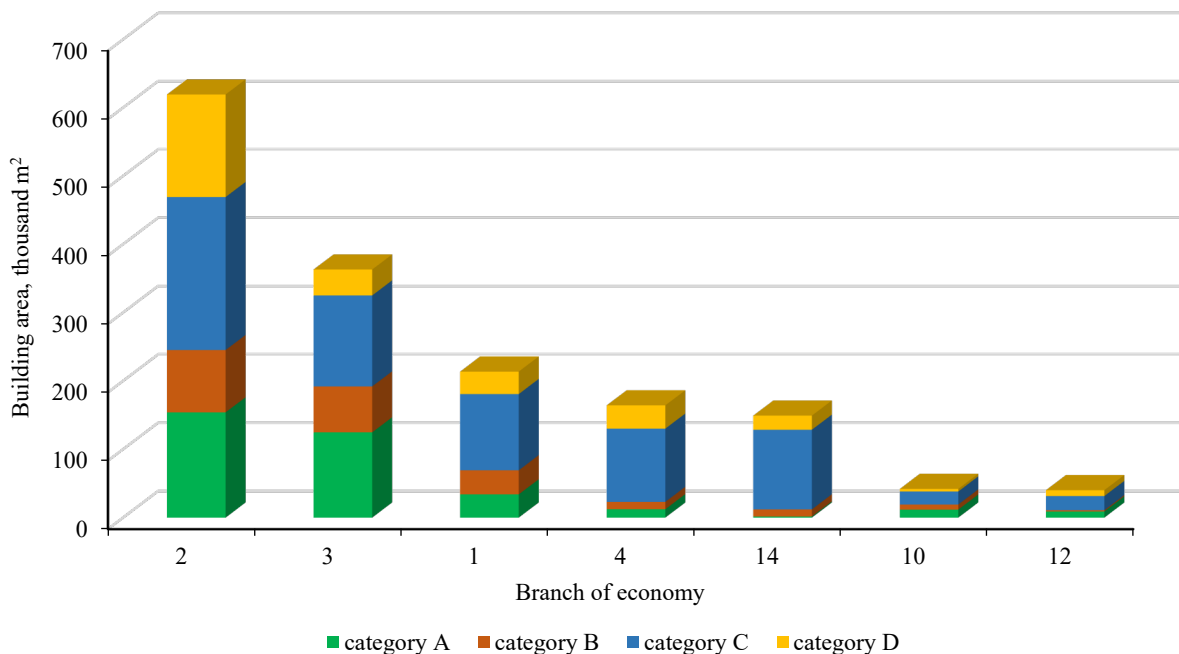


Fig. 4. Building area of enterprises with buildings (structures) classified into certain categories of explosion and fire hazard, by economic sectors. Economic sectors are listed in the caption to Figure 1

Figure 4 shows the distribution of economic sectors by area covered by buildings of enterprises with buildings (structures) classified into certain categories of explosion and fire hazard. The largest average building area was in machine-building and metalworking enterprises — 154 thousand m² for category A, 91 thousand m² for category B, 224 thousand m² for category C, and 150 thousand m² for category D. The average building area for all enterprises in these categories was 52 thousand, 63 thousand, 91 thousand and 36 thousand m², respectively.

The average number of fires at enterprises with fire protection units over a 5-year period was 1.2 fires per enterprise. Enterprises in the ferrous metallurgy industry had the highest number of fires, averaging 11.5 over 5 years, while enterprises in the light industry had the lowest number, averaging 0.07 over 5 years.

The average distance to local fire department, arriving at the facility in accordance with the predetermined attendance, was 12.6 km. The longest distance was for chemical and petrochemical enterprises, with an average distance of 28.7 kilometers, while the shortest distance was for mechanical engineering enterprises, with an average distance of only 3.5 kilometers.

Results. Based on the analysis results, dimensionless computing complex $U_{\text{по}}$ has been developed to assess the fire hazard level of industrial facilities, which is calculated using the formula:

$$U_{\text{по}} = \left(1 + (S_1 + S_2)^{-1}\right)^{-1}. \tag{1}$$

S_1 dimensionless complex, included in (1), characterizes the fire hazard level of the industry to which the production facility in question belongs. To calculate S_1 , the formula is used:

$$S_1 = w_1 \frac{N_{\text{пож}}}{N_{\text{пож.ср}}} + w_2 \frac{N_{\text{ГТ}}}{N_{\text{ГТ.ср}}} + w_3 \frac{Y_{\text{М}}}{Y_{\text{М.ср}}}, \tag{2}$$

where w_i — dimensionless weighting factors, taken equal to 2/19; $N_{\text{пож}}$, $N_{\text{ГТ}}$, $Y_{\text{М}}$ — indicators characterizing the fire hazard of the industry, shown in Table 1; $N_{\text{пож.ср}}$, $N_{\text{ГТ.ср}}$, $Y_{\text{М.ср}}$ — average values of fire hazard indicators for all industries.

Table 1

Indicators characterizing the fire hazard of the industry

No.	Symbol	Name of the indicator	Unit of measurement
1	$N_{\text{пож}}$	Number of fires per 100 enterprises per year	units
2	$N_{\text{ГТ}}$	Number of people affected by fires, per 1,000 fires	people
3	$Y_{\text{М}}$	Average damage from one fire	rub.

S_2 dimensionless complex describes technical, economic and operational characteristics of a specific production facility. To calculate S_2 , the formula is used:

$$S_2 = w_4 \frac{S_{\text{тер}}}{S_{\text{тер.ср}}} + w_5 \frac{S_{\text{зд}}}{S_{\text{зд.ср}}} + w_6 \frac{S_{\text{уст}}}{S_{\text{уст.ср}}} + w_7 \frac{N_{\text{перс}}}{N_{\text{перс.ср}}} + w_8 \frac{N_{\text{загр}}}{N_{\text{загр.ср}}} + w_9 \frac{M_{\text{сред}}}{M_{\text{сред.ср}}} + w_{10} \frac{S_{\text{огн}}}{S_{\text{огн.ср}}} + w_{11} \frac{S_{\text{А}}}{S_{\text{А.ср}}} + w_{12} \frac{S_{\text{Б}}}{S_{\text{Б.ср}}} + w_{13} \frac{S_{\text{В}}}{S_{\text{В.ср}}} + w_{14} \frac{S_{\text{Г}}}{S_{\text{Г.ср}}} + w_{15} \frac{N_{\text{пож}}}{N_{\text{пож.ср}}} + w_{16} \frac{L_{\text{ПО}}}{L_{\text{ПО.ср}}}, \tag{3}$$

where w_i — dimensionless weighting factors, taken equal to 1/19; $S_{\text{тер}}$, $S_{\text{зд}}$, $S_{\text{уст}}$, $N_{\text{перс}}$, $N_{\text{загр}}$, $M_{\text{сред}}$, $S_{\text{огн}}$, $S_{\text{А}}$, $S_{\text{Б}}$, $S_{\text{В}}$, $S_{\text{Г}}$, $N_{\text{пож}}$, $L_{\text{ПО}}$ — indicators characterizing technical, economic and operational characteristics of the facility (Table 2); $S_{\text{тер.ср}}$, $S_{\text{зд.ср}}$, $S_{\text{уст.ср}}$, $N_{\text{перс.ср}}$, $N_{\text{загр.ср}}$, $M_{\text{сред.ср}}$, $S_{\text{огн.ср}}$, $S_{\text{А.ср}}$, $S_{\text{Б.ср}}$, $S_{\text{В.ср}}$, $S_{\text{Г.ср}}$, $N_{\text{пож.ср}}$, $L_{\text{ПО.ср}}$ — average values of indicators for facilities with fire protection units.

Table 2

Indicators characterizing technical, economic and operational characteristics of a production facility

No.	Symbol	Name of the indicator	Unit of measurement
1	$S_{\text{тер}}$	Area of the territory	ha
2	$S_{\text{зд}}$	Area covered by buildings and structures	m ²
3	$S_{\text{уст}}$	Area covered by open-air plants	m ²
4	$N_{\text{перс}}$	Total number of staff	people
5	$N_{\text{загр}}$	Number of facility staff working during the busiest shift	people
6	$M_{\text{сред}}$	Mass of fire hazardous and explosive technological environments simultaneously circulating in open-air plants	t
7	$S_{\text{огн}}$	Area of buildings and structures belonging to the V degree of fire resistance	m ²
8–11	$S_{\text{А}}$, $S_{\text{Б}}$, $S_{\text{В}}$, $S_{\text{Г}}$	Area of buildings (structures) classified as explosion and fire hazard categories A, B, C, D	m ²
12	$N_{\text{пож}}$	Number of fires at the enterprise over 5 years	units
13	$L_{\text{ПО}}$	Distance to the local fire department unit arriving at the production facility in accordance with the predetermined attendance	km

The distribution of U_{no} complex values for production facilities with fire protection units is described by a normal law with average value $m = 0.47$ and standard deviation $\sigma = 0.19$. Table 3 provides the criteria for classifying a production facility as a certain category of fire hazard.

Table 3

Fire hazard levels of the production facility and their corresponding values of U_{no} complex

Fire hazard category	Criteria	Range of values
Low	$0 \leq U_{no} < m$	$0 \leq U_{no} < 0.47$
Average	$m \leq U_{no} < m + \sigma$	$0.47 \leq U_{no} < 0.66$
High	$m + \sigma \leq U_{no} < m + 2\sigma$	$0.66 \leq U_{no} < 0.85$
Extremely high	$m + 2\sigma \leq U_{no} < 1$	$0.85 \leq U_{no} < 1$

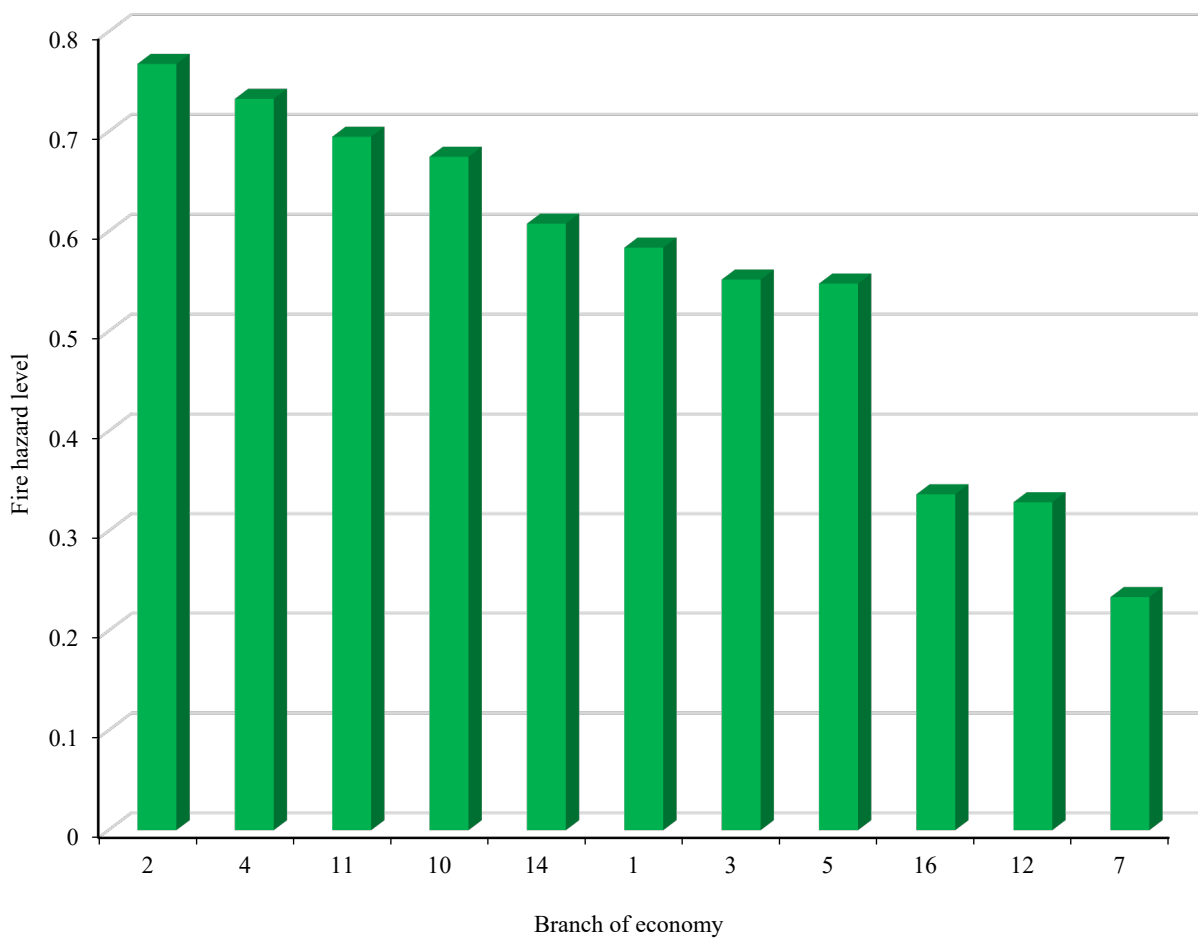


Fig. 5. Distribution of economic sectors by fire hazard level. Economic sectors are listed in the caption to Figure 1

Figure 5 provides the average values of U_{no} complex for economic sectors. As can be seen in the figure, ferrous metallurgy, mechanical engineering, metalworking, and non-ferrous metallurgy as well as the fuel industry fall into the category of high fire danger. The category of medium fire danger includes the following industries: shipbuilding and ship repair, electric power industry, chemical and petrochemical industry, forestry, woodworking and pulp and paper industry. Other industries belong to the category of low fire danger.

As an example, the fire hazard level for electric power industry enterprises is calculated. Table 4 shows the significance of technical, economic, and operational characteristics of the enterprise.

Values of indicators characterizing the fire hazard state of an electric power production facility

Indicator	Value	Indicator	Value
Y_1 , ha	17.0	Y_8 , hous. m ²	2.6
Y_2 , thous. m ²	33.5	Y_9 , thous. m ²	0.5
Y_3 , thous. m ²	0.0	Y_{10} , thous. m ²	8.0
Y_4 , people	236.0	Y_{11} , thous. m ²	12.5
Y_5 , people	184.0	Y_{12} , units	0.0
Y_6 , thous. tons	2,540.5	Y_{13} , km	13.0
Y_7 , thous. m ²	0.0		

Using formulas (2) and (3), we find the value of complexes $S_1 = 0.962$ and $S_2 = 1.424$. The value of U_{no} computing complex is determined by formula (1), $U_{no} = 0.705$. According to Table 3, the company is considered to have a high fire risk, while the electricity industry in general is considered to be at medium risk (Fig. 5).

Discussion. In the course of our research, we aimed to identify the level of fire hazard at production facilities, considering technical and economic characteristics of individual enterprises. The implemented model allows for the assessment of risks, taking into account the specific features of various industries. The main findings indicate that the level of fire hazard depends on the type of activity, with industries such as ferrous and non-ferrous metallurgy, mechanical engineering, metalworking, and the fuel sector having significantly higher levels of risk than the average.

The created dimensionless computing complex — U_{no} — makes it possible to analyze the fire hazard of production facilities more deeply, taking into account various factors, including the distance to the local fire protection unit, the mass of fire hazardous and explosive technological environments in circulation, the area occupied by buildings and structures classified into certain categories of explosion and fire hazard, the number of fires at the enterprise, etc. These factors should be taken into account when determining the resource requirements of fire protection units.

Thus, the results of the work not only confirm the existing hazards in the field of fire safety, but also emphasize the need to adapt the system to the conditions of specific industries for effective risk management. This creates the basis for further recommendations and actions aimed at reducing the number and consequences of fires.

Conclusion. The results obtained were used to develop a new version of the Methodology for calculating the number and technical equipment of fire protection units created to extinguish fires and conduct emergency rescue operations in organizations. This Methodology was approved by Order of the Ministry of Emergency Situations of Russia No. 700 dated October 15, 2021. In the new version of the Methodology, it is proposed to calculate the service radius of the fire department depending on the level of fire danger of the production facility, determined by U_{no} indicator. The fire hazard of the facility is also taken into account to determine the required consumption of extinguishing agent for outdoor firefighting when calculating the composition of fire protection forces and equipment. Furthermore, the areas under fire safety control during fire prevention are determined based on the value of U_{no} complex indicator.

The results of the research on the rationing of fire protection facilities will be discussed in more detail in a series of future publications.

References

- Smirnov AV. On Fire Safety Management Structure at a Typical Chemical Industry Facility. In: *Problems of Technosphere Safety: Proceedings of the International Scientific and Practical Conference of Young Scientists and Specialists*. 2017;(6):426–430. (In Russ.)
- Fedorov VA. Assessment of Fire and Explosion Safety of Metallurgical Industry Enterprises in Terms of Production Related to the Handling of Combustible Dust. *Fire and Technosphere Safety: Problems and Ways of Improvement*. 2021;3(10):456–460. (In Russ.)
- Moroń W, Ferens W. Analysis of Fire and Explosion Hazards Caused by Industrial Dusts with a High Content of Volatile Matter. *Fuel*. 2024;355:129363. <https://doi.org/10.1016/j.fuel.2023.129363>

4. Polyenin AV. Increasing the Level of Safety for Participants of Fire Extinguishing at the Facilities of the Metallurgical Industry. In: *Proceedings of the III International Scientific and Practical Conference "Scientific Research 2022"*, Penza, September 15, 2022. Penza: Science and Education (IP Gulyaev G.Yu.); 2022. P. 30–32. (In Russ.)
5. Korniyukhin IS, Ermilov AV. Analysis of Statistical Data on Fires in the Woodworking Industry. In: *Proceedings "Current Issues of Firefighting"*, Ivanovo, May 15, 2020. 2020. Ivanovo: Federal State Budgetary Educational Institution of Higher Education "Ivanovo Fire and Rescue Academy of the State Fire Service of the Ministry of the Russian Federation for Civil Defense, Emergencies and Elimination of Consequences of Natural Disasters"; P. 68–73. (In Russ.)
6. Kundysheva MV. Analysis of Sources of Danger in a Woodworking Enterprise. In: *Proceedings of the International Scientific and Practical Conference "The Arctic: Modern Approaches to Industrial and Environmental Safety in the Oil and Gas Sector"* Tyumen, November 29, 2023. Tyumen: Tyumen Industrial University; 2024. P. 109–112. (In Russ.)
7. Aleshkov MV, Pushkin DS, Kolbasin AA. Features of Development and Suppression of Fires on Objects of Power. *Technosphere Security Technologies*. 2010;(3(31));9. (In Russ.)
8. Maltsev AV. Analysis of the Causes of Fires at Oil Refining Facilities. *Fire Safety: Problems and Prospects*. 2017;1(8):278–280. (In Russ.)
9. Pshenichnyi DS. Analysis of the causes and Methods of Extinguishing Fires at Gas Industry Facilities. In: *Proceedings of the X All-Russian Scientific and Technical Conference of Young Researchers "Actual Problems of Construction, Housing and Communal Services and Technosphere Safety"*, Volgograd, April 24–29, 2023. Volgograd: Volgograd State Technical University; 2023. P. 260–262. (In Russ.)
10. Fedorov AV, Ospanov KK, Lomaev EN, Aleshkov AM, Mintshev MSh. Statistical and Causal Factors Analysis of Accidents at Oil Refining and Petrochemical Industry of Russia and Kazakhstan. *Technosphere Security Technologies*. 2021;(2(92)):156–168. (In Russ.) <https://doi.org/10.25257/TTS.2021.2.92.156-168>
11. Kalach AV, Cherepakhin AM, Sushko EA, Kalach EV, Sysoeva TP. The Dangerous Fire Factors Formation the on an Oil and Gas Complex Objects When Using the Combustible Environment on the Tetrachlormethane Basis. *IOP Conference Series: Earth and Environmental Science*. 2020;459:042046. <https://doi.org/10.1088/1755-1315/459/4/042046>
12. Gvozdev E. Development of an Integrated Safety System for Production Facilities: the Problem Statement and the Proposed Solution. *Reliability: Theory & Applications*. 2024;19(1(77)):474–487. <https://doi.org/10.24412/1932-2321-2024-177-474-487>
13. Aldiyansyah Aldiyansyah, Al Amin Siharis, Abriansyah Abriansyah, Fitriani Amin, Aqsal Ramadhan. Kegiatan Sosialisasi Keselamatan Dan Kesehatan Kerja Pada Tambang Batu Gamping di PT. Diamond Alfa Propertindo Kabupaten Buton Tengah. *Anoa: Jurnal Pengabdian Masyarakat Fakultas Teknik*. 2023;2(1):58–62. <https://doi.org/10.51454/anoa.v2i01.453>
14. Savelyev AP, Glotov SV, Chugunov MN, Enaleeva SA. Fire Safety at Medium-Size Machine-Building Facilities. *Russian Engineering Research*. 2022;42(4):373–375. <https://doi.org/10.3103/S1068798X22040268>
15. Marakhov PA, Poroshin AA, Streltsov OV, Kondashov AA, Bobrinev EV, Udavtsova EY. Formation of an Information Base for Calculating the Resource Provision of Fire Protection to Protect Organizations from Fires. *Modern Problems of Civil Protection*. 2024;(3(52)):22–29. (In Russ.) URL: https://ntp.edufire37.ru/uploads/2024/09/%D0%A1%D0%9F%D0%93%D0%97_352_2024.pdf (accessed: 11.05.2025).

About the Author:

Andrey A. Kondashov, Cand. Sci. (Phys.-Math.), Leading Researcher of the All-Russian Research Institute of Fire Protection of the Ministry of the Russian Federation for Civil Defense, Emergencies and Elimination of Consequences of Natural Disasters (12, VNI IPO, Balashikha, mkr., 143903, Russian Federation), [SPIN-code](#), [ORCID](#), [ScopusID](#), akond2008@mail.ru

Conflict of Interest Statement: the author declares no conflict of interest.

The author has read and approved the final version of manuscript.

Об авторе:

Андрей Александрович Кондашов, кандидат физико-математических наук, ведущий научный сотрудник Всероссийского ордена «Знак почета» научно-исследовательского института противопожарной обороны МЧС России» (143903, Российская Федерация, г. Балашиха, мкр. ВНИИПО, 12), [SPIN-код](#), [ORCID](#), [ScopusID](#), akond2008@mail.ru

Конфликт интересов: автор заявляет об отсутствии конфликта интересов.

Автор прочитал и одобрил окончательный вариант рукописи.

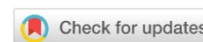
Received / Поступила в редакцию 02.06.2025

Reviewed / Поступила после рецензирования 24.06.2025

Accepted / Принята к публикации 10.07.2025

TECHNOSPHERE SAFETY

ТЕХНОСФЕРНАЯ БЕЗОПАСНОСТЬ



UDC 504.054, 504.53

Original Empirical Research

<https://doi.org/10.23947/2541-9129-2025-9-3-196-207>

Investigation of the Sorption of Heavy Metals by Terrestrial Ecosystems in Areas of the City of Chita with Various Anthropogenic Loads



EDN: YKMQQT

Tatyana V. Turusheva  , Vyacheslav E. Esipov
Transbaikal State University, Chita, Russian Federation
 turusheva_tanya@mail.ru

Abstract

Introduction. Environmental pollution with heavy metals is one of the most pressing environmental problems, as these substances can have a negative impact on ecosystems and living organisms. In particular, the accumulation of heavy metals in plants in urban ecosystems is an issue that has been widely studied, but many aspects of the problem remain unintelligible. For example, existing research does not always consider the influence of different environmental factors on metal sorption processes. This creates gaps in understanding the mechanisms of interaction between plants and pollutants. The current study aims to investigate the dependence of heavy metal sorption by the Scots pine (*Pinus sylvestris*) on the level of environmental pollution. The goal is to determine how metal accumulation indicators change depending on the growing conditions, allowing for a more accurate assessment of this plant's role in urban ecology.

Materials and Methods. The research was conducted in the city of Chita in the Trans-Baikal Territory. Scots pine is a widespread species of pine in this region, therefore, the bark of the Scots pine, as well as soil samples from sites in Chita that were exposed to high levels of human activity served as the basis for the study. Selection of sites was based, among other factors, on complex air pollution index (API5) in Chita. After collecting samples, they were quartered, dried, and ground into a fine powder. Then, the bark and soil were heated in a muffle furnace at 600°C. The burnt soil and pine bark ash were analyzed using methods commonly used in wood chemistry, including a spectrometric analysis on a Shimadzu AA-6200 atomic absorption spectrometer. The acidity was determined by the potentiometric method in a chloride extract. For this purpose, a 1M KCl solution (pH = 6.0) was used, as well as standard buffer solutions (pH 4.01; 6.86; 9.18) for instrument calibration. Suspensions were prepared by adding 75 ml of extractant to 30 g of soil, stirring for one minute. The pH was then measured after the readings stabilized. In parallel, a control experiment was conducted without a soil sample.

Results. Analysis of the data on seasonal changes in the ash and moisture content of Scots pine bark showed that they slightly increased in the summer and autumn months. During the study, we also obtained data on the distribution of heavy metals in the soil and bark of Scots pine depending on the season of the year. It was found that the highest levels of copper in the soil and bark of Scots pine were observed in Batareinaya Sopka, exceeding the maximum permissible concentration by 11 times, followed by Granitnaya Street, where the maximum permissible concentration was exceeded by 5 times. Zinc levels in the soil were high at three locations: Sosnovy Bor, Memory Park, and Batareinaya Sopka, exceeding the maximum permissible concentration by 1.77, 1.74 and 1.5 times, respectively. Lead levels were within the MPC at all seven locations. There were no seasonal changes in the content of heavy metals in the soil and bark. Thus, the study revealed the dependence of the content of heavy metals in the soil and bark of the Scots pine on the degree of anthropogenic load in the districts of Chita in the Trans-Baikal Territory.

Discussion. The results of the study demonstrated the correlation between the concentration of heavy metals in soil and bark samples of Scots pine and the degree of anthropogenic load. Therefore, the Scots pine can be considered a valuable object for monitoring heavy metal pollution, as it combines high sensitivity to man-made effects, resistance to adverse conditions and long-term ability to accumulate toxic substances. The data obtained support the idea of including the Scots pine in environmental monitoring systems, particularly in areas with developed industrial and transportation infrastructure. Future research could focus on developing standardized methods for using pine in bioindication, as well as studying its phytoremediation potential in conditions of chronic pollution.

Conclusion. The study expands our understanding of the mechanisms behind the migration and accumulation of heavy metals in urban ecosystems, especially in areas with a harsh continental climate. The findings can be used to improve urban planning, reduce the negative impact on public health, and develop sustainable strategies for areas with high levels of anthropogenic load.

Keywords: heavy metals, soil pollution, scots pine, monitoring, negative impact

Acknowledgements. The authors would like to thank the staff of the Laboratory of Physical-Chemical Research of Natural Objects and Synthesized Substances of the Financial and Economic Institute for the Development of Siberia and the East of Transbaikal State University for their help in obtaining and discussing the results.

For Citation. Turusheva TV, Esipov VE. Investigation of the Sorption of Heavy Metals by Terrestrial Ecosystems in Areas of the City of Chita with Various Anthropogenic Loads. *Safety of Technogenic and Natural Systems*. 2025;9(3):196–207. <https://doi.org/10.23947/2541-9129-2025-9-3-196-207>

Оригинальное эмпирическое исследование

Исследование сорбции тяжелых металлов наземными экосистемами на участках города Чита с различной антропогенной нагрузкой

Т.В. Турушева  , В.Е. Есипов

Забайкальский государственный университет, г. Чита, Российская Федерация

 turusheva_tanya@mail.ru

Аннотация

Введение. Загрязнение окружающей среды тяжелыми металлами представляет собой одну из наиболее актуальных экологических проблем, поскольку эти вещества негативно влияют на экосистемы и здоровье живых организмов. В литературе активно исследуется вопрос о накоплении тяжелых металлов растениями в урбоэкосистемах, однако многие аспекты данной проблемы остаются недостаточно раскрытыми. Например, существующие исследования не всегда учитывают влияние различных факторов окружающей среды на процесс сорбции металлов. Это создает пробелы в понимании механизмов взаимодействия растений и загрязняющих веществ. Настоящее исследование нацелено на детальное изучение зависимости сорбции тяжелых металлов сосной обыкновенной (*Pinus sylvestris*) от уровня загрязнения среды. Авторы ставят задачу определить, как изменяются показатели накопления металлов в зависимости от условий произрастания, что позволит более точно оценить роль данного растения в экологии городских территорий.

Материалы и методы. Исследования проводились на территории города Чита Забайкальского края. Сосна обыкновенная является широко распространенным видом рода сосна в Забайкальском крае, поэтому материалом для исследования послужила кора сосны обыкновенной, а также почвенные образцы, взятые на участках города Чита, отличающихся интенсивностью антропогенной нагрузки. Выбор участков для отбора материала осуществлялся, в том числе, по показателю комплексного загрязнения атмосферного воздуха (ИЗА5) на территории города Чита. После отбора пробы подвергались квартованию, сушке и измельчению до мелкозернистого состояния, после чего кора и почва подвергались термической обработке в муфельной печи при 600 °С. Обожженную почву и золу коры сосны исследовали по методикам, общепринятым в химии древесины, с использованием спектрометрического метода на атомно-абсорбционном спектрометре Shimadzu AA–6200. Кислотность определяли потенциометрическим методом в хлоридной вытяжке. Для этого использовали 1М раствор KCl (pH = 6,0), а также стандартные буферные растворы (pH 4,01; 6,86; 9,18) для калибровки прибора. Суспензии готовили, добавляя к 30 г почвы 75 мл экстрагента, перемешивали в течение одной минуты и измеряли pH после стабилизации показаний. Параллельно выполняли контрольный эксперимент без образца почвы.

Результаты исследования. Проведенный анализ полученных данных по сезонному изменению зольности и влажности коры сосны обыкновенной показал, что они незначительно возрастают в летне-осенний период. В ходе работы была получена динамика распределения тяжелых металлов в почве и коре сосны обыкновенной в зависимости от сезона года. Выяснено, что наибольшее содержание меди в почве и в коре сосны обыкновенной наблюдается на участке Батарейной сопки, превышая ПДК в 11 раз, далее ул. Гранитная, где ПДК превышен в 5 раз. Высокое содержание цинка в почве сосны обыкновенной наблюдается сразу в трех точках: Сосновый бор, Парк Памяти и Батарейная сопка, с превышением ПДК в 1,77; 1,74 и 1,5 раза соответственно. Содержание свинца в почве на всех семи точках находится в пределах ПДК. Сезонных изменений содержания тяжелых металлов в почве и коре не наблюдается. Таким образом, в ходе исследования была выявлена зависимость содержания тяжелых металлов в почве и коре сосны обыкновенной от степени антропогенной загруженности районов города Чита Забайкальского края.

Обсуждение. Результаты исследования показали зависимость содержания тяжелых металлов в исследованных образцах почвы и коры сосны обыкновенной от степени интенсивности антропогенной нагрузки. Таким образом, сосна обыкновенная представляет собой ценный объект для мониторинга загрязнения тяжелыми металлами, так как сочетает в себе высокую чувствительность к техногенному воздействию, устойчивость к неблагоприятным условиям и долговременную способность накапливать токсиканты. Полученные данные обосновывают целесообразность включения этого вида в системы экологического контроля, особенно в регионах с развитой промышленностью и транспортной инфраструктурой. Дальнейшие исследования могут быть направлены на разработку стандартизированных методик использования сосны в биоиндикации, а также на изучение её фиторемедиационного потенциала в условиях хронического загрязнения.

Заключение. Проведенное исследование расширяет понимание механизмов миграции и аккумуляции тяжелых металлов в урбанизированных экосистемах, особенно в условиях резко-континентального климата. Полученные результаты могут быть использованы для оптимизации городского планирования, минимизации негативного воздействия на здоровье населения и разработки стратегий устойчивого развития территорий с высокой антропогенной нагрузкой.

Ключевые слова: тяжелые металлы, загрязнение почвы, сосна обыкновенная, мониторинг, негативное воздействие

Благодарности. Авторы благодарят сотрудников лаборатории физико-химических исследований природных объектов и синтезированных веществ Финансово-хозяйственного института проблем освоения Сибири и Востока Забайкальского государственного университета за помощь в получении и обсуждении результатов.

Для цитирования. Турушева Т.В., Есипов В.Е. Исследование сорбции тяжелых металлов наземными экосистемами на участках города Чита с различной антропогенной нагрузкой. *Безопасность техногенных и природных систем.* 2025;9(3):196–207. <https://doi.org/10.23947/2541-9129-2025-9-3-196-207>

Introduction. One of the most urgent problems in modern ecology is environmental pollution by heavy metals. These substances [1] belong to the first and second hazard classes, as they have a significant negative impact on biological processes in ecosystems [2]. In addition, heavy metals can accumulate in living organisms, soil, and water bodies [3]. Entering the human body in small doses through the gastrointestinal tract, respiratory system, or skin, these substances are invisible to the naked eye, as they lack taste, smell, and color. However, their long-term accumulation [4] in human bones, liver, and brain can lead to severe diseases such as neurological disorders and cancer. Recently, there has been a growing interest in the scientific community [6] in the topic of heavy metal accumulation [5] by plants in urban ecosystems. In his work, the author [7] conducts a comparative analysis of the accumulation of heavy metals in the leaves, root and bark of the Siberian peashrub (*Caragana arborescens*) under conditions of anthropogenic impact on the territory of the Trans-Baikal Territory. Studies by another author show [8] that in urbanized landscapes, especially near highways, pine bark can accumulate significant concentrations of lead, cadmium, zinc, and copper, acting as kind of "storehouse" for these pollutants. Due to the mountainous and hollow location of the city of Chita and its high level of air pollution, the Scots pine tree absorbs pollutants on its needles and bark throughout the year. Therefore, research on the accumulation of heavy metals in coniferous trees in the climatic conditions of the Trans-Baikal Territory remains insufficiently explored, making this work particularly relevant.

It has been established [9] that the place of growth significantly affects the quantitative content of heavy metals in plants. The main sources of heavy metal pollution in the environment of the Trans-Baikal Territory are industry, vehicle emissions, and private sector using coal for furnace heating. The problem of air pollution in the Trans-Baikal Territory is particularly acute, as the city of Chita has been among the cities with the highest levels of air pollution for several years. This problem is aggravated by natural and climatic conditions and the mountainous and hollow location of the city. In winter, the Siberian anticyclone dominates the territory of the Trans-Baikal Territory, which is characterized by low temperatures and lack of air mass transfer. This results in a temperature inversion over Chita that prevents normal dispersion of emissions. Therefore, monitoring of the state of atmospheric air by priority pollutants is necessary in many cities [10].

The Scots pine (*Pinus sylvestris*) is of considerable interest in the context of phytoremediation of urban areas contaminated with heavy metals due to a number of unique adaptive mechanisms and high resistance to adverse environmental conditions. As an evergreen coniferous species, the pine accumulates pollutants all year round [11], especially effectively trapping metal-containing aerosols and dust particles that settle on the surface of the needles.

The bark of the Scots pine is a unique biological filter that plays a significant role in the accumulation of heavy metals from the urban environment. Unlike other tree tissues, the bark has a strong sorption capacity due to its porous structure and high lignin content, as well as the presence of phenolic compounds that bind metal ions actively. The process of metal accumulation in the bark is complex. Primary deposition occurs through direct contact with airborne particles, such as particles of tire wear, brake pads and pavement, which settle on the rough bark surface. Secondary accumulation occurs through bark diffusion processes, when soluble forms of metals enter the outer layers of bark through rainwater or condensation, becoming bound to cell walls through chelation with organic acids and tannins.

Thus, the aim of this research is to investigate the relationship between the sorption of heavy metals by the Scots pine and the level of pollution in their growing environment, taking into account the sharply continental climate and the mountainous and hollow location of the city of Chita in the Trans-Baikal Territory.

Materials and Methods. The bark of the Scots pine and soil samples taken from seven sites in Chita, which differed in the level of anthropogenic load, were used as the object of research (Fig. 1): site No. 1 — Pioneer Park (Zhuravleva St.); site No. 2 — Memorial Park (Petrovsko-Zavodskaya St.); site No. 3 — stadium SibVO (Kaidalovskaya St.); site No. 4 — Batareinaya Sopka; site No. 5 — Sosnovy Bor; site No. 6 — Bypass Highway; site No. 7 — Granitnaya St..

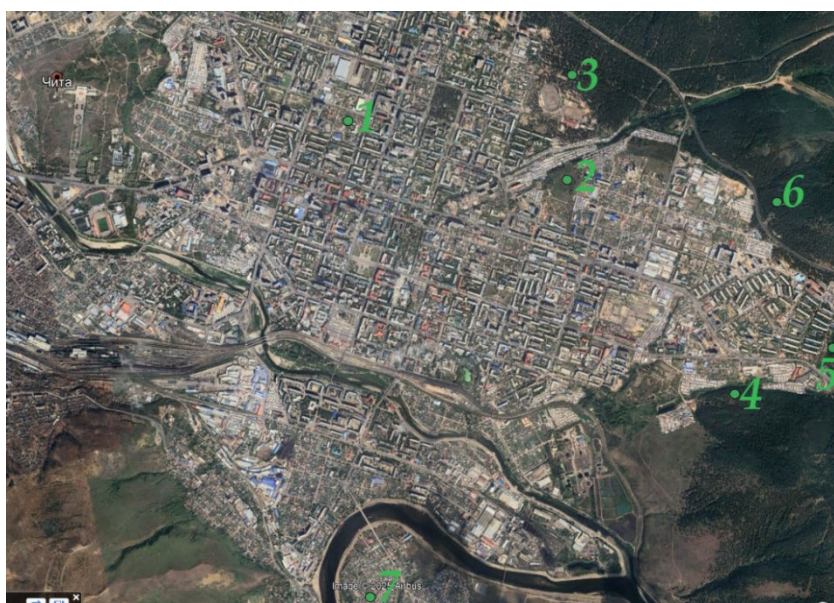


Fig. 1. Sampling map

Sampling was conducted during the seasons from spring 2024 to winter 2025. At each sampling location, 10–12 trees were selected and bark samples were collected. The top layer of bark was discarded, and then the fresh layer below was carefully removed using a knife. Soil samples were collected at a distance of 1.5 meters from the trees at a depth of 10 cm below the surface.

The samples were quartered, dried, and ground to a fine-grained state, after which the bark and soil were thermally treated in a muffle furnace at 600°C. The burnt soil and ash of the bark of the Scots pine were studied according to the methods adopted in wood chemistry [12], using the spectrometric method on a Shimadzu AA-6200 atomic absorption spectrometer. Sample preparation for analysis on an atomic absorption spectrometer included taking a 5.00 g sample, placing it in a conical flask, wetting it with water and adding 15 ml of chemically pure hydrochloric acid. Then the mixture was boiled for 2–3 minutes, 5 ml of 2M chemically pure nitric acid was added and the contents of the flask were brought to the state of dry salts. After that, the flasks were removed from the stove, 30 ml of 5M hydrochloric acid 1:1 was added and boiled again until dry salts were obtained, then HCl 1:1 was added again and boiled for 3 minutes. The flasks were cooled to room temperature, and then the volume of the solution was adjusted to 200 ml and filtered through blue ribbon filters. The resulting filtrate was analyzed on Shimadzu AA-6200 and Agilent 240 FS AA devices. The data was processed and organized into tables, and then the diagrams were constructed indicating the MPC in the soil (HN 2.1.7.2041–06). Acidity was determined by the potentiometric method in a chloride extract using a 1M KCl solution (pH=6.0), as well as standard buffer solutions (pH 4.01; 6.86; 9.18) for calibration of the device. The suspension was prepared by adding 75 ml of extractant to 30 g of soil, stirring for a minute, and pH was measured after stabilization of the readings. In parallel, a control experiment was conducted without a soil sample.

Results. During the course of the study, the moisture content and ash content of Scots pine bark, as well as soil moisture levels, were measured. An increase in moisture levels led to an increase in the mobility of heavy metals in the soil, and as a result, their bioavailability to plants increased (Tables 1–3).

Table 1

Seasonal dynamics of moisture changes in the Scots pine bark in 2024, %

Sampling site	Season			Standard deviation
	Spring	Summer	Autumn	
Pioneer Park	6.4	7.6	8.1	0.8737
Memory Park	5.9	7.3	7.9	1.0263
SibVO Stadium	8.3	9.1	10.1	0.9018
Batareinaya Sopka	10.2	11.3	12.6	1.2014
Sosnovy Bor	7.3	8.7	9.8	1.2530
Bypass Highway	6.1	7.5	8.2	1.0693
Granitnaya St.	8.5	9.2	10.3	0.9074

Table 2

Seasonal dynamics of ash content in the Scots pine bark in 2024, %

Sampling site	Season			Standard deviation
	Spring	Summer	Autumn	
Pioneer Park	6.7	7.1	6.9	0.2000
Memory Park	4.9	5.3	5.5	0.3055
SibVO Stadium	4.8	5.1	5.4	0.3000
Batareinaya Sopka	5.2	4.5	4.7	0.3606
Sosnovy Bor	4.9	4.7	5.2	0.2517
Bypass Highway	3.9	4.2	4.3	0.2082
Granitnaya St.	4.8	5.0	5.4	0.3055

An analysis of the data on moisture and ash content of pine bark revealed that, on average, the bark had low humidity levels in all areas except for Batareinaya Sopka and Granitnaya Street. This could be explained by the fact that these locations were further away from the city and therefore received more moisture and lost it to a lesser extent due to sunlight exposure. The humidity increased slightly from winter to autumn throughout the year, while the ash content remained approximately the same. Although the ash content of the bark did not directly influence the accumulation of heavy metals, it could indirectly affect this process through the ratio of organic and inorganic substances in the bark. This, in turn, could influence the plant's ability to accumulate heavy metals [13].

Table 3

Seasonal dynamics of soil moisture changes in 2024, %

Sampling site	Season			Standard deviation
	Spring	Summer	Autumn	
Pioneer Park	3.0	3.1	3.6	0.3215
Memory Park	2.1	2.3	2.5	0.2000
SibVO Stadium	1.7	1.8	2.1	0.2082
Batareinaya Sopka	2.4	2.5	3.0	0.3215
Sosnovy Bor	3.0	3.2	3.8	0.4163
Bypass Highway	3.7	3.9	4.2	0.2517
Granitnaya St.	2.6	2.7	3.1	0.2646

According to the data collected, soil moisture in these areas was low and increased slightly during the summer and autumn periods.

Another important factor in the sorption of heavy metals from soil was its acidity. Podzolic soils were the most common type in the studied region. Their type was previously assessed by morphological features such as color and structure, which allowed us to identify genetic horizons. The analyzed samples were characterized by a gray-brown color and contained small aggregates, which was typical for sod-podzolic soils with a pH ranging from 4 to 7.

The data collected are presented in Table 4.

Table 4

pH values of soil extracts

Sampling site	pH value
Pioneer Park	6.3
Memory Park	5.5
SibVO Stadium	6.3
Batareinaya Sopka	4.9
Sosnovy Bor	5.3
Bypass Highway	6.6
Granitnaya St.	5.6

The conducted studies of Chita's soil cover revealed a number of interesting patterns. Among them, the data from the territories of Batareinaya Sopka and Sosnovy Bor were of particular concern. There, abnormally low pH values were recorded, which was surprising for coniferous forests. The analysis of the wind rose and the locations of industrial facilities indicated that these natural ecosystems actually became accumulators of pollutants from thermal power plants, boiler houses, and busy highways. The SibVO Stadium and the Bypass Highway showed good performance. These territories were characterized by acidity values in the range of 6.3–6.6 pH, which was consistent with the results of morphological studies of the soil cover and indicated its compliance with the sod-podzolic type. Granitnaya Street with its moderately acidic soils was a typical example of an urbanized area with a predominance of traffic load. Such results require further investigation, especially considering long-term trends and potential consequences for urban ecosystems.

When studying the soil [14] and the bark of the Scots pine, special attention was paid to the following heavy metals: Cu, Zn, Pb. Each element has its own lamp emitting light with a certain wavelength: copper — 324.7 nm, lead — 283.3 nm, zinc — 213.9 nm. The obtained laboratory data are presented in Figures 2–7.

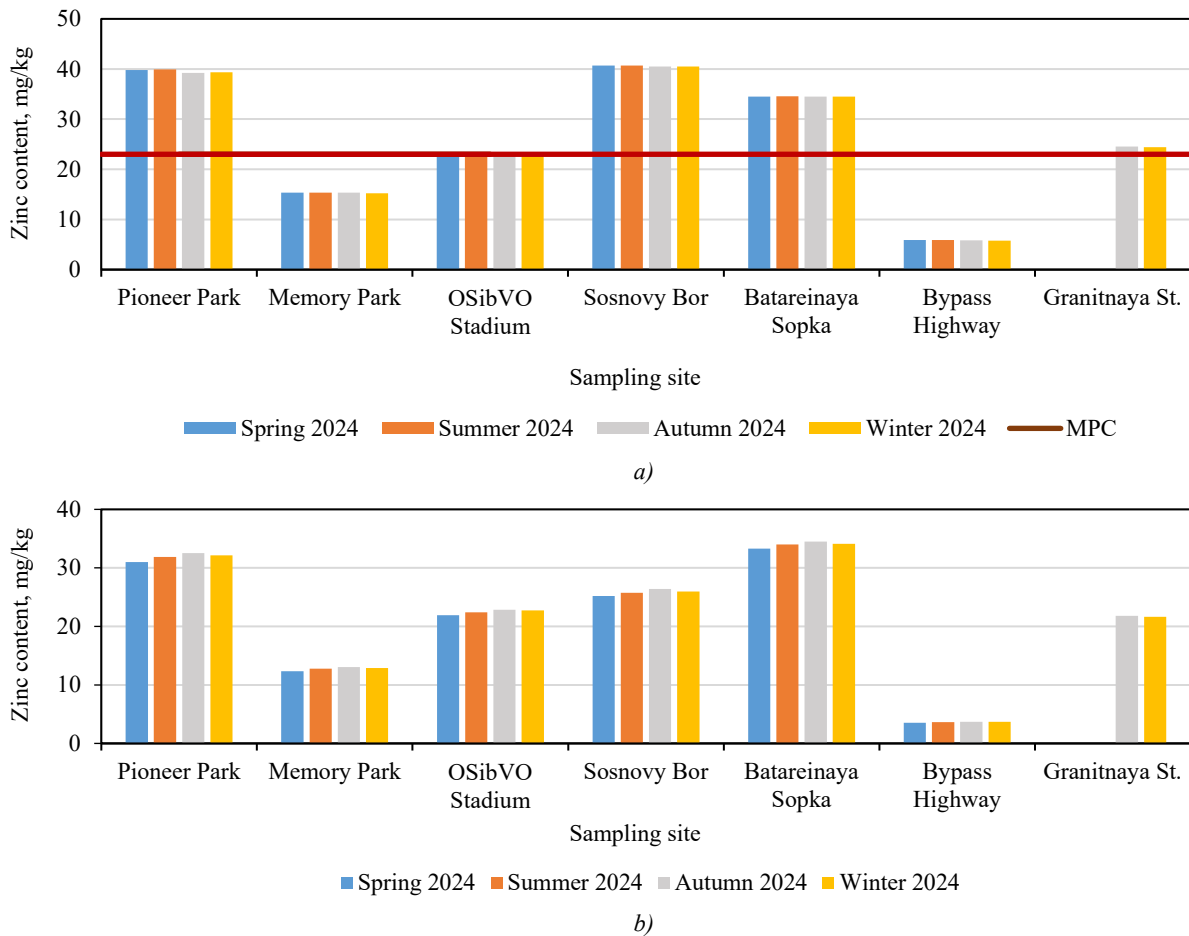


Fig. 2. Zinc content: a — in the soil; b — in the bark

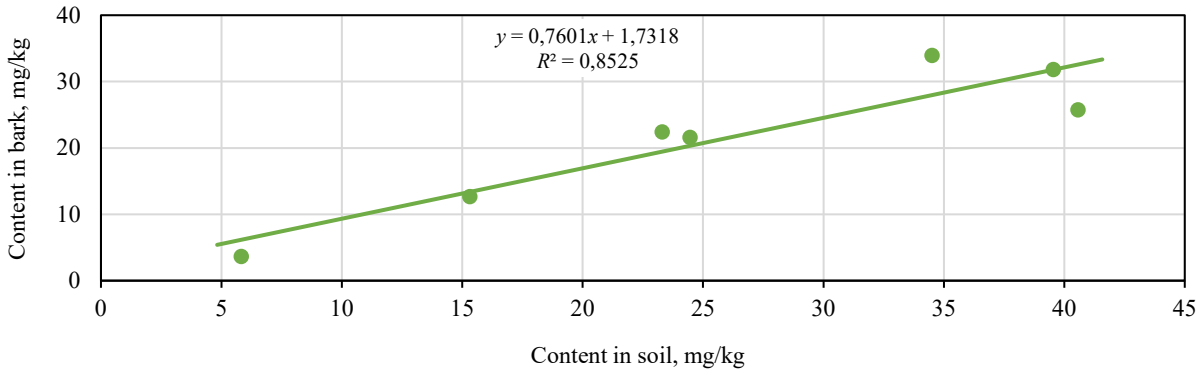
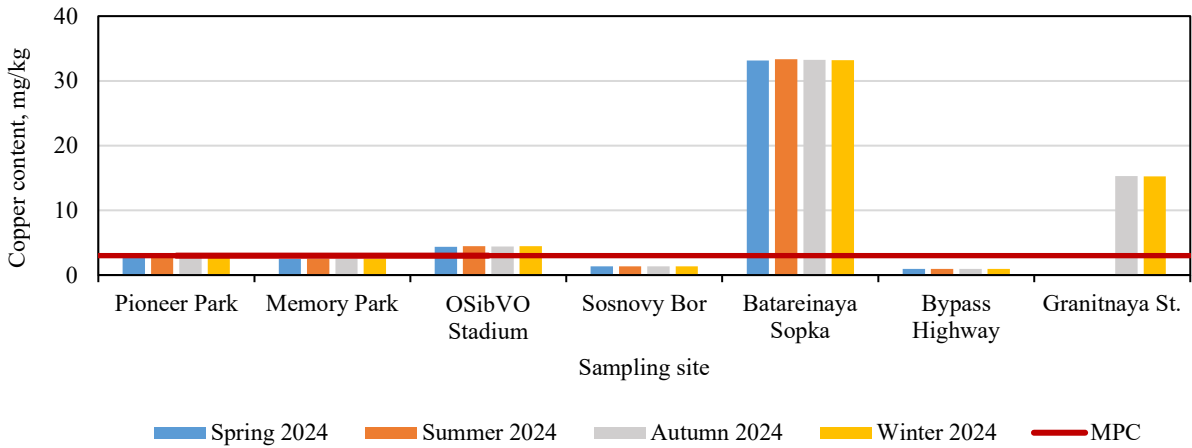
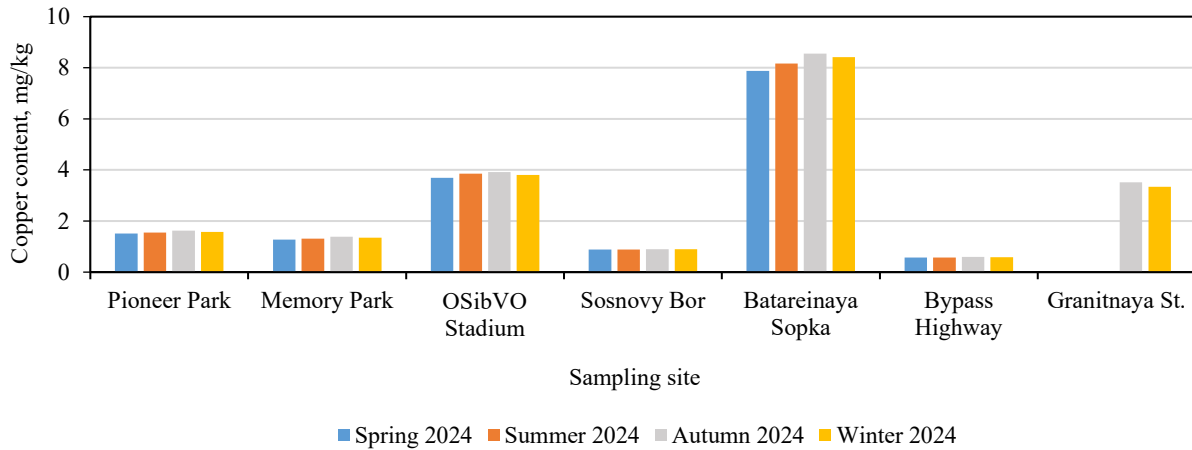


Fig. 3. Dependence of zinc content in the bark on the content in the soil



a)



b)

Fig. 4. Copper content: a — in the soil; b — in the bark

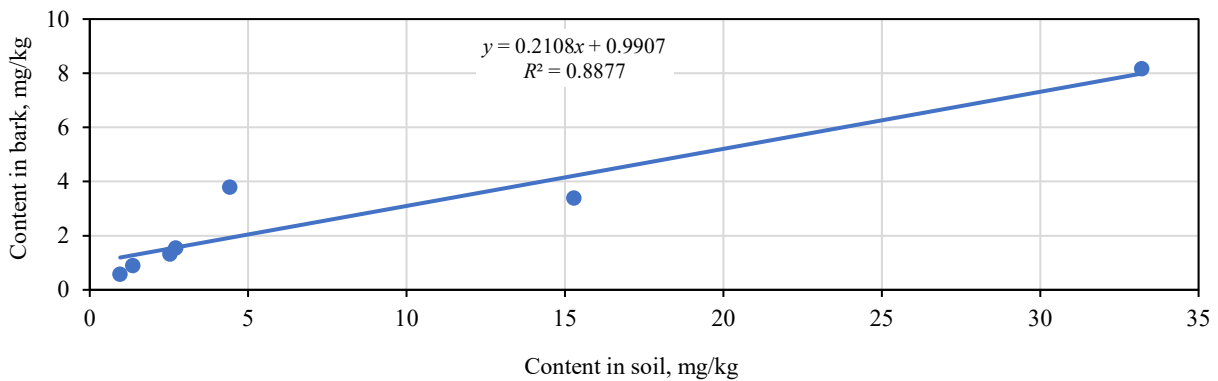


Fig. 5. Dependence of copper content in the bark on the content in the soil

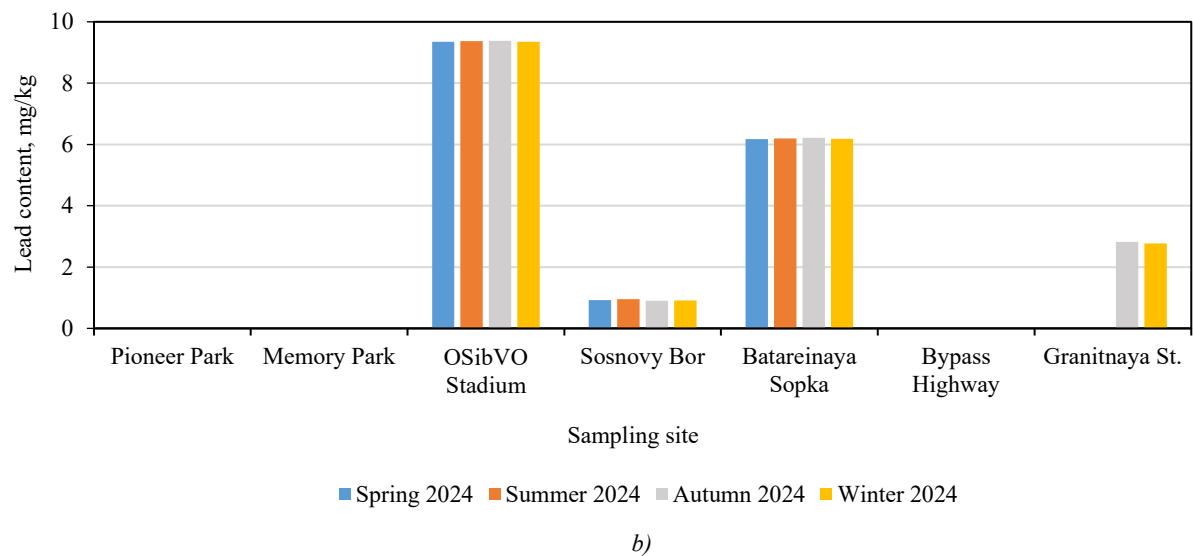
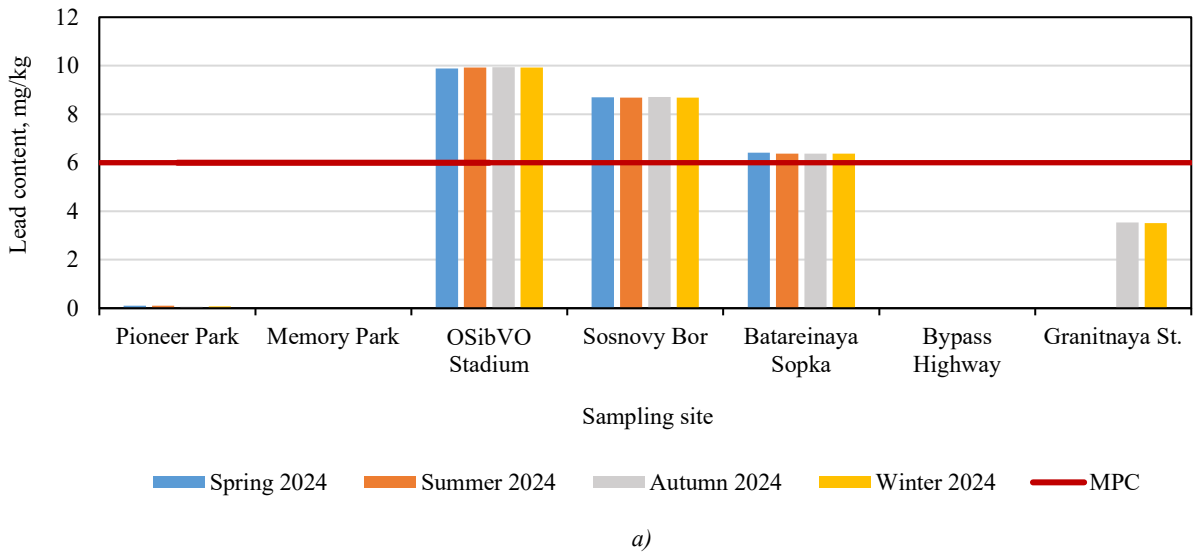


Fig. 6. Lead content: a — in the soil; b — in the bark

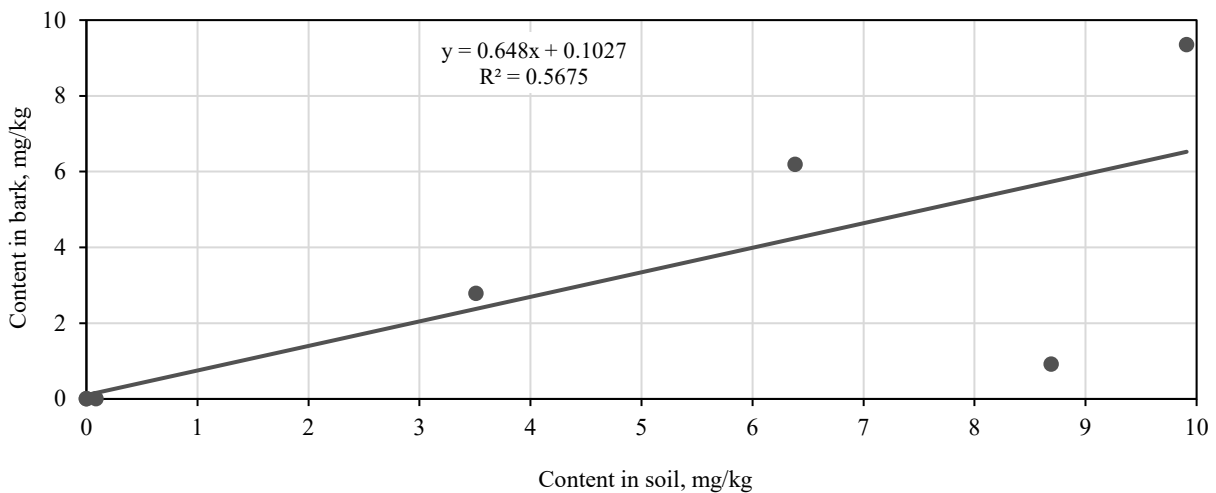


Fig. 7. Dependence of lead content in the bark on the content in the soil

After analyzing the results, it can be noted that the levels of heavy metals in the Scots pine bark showed a slight increase from spring to autumn, while soil levels remained relatively stable. The highest levels of soil pollution were observed in areas such as Batareinaya Sopka, Sosnovy Bor, Memory Park, Granitnaya Street, and SibVO. The analysis revealed the dependence of levels of heavy metal contamination in the Scots pine soil and bark on the level of anthropogenic load in the respective areas.

The research found a high concentration of copper in the soil at Batareinaya Sopka, which was 11 times higher than the maximum permissible level. This could be due to the presence of car repair shops and highways nearby, which could lead to increased levels of heavy metals in wastewater. Site No. 4 had a high level of air pollution due to its location on the leeward side of Chitinskaya CHPP-2. The samples taken near Granitnaya Street and the SibVO Stadium showed that the copper content was 5 and 1.5 times higher than the MPC, respectively. However, in other areas, the concentration remained within the sanitary standards.

High zinc content in the soil has been observed at three locations: Sosnovy Bor, Memory Park, and Batareinaya Sopka, with excesses of MPC by 1.77, 1.74 and 1.5 times, respectively. Additionally, a slight excess of the maximum permissible concentration was detected in the areas of the SibVO Stadium and Granitnaya Street. In other areas the indicators were within the normal range. Lead content in the soil exceeded the maximum permissible concentration in near the SibVO Stadium by 1.6 times, near the Sosnovy Bor by 1.45 times and near the Batareinaya Sopka. No lead was found in areas such as Memorial Park, Pioneer Park and Bypass Highway.

The excess of the maximum permissible concentration of lead was explained by the negative impact of energy and motor transport enterprises. Thus, in the ash deposits at CHPP-2 after coal combustion, lead content was 50–60% higher than the toxicity threshold. The wind carried toxic dust from the ash and slag dumps to all adjacent areas [15]. High levels of lead in soil were also caused by the slow removal of lead from soil. The rate of leaching varied between 4 and 30 grams per hectare per year, which led to an increase in lead concentration, especially in areas near highways.

There were no seasonal changes in the content of heavy metals in the soil. A slight fluctuation in the heavy metals content was observed in the bark. The levels increased gradually from spring to autumn, and then decreased slightly in winter and spring. This could be related to the growth cycle of the trees.

At the Sosnovy Bor site, lead content in the bark was almost not detected. This discrepancy in the overall picture could be explained by lead's strong binding [16] to organic matter in soils with high humus content, as well as its formation of phosphates and carbonates, making it practically inaccessible to plants. Additionally, the absorption of heavy metals by plants was influenced by the ionic composition of the soil. For example, the presence of competing Ca^{2+} and Al^{3+} ions could inhibit the absorption of lead by roots [17]. In soils with high concentrations of these elements, Pb^{2+} supply to plants decreased, while zinc and copper [18] continued to accumulate due to specialized transport mechanisms.

The cleanest section in this study was the Bypass Highway, since the sampling site in this case was far from the sources of pollution.

Discussion. The results of the study revealed significant soil contamination with heavy metals (Pb, Zn, Cu) in several areas of the city. The maximum permissible concentration (MPC) was exceeded in some areas, with the highest levels recorded at Batareinaya Sopka (copper — 11 times, zinc — 1.5 times), Granitnaya Street (copper — 5 times) and in the area of the SibVO Stadium (lead — 1.6 times). These findings indicate a high anthropogenic load due to the proximity of industrial enterprises, highways and historical sources of pollution, such as landfills and boiler houses. At the same time, seasonal fluctuations in the content of heavy metals in the soil were found to be relatively minor, suggesting that the pollution is more likely to be chronic in nature.

Special attention was paid to the impact of the hollow location of Chita on the environmental situation. The mountainous and hollow relief contributes to the accumulation of pollutants in the surface layer of the atmosphere and soil, limiting their natural dispersion. This is aggravated by the prevailing climatic conditions, such as a sharply continental climate with low precipitation, which increases the concentration of pollutants. The research results confirm that these factors create unfavorable conditions for natural self-purification of ecosystems, especially in areas with high anthropogenic load.

An important aspect of the research was the study of the effect of soil acidity on the mobility and accumulation of heavy metals. It has been found that in acidic soils (pH 4.9–5.6), such as in the areas of Batareinaya Sopka and Sosnovy Bor, the availability of metals to plants increased, which contributed to their accumulation in the bark of pine trees. At the same time, neutral and slightly alkaline soils (pH 6.3–6.6) demonstrated lower mobility of heavy metals, which reduced their bioavailability. These data emphasize the importance of considering pH when assessing pollution risks and designing remediation measures.

Thus, the Scots pine is a valuable tool for monitoring environmental pollution by heavy metals in a sharply continental climate and the hollow location of the city of Chita, combining high sensitivity to man-made impacts, resistance to adverse conditions and the long-term ability to accumulate toxins, thereby removing them from the circulation of substances. The data obtained substantiate the expediency of including this species in environmental control systems, especially in regions with developed industry and transport infrastructure. Further research could focus on developing standardized methods for utilizing the pine in bioindication, as well as studying its phytoremediation potential in conditions of chronic pollution.

Conclusion. The results of the study indicate that the city of Chita has a significant level of soil pollution by heavy metals. These metals are then absorbed by plants, which makes it possible to temporarily remove harmful compounds from the circulation and reduce their negative impact on the environment. The analysis of the results confirms the findings of previous researchers [19] that the absorption of heavy metals by the components of the natural environment is directly related to the proximity and intensity of their source of pollution [20].

Pine bark, being a passive but effective accumulator of heavy metals, deserves special attention in the strategies of phytoremediation of urban areas. Its ability to retain pollutants for a long time without significant damage to the vital activity of the tree makes this species a valuable component in protective plantings along transport arteries. However, for the maximum efficiency, it is essential to consider the dynamics of metal accumulation, the spatial distribution of metals, and develop methods for safely removing and processing contaminated bark to prevent it from returning to the biogeochemical cycle.

The study expands our understanding of the mechanisms of migration and accumulation of heavy metals in urban ecosystems, especially in areas with a sharply continental climate. The results can be used to optimize urban planning and minimize the negative impact on public health. They can also help develop strategies for sustainable development in the areas with high levels of anthropogenic activity.

References

1. Dubrovina O, Zubkova T, Masina T, Vinogradov D, Gogmachadze G. Accumulation of Lead and Cadmium in Vegetative Organs of *Betula Pendula*, *Tilia Cordata* L., *Populus Pyramidalis* in Urban Parks of Yelets, Zadonsk, Lebedyan, Lipetsk Region. *AgroEcoInfo*. 2024;4(64):1–13. (In Russ.) <https://doi.org/10.51419/202144416>
2. Zubairov RR, Mustafin RF, Odintsov GE. The Content of Elements of the First Hazard Class in Soils and Wood in the Catchment Area of the Bolshaya Balykly River. In: *Prospects for the Introduction of Innovative Technologies in Agriculture: Proceedings of the III All-Russian (National) Scientific and Practical Conference with International Participation, Dedicated to the 80th Anniversary of the Faculty of Agronomy of Altai State Agrarian University, Barnaul, November 22, 2023*. Barnaul: Altai State Agrarian University; 2023. P. 203–207. (In Russ.)
3. Gyl'byakov NR, Davydova SA, Gyl'byakova KhN. Changes in the Numerical Parameters and Content of Tannins in the Bark of Small-Leaved Linden Depending on the Place of Growth. In: *Collection of Scientific Papers "Development, Research and Marketing of New Pharmaceutical Products"*. Pyatigorsk: Advertising and Information Agency on Kavminvody; 2021. P. 24–29. (In Russ.)
4. Vetchinnikova LV, Kuznetsova TYu, Titov AF. Patterns of Heavy Metal Accumulation in Leaves of Trees in Urban Areas in the North. *Transactions of the Karelian Research Centre of the Russian Academy of Sciences*. 2013;(3):68–73. (In Russ.)
5. Churakov BP, Zyryanova UP, Zagidullin RA, Paramonova TA, Mitrofanova NA, Mikheeva AV. Dynamics of Heavy Metal Accumulation in Trophic Levels of Forest Ecosystems. *Ulyanovsk Medico-Biological Journal*. 2024;(1):105–114. (In Russ.) <https://doi.org/10.34014/2227-1848-2024-1-105-114>
6. Petukhov AS, Kremleva GA, Petukhova GA, Khritokhin NA. Heavy Metal Accumulation and Migration in Soils and Plants under Contamination in Urban Environments. *Proceedings of the Karelian Scientific Center of the Russian Academy of Sciences*. 2022;(3):53–66. <https://doi.org/10.17076/eco1342>
7. Kravtsov VN. The Content of Heavy Metals in the Leaves and Conifers of Woody Plants Growing on the Territory of the Far Eastern Higher Combined Arms Command School. In: *Proceedings of the 23d Regional Scientific and Practical Conference "Youth of the 21st Century: A Step into the Future"*, Blagoveshchensk, May 24, 2022. Vol. 4, Blagoveshchensk: Far Eastern State Agrarian University; 2022. P. 253–255. (In Russ.)
8. Kopylova LV. Accumulation of Heavy Metals *Caragana Arborescens* Lam. in the Conditions of Anthropogenic Influence (Zabaikalsky Krai). *Scholarly Notes of Transbaikalian State University*. 2017;12(1):20–25. (In Russ.)
9. Saidyasheva GV, Zakharov SA. The Results of Monitoring the Content of Heavy Metals in Soil, Plants and Snow Cover near Highways Selected Can Be Removed at Various Distances from the City of Ulyanovsk. *Vestnik of Kazan State Agrarian University*. 2023;17(4):45–49. (In Russ.) <https://doi.org/10.12737/2073-0462-2023-45-49>
10. Gavrilova AA, Makarova EI, Akhtyamov RG. Accumulation of Heavy Metals in Soils and Phytomass in Urbanized Areas. *Proceedings of Petersburg Transport University*. 2023;20(3):706–714. (In Russ.) <https://doi.org/10.20295/1815-588X-2023-3-706-714>

11. Soboleva SV, Chentsova LI, Pochekutov IS. The Research of the Heavy Metal Accumulation in the Soil and Poplar Bark in the Krasnoyarsk City Territory. *Bulletin of KSAU*. 2013;9(84):122–126. (In Russ.) <https://kgau.editorum.ru/ru/storage/viewWindow/146397>(accessed: 11.04.2025).
12. Kashina EM, Malkov AV, Bogolitsyn KG. Determination of Heavy Metal Content in Wood by X-Ray Fluorescence Spectroscopy. *Bulletin of Higher Educational Institutions. Russian Forestry Journal*. 2011;(6):140–143. (In Russ.)
13. Chichigina Y, Shigabaeva G, Emelyanova E, Galunin E, Yakimov A, Isaev A, Bekker M. Heavy Metal Contents in the Tyumen City Residential Area Soils. *Journal of Advanced Materials and Technologies*. 2023;8(2):141–156. <https://doi.org/10.17277/jamt.2023.02.pp.141-156>
14. Vedernikov K, Zagrebina E, Bukharina I. Specific Nature of the Biochemical Composition of Spruce Wood from the Forest Stands Exposed to Drying out in European Russia. *Kastamonu University Journal of Forestry Faculty*. 2020;20(3):208–219. <https://doi.org/10.17475/kastorman.849461>
15. Menahem Edelstein, Meni Ben-Hur. Heavy Metals and Metalloids: Sources, Risks and Strategies to Reduce Their Accumulation in Horticultural Crops. *Scientia Horticulturae*. 2018;234:431–444. <https://doi.org/10.1016/j.scienta.2017.12.039>
16. Kočevlar Glavač N, Mračević SD, Ražić SS, Kreft S, Veber M Accumulation of Heavy Metals from Soil in Medicinal Plants. *Archives of Industrial Hygiene and Toxicology*. 2017;68(3):236–244. <https://doi.org/10.1515/aiht-2017-68-2990>
17. Konstantinova E, Minkina T, Konstantinov A, Sushkova S, Antonenko E, Kurasova A, et al. Pollution Status and Human Health Risk Assessment of Potentially Toxic Elements and Polycyclic Aromatic Hydrocarbons in Urban Street Dust of Tyumen City, Russia. *Environmental Geochemistry and Health*. 2020;44:409–432. <https://doi.org/10.1007/s10653-020-00692-2>
18. Stepanova NV, Fomina SF, Valeeva ER, Ziyatdinova AI. Heavy Metals as Criteria of Health and Ecological Well-Being of the Urban Environment. *Journal of Trace Elements in Medicine and Biology*; 2018;50:646–651. <https://doi.org/10.1016/j.jtemb.2018.05.015>
19. Dyomina EB, Savchenkova VA. The Content of Heavy Metals in Soils and Leaves of Silver Birch Plantations (Moscow). *Russian Forestry Journal*; 2024;4(400):37–48. <https://doi.org/10.37482/0536-1036-2024-4-37-48>
20. Tsegay MK, Sukhenko LT. Pilot Survey of Three Soil Heavy Metals at Abandoned Industrial Farmland, and Determination of Its Potential Health Risk. *International Journal of Humanities and Natural Sciences*; 2023;10–1(85):23–30. <https://doi.org/10.24412/2500-1000-2023-10-1-23-30>

About the Authors:

Tatyana V. Turusheva, Cand. Sci. (Eng.), Associate Professor of the Department of Technosphere Safety, Transbaikal State University (30, Aleksandro-Zavodskaya Str., Chita, 672039, Russian Federation), [SPIN-code](#), [ORCID](#), turusheva_tanya@mail.ru

Vyacheslav E. Esipov, Master's Degree Student of the Department of Technosphere Safety, Transbaikal State University (30, Aleksandro-Zavodskaya Str., Chita, 672039, Russian Federation), slavel.chapp@gmail.com

Claimed Contributorship:

TV Turusheva: supervision, conceptualization.

VE Esipov: investigation.

Conflict of Interest Statement: the authors declare no conflict of interest.

All authors have read and approved the final manuscript.

Об авторах:

Татьяна Викторовна Турушева, кандидат технических наук, доцент, кафедра «Техносферная безопасность» Забайкальского государственного университета (672039, Российская Федерация, г. Чита, ул. Александрo-Заводская, д. 30), [SPIN-код](#), [ORCID](#), turusheva_tanya@mail.ru

Вячеслав Евгеньевич Есипов, магистрант, кафедра «Техносферная безопасность» Забайкальского государственного университета (672039, Российская Федерация, г. Чита, ул. Александрo-Заводская, д. 30), slavel.chapp@gmail.com

Заявленный вклад авторов:

Т.В. Турушева: научное руководство, разработка концепции.

В.Е. Есипов: проведение исследования.

Конфликт интересов: авторы заявляют об отсутствии конфликта интересов.

Все авторы прочитали и одобрили окончательный вариант рукописи.

Received / Поступила в редакцию 28.05.2025

Reviewed / Поступила после рецензирования 14.06.2025

Accepted / Принята к публикации 02.07.2025

TECHNOSPHERE SAFETY

ТЕХНОСФЕРНАЯ БЕЗОПАСНОСТЬ



UDC 621.433: 547.211

Perspective Article

<https://doi.org/10.23947/2541-9129-2025-9-3-208-220>

The Use of Coal Mine Methane as a Natural Gas Motor Fuel for Commercial Motor Transport in Donbass Cities

Nikita V. Savenkov^{ID}, Ekaterina L. Golovatenko^{ID}✉

Donbas National Academy of Civil Engineering and Architecture, Makeyevka, Donetsk People's Republic, Russian Federation

✉ e.l.golovatenko@donnasa.ru

EDN: HTLYBN

Abstract

Introduction. Coal mine methane, a greenhouse gas released during underground coal mining, is considered to be a cause of global climate change. However it is also a valuable energy resource. Currently, the global utilization rate of coal mine methane is low, and the amount of methane released into the atmosphere is increasing every year. To limit greenhouse gas emissions, several legislative initiatives have been implemented, including the Kyoto Protocol, the Paris Agreement, and Federal Law No. 296-FZ “On Limiting Greenhouse Gas Emissions”¹. In the conditions of Donbass, the task of mine methane utilization is relevant due to the dense location of emission sources and the need to improve the safety of mining operations, as well as to ensure the implementation of the principle of integrated field development. In addition, the ongoing hostilities have led to an increase in fuel prices in the region and an increase in road transport due to the limited availability of rail, sea, and air transportation. The aim of the research is to conduct a calculated assessment of the energy efficiency of using mine methane from Donbass coal deposits as motor fuel for commercial vehicles with internal combustion engines.

Materials and Methods. As an example, the studies were conducted on BAZ-2215 vehicles on the GAZelle Business chassis, GAZelle Next Citiline, and PAZ 3203, which were commonly used on urban routes in Makeyevka (DPR). These vehicles were equipped with UMZ, ZMZ, and Cummins spark and diesel engines. The full composition of methane-air mixture samples from several mines (Chaykino Mine, Makeyevka, Komsomolets Donbassa Mine, Kirovskoye), taken from degassing systems, was determined in the laboratories of Makeyevka Research Institute for Mining Safety and Donetskavtogaz using a Kristallyuks 4000M gas chromatograph. The energy efficiency of engines operating on various types of fuel, including mine methane, as well as the performance characteristics of selected buses (fuel consumption, distance-to-empty, and carbon dioxide emissions) under urban driving cycles according to GOST R 54810–2011², were determined through a series of calculations using well-established methods.

Results. An estimation of the energy efficiency of mine methane as a gas engine fuel has been performed. In the range of concentrations of the studied samples of gas-air mixtures, the calculated maximum loss of effective power for ZMZ and UMZ spark engines was up to 15%. For gas-diesel engines, such as Cummins, power could be increased by up to 29%. These findings did not prevent selected buses from operating under driving cycles in accordance with GOST R 54810–2011³. Under these conditions, fuel consumption and range per refueling depended significantly on the component composition of mine methane. For the samples studied, it was 1.8–3.5 times worse than for natural gas used for refueling. Emissions of carbon dioxide were reduced by 62–73% compared to gasoline.

¹ On Limiting Greenhouse Gas Emissions. Federal Law No. 296–FZ dated 02 July, 2021. Electronic Fund of Legal and Regulatory and Technical Documents. (In Russ.) URL: <https://docs.cntd.ru/document/607142402> (accessed: 21.05.2025).

² GOST R 54810 2011. Motor Vehicles. Fuel Economy. Test Methods. Electronic Fund of Legal and Regulatory and Technical Documents. (In Russ.) URL: <https://docs.cntd.ru/document/1200093157> (accessed: 21.05.2025).

³ Ibid

Discussion. Due to the specific features of degassing processes and the mining and geological conditions of different mines, the alternative fuel discussed in this article has a variable component composition. In this regard, the transfer of PAZ and GAZ bus rolling stock to a byproduct of coal mining — mine methane — is associated with several challenges. These include the need for more powerful fuel systems (three times or more than the power supply systems of internal combustion engines of comparable power, operating on compressed gas) and deterioration in fuel-economic and traction-speed properties of vehicles, as well as reduced range. A quantitative assessment of these changes has been obtained through research. The positive impact of the proposed measures stems from the reduction in negative environmental impact by using mine methane as a fuel for vehicles, which reduces the carbon footprint of road transport and decreases the consumption of liquid hydrocarbon fuel.

Conclusion. As a result of the study, it has been found that the methane from the Donbass coal mines can be used as motor fuel for commercial vehicles such as city buses. The study has determined the corresponding energy efficiency parameters (the effective power generated by internal combustion engines, the specific fuel consumption, the range of vehicles under driving cycles, etc.), as well as the degree of their reduction compared to traditional fuels. It has been established that this does not affect the performance of transportation work (in compliance with GOST R 54810–2011⁴) and is beneficial from the perspective of saving non-renewable resources and improving environmental safety in the region.

Keywords: methane utilization, gas engine fuels, internal combustion engines, motor vehicles

Acknowledgements. The authors would like to express their gratitude to the staff of the laboratories (SE “Donetskavtogaz”, SE “Makeevka Research Institute for Mining Safety”, and SE “Donbasstransgaz”), on the basis of which the component composition of methane-air mixtures was studied, coal mining enterprises (SE “Makeevugol” “Chaykino Mine”, SUE DNR “Komsomolets Donbass Mine”), for the opportunity to perform sampling, as well as to the reviewers for their critical assessment of the submitted materials and their suggestions for improvement the quality of this work.

Financing. This research is an integral part of the scientific research topic “Improving the operational efficiency of motor vehicles by improving their technological, structural and operational parameters” (State Task No. 075-01620-23-00 dated May 12, 2023).

For citation. Savenkov NV, Golovatenko EL. The Use of Coal Mine Methane as a Natural Gas Motor Fuel for Commercial Motor Transport in Donbass Cities. *Safety of Technogenic and Natural Systems*. 2025;9(3):208–220. <https://doi.org/10.23947/2541-9129-2025-9-3-208-220>

Статья-перспектива

Применение шахтного метана в качестве газомоторного топлива для коммерческого автомобильного транспорта городов Донбасса

Н.В. Савенков , Е.Л. Головатенко  

Донбасская национальная академия строительства и архитектуры, г. Макеевка, Донецкая Народная Республика

 e.l.golovatenko@donnasa.ru

Аннотация

Введение. Шахтный метан, выделяющийся в процессе подземной добычи угля, с одной стороны рассматривается в качестве причины глобального изменения климата (парниковый газ), а с другой стороны является ценным энергетическим ресурсом. В настоящее время доля его утилизации в мировом масштабе невысока, количество метана, поступающее в атмосферу, ежегодно увеличивается. С целью ограничения выбросов парниковых газов принят ряд законодательных инициатив: Киотский протокол, Парижское соглашение, Федеральный закон № 296–ФЗ «Об ограничении выбросов парниковых газов».

В условиях Донбасса задача утилизации шахтного метана является актуальной в связи с плотным размещением источников выбросов и необходимостью повышения безопасности горных работ, а также обеспечивает реализацию принципа комплексного освоения месторождения. Кроме того, боевые действия обусловили повышение стоимости топлива в регионе и увеличение грузооборота автомобильным транспортом ввиду практически не функционирующих ж/д, морского и авиасообщения. Цель исследования — выполнить расчетную оценку энергетической эффективности применения шахтного метана угольных месторождений Донбасса в качестве моторного топлива автомобильных двигателей внутреннего сгорания коммерческого транспорта.

⁴ GOST R 54810 2011. *Motor Vehicles. Fuel Economy. Test Methods*. Electronic Fund of Legal and Regulatory and Technical Documents. (In Russ.) URL: <https://docs.cntd.ru/document/1200093157> (accessed: 21.05.2025).

Материалы и методы. В качестве примера для выполнения исследований выбраны распространённые на городских маршрутах г. Макеевки (ДНР) автотранспортные средства БАЗ-2215 на шасси «Газель Бизнес», ГАЗель Next «Citiline» и ПАЗ 3203, оснащённые искровыми и дизельными двигателями марок УМЗ, ЗМЗ и Cummins. Полный состав проб метановоздушной смеси ряда шахт («Шахта им. Чайкино», г. Макеевка, «Шахта Комсомолец Донбасса», г. Кировское), отобранных из дегазационных систем, определён в лабораториях ГУ «МАКНИИ» и ГП «Донецкавтогаз» с помощью газового хроматографа «Кристаллюкс 4000М». Энергетические показатели автомобильных двигателей при работе на различных видах топлива, в том числе на шахтном метане, а также эксплуатационные свойства выбранных автобусов (путевой расход топлива, запасы хода и выбросы диоксида углерода) в условиях городских ездовых циклов по ГОСТ Р 54810–2011 определены в результате выполненной серии расчётов по известным методикам.

Результаты исследований. Выполнена расчётная оценка энергетической эффективности применения шахтного метана в качестве газомоторного топлива. В диапазоне концентраций исследованных образцов газоздушных смесей максимальная расчётная потеря развиваемой эффективной мощности искровых двигателей ЗМЗ и УМЗ составляет до 15 %, а для газодизелей на примере Cummins мощность может быть увеличена до 29 %. Это не препятствует движению выбранных автобусов в условиях ездовых циклов по ГОСТ Р 54810–2011. В этих условиях путевой расход топлива и запасы хода на одной заправке существенно зависят от компонентного состава шахтного метана и для исследуемых образцов ухудшаются в 1,8–3,5 раза по отношению к показателям на природном газе, используемом для заправки автомобилей, а эмиссия диоксида углерода сокращается на 62–73 % от эмиссии на бензине.

Обсуждение. В связи с особенностями дегазационных процессов и горно-геологических условий разных шахт рассматриваемое в статье альтернативное топливо обладает непостоянным компонентным составом. В связи с этим перевод подвижного состава марок ПАЗ и ГАЗ на побочный продукт угледобычи — шахтный метан — сопряжён со следующими сопутствующими сложностями: необходимость применения топливных систем повышенной производительности (в 3 и более раз по отношению к системам питания ДВС сопоставимой мощности, работающим на сжатом газе), ухудшение топливно-экономических и тягово-скоростных свойств автотранспортных средств, а также их запаса хода. В исследовании получена количественная оценка данных изменений. Положительный эффект предлагаемых мероприятий обусловлен снижением негативного воздействия на окружающую среду путём утилизации шахтного метана его применением в качестве газомоторного топлива, уменьшением углеродного следа от автомобильного транспорта, сокращением потребления жидкого углеводородного топлива.

Заключение. В результате исследования установлено, что шахтный метан угольных месторождений Донбасса может быть применён в качестве моторного топлива автомобильных двигателей внутреннего сгорания коммерческого транспорта на примере городских автобусов. Определены соответствующие параметры энергетической эффективности (развиваемая ДВС эффективная мощность, удельные расходы топлива, запасы хода автомобилей в условиях ездовых циклов и т.д.), а также степень их снижения относительно применения традиционных видов топлива. Установлено, что это не препятствует выполнению транспортной работы (в условиях ГОСТ Р 54810–2011) и является оправданным с позиции экономии невозобновляемых ресурсов и повышения экологической безопасности региона.

Ключевые слова: утилизация метана, газомоторное топливо, двигатели внутреннего сгорания, автотранспортные средства

Благодарности. Авторы выражают благодарность сотрудникам лабораторий (ГП «Донецкавтогаз», ГУ «МакНИИ» и ГП «Донбасстрансгаз»), на базе которых исследован компонентный состав метановоздушных смесей, угледобывающих предприятий (ГП «Макеевуголь» «Шахта им. Чайкино», ГУП ДНР «Шахта Комсомолец Донбасса»), предоставившим возможность выполнить отбор проб, а также рецензентам, чья критическая оценка представленных материалов и высказанные предложения по их усовершенствованию способствовали повышению качества настоящей работы.

Финансирование. Исследование является составной частью госбюджетной научной темы «Повышение эксплуатационной эффективности автотранспортных средств совершенствованием их технологических, конструкционных и режимных параметров» (Государственное задание № 075-01620-23-00 от 12.05.2023 г.).

Для цитирования: Савенков Н.В., Головатенко Е.Л. Применение шахтного метана в качестве газомоторного топлива для коммерческого автомобильного транспорта городов Донбасса. *Безопасность техногенных и природных систем.* 2025;9(3):208–220. <https://doi.org/10.23947/2541-9129-2025-9-3-208-220>

Introduction. Coal mine methane is a valuable fuel and energy source that is produced during coal mining [1] and during coal seam degassing [2] processes. Its efficient utilization can reduce greenhouse gas emissions [3], increase the economic efficiency of coal mining, and provide additional energy sources for road transport [4]. In conditions of limited global oil reserves and growing energy costs, the use of coal mine methane as a motor fuel is a promising direction [5], which makes it possible to reduce our dependence on fossil fuels and the environmental impact [6]. Within the Russian Federation, the share of methane in greenhouse gas emissions ranks second after carbon dioxide and amounts to 14%, almost half of which is the contribution of coal mines (400 million tons of CO₂ equivalent per year) [7]. An increase in coal mining leads to an increase in the formation of coal mine methane [8], which requires an intensification of degassing⁵.

In a number of countries, the share of degassed methane used in the energy sector reaches 50–80% [7]. However, in Russia, a significant amount of it (more than 1 billion m³ per year [7]) is released into the atmosphere [9].

In world practice, coal mine methane is used in several ways, including combustion, cogeneration [10], chemical processing and injection into coal seams [11]. The choice of the most suitable technology depends on the component composition of the gas [12] and the characteristics of the deposit (Fig. 1) [13].

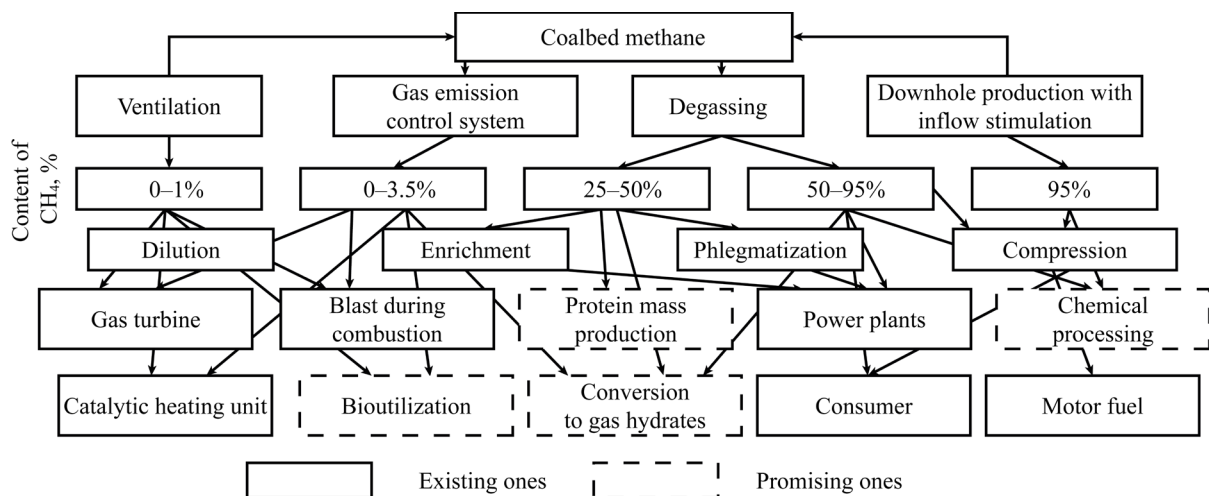


Fig. 1. The main uses of coal mine methane [13]

However, existing technologies only cover limited concentrations of methane [14] and, when used as a motor fuel, further research is needed on the effect of gas mixture composition on engine efficiency and car performance [5]. These factors create a need for a systematic analysis of the potential of coal mine methane as an alternative fuel and the development of methods for assessing its efficiency for commercial vehicles.

Existing studies mainly focus on stationary gas piston units [15] and a separate analysis relates to motor-car engines [16]. However, there is a key gap in the lack of data on the impact of variations in the composition of mine methane mixture on the energy performance of internal combustion engines in real-world driving cycles. Additionally, there is no assessment of the economic and environmental effectiveness of these solutions on a large regional scale. Therefore, a comprehensive theoretical justification for the use of coal mine methane in transportation is needed, as well as a method for calculating energy efficiency that considers the composition of gas, engine modes, and vehicle cycles.

The aim of the work is to conduct a calculated assessment of the energy efficiency of using coal mine methane from Donbass coal deposits as a motor fuel for automotive internal combustion engines of commercial vehicles. The tasks include: reviewing the features of coal mine methane degassing at domestic and foreign mines; analyzing its composition at coal companies in the Donbass region; modeling the operation of automotive internal combustion engines in various modes when using coal mine gas as fuel; quantifying energy efficiency (including performance and developed effective indicators) for mine gas-fueled motor transport power units compared to traditional fuels; identifying of conditions and limitations for safe and environmentally friendly operation of mine gas-fueled vehicles; and formulating recommendations on degassing and gas treatment technologies for widespread use in commercial transportation.

⁵ *Global Methane Tracker*. URL: https://iea.blob.core.windows.net/assets/b5f6bb13-76ce-48ea-8fdb-3d4f8b58c838/GlobalMethaneTracker_documentation.pdf (accessed 27.05.2025).

Materials and Methods. The work used laboratory methods for studying the composition of coal mine methane from the State Enterprise “Makeyevugol” “Chaikino Mine” (Makeyevka) and the State Unitary Enterprise of the DPR “Komsomolets Donbass Mine” (Kirovskoye). An integrated technological process was used to prepare laboratory gases. The degassing systems of these mines were equipped with two types of vacuum pumping stations — VN-50 water-ring vacuum pumps (manufactured in China), in which water was used as a working fluid; gas sampling was conducted in front of vacuum pumping stations; silica gel was used to remove moisture; rotary pumps with means of dedusting and removing moisture, gas sampling was conducted at the outlet into cylinders with a capacity of 2 liters. The processes of dilution of laboratory gas to the required concentration, as well as additional enrichment with natural gas, were not used. The full composition of the selected gas was determined in two laboratories: the gas analytical laboratory of the State Institution MAKNI (Makeevka Research Institute for Mining Safety) and the chemical laboratory of the State Enterprise Donbasstransgaz. A Crystallux 4000M gas chromatograph was used to analyze the composition of gases.

As an example, BAZ-2215 on the Gazelle Business chassis, Gazelle Next Citiline and PAZ 3203 were selected for research. These vehicles were common on urban routes in Makeyevka (DPR). According to the Municipal Unitary Enterprise “Dispatch Service” of the Makeyevka City Administration, 231 units of rolling stock of these brands were involved on 52 urban and 28 suburban routes of the city. Among them 122 units were of medium capacity (M3) and 109 units were of small capacity (M2). The prevailing number of buses was equipped with ZMZ, UMZ and Cummins engines. The main technical characteristics of the selected vehicles and their engines are shown in Table 1. The indicators of the engines selected as an example when running on coal mine methane of various compositions, as well as on traditional liquid fuels (developed effective power, effective specific and hourly fuel consumption, etc.), were determined based on the results of a series of thermal calculations performed using methodology [17].

The operational properties of motor vehicles (fuel consumption, range and carbon dioxide emissions), were measured under driving cycle (DC) conditions according to GOST R 54810–2011⁶. These properties were obtained by numerical simulation of the movement process in accordance with methodology [18] when their engines were running on the fuels considered in the study.

Table 1

Characteristics of the vehicles in question and their internal combustion engines

Vehicle model	GAZelle Next Citiline	BAZ-2215	PAZ 3203
Category according to TR CU 018/2011	M ₂	M ₂	M ₃
Class according to GOST R 54810–2011 ⁷	II	II	II
Passenger capacity, person	17	15	48
Gross weight, kg	4950	3980	8500
Power-weight ratio, W/kg	17.84	19.72	11.3
Engine type	CUMMINS ISF2.8S4R129	EVOTECH A274	ZMZ-5234
Type	Diesel, turbocharged and charge air cooler	Petrol, 4-cycle, injected	Petrol, 4-cycle, carburetor
Number of cylinders and their arrangement	4, in-line	4, in-line	8, V-engine
Cylinder diameter and piston stroke, mm	94×100	96.5×92	92x88
Cylinder capacity, l	2.8	2.69	4.67
Compression ratio	16.9	10	7.6
Rated power, net kW (hp) at crankshaft speed, rpm	88.3 (120) 3,600	78.5 (106.8) 4000	96 (130) 3200–3400
Maximum torque, net, Nm (kgfm) at crankshaft speed, rpm	295 (30.0) 1,600–2,700	220.5 (22.5) 2,350±150	314(32) 2,250–2,500

⁶ GOST R 54810–2011. *Motor Vehicles. Fuel Economy. Test Methods.* Electronic Fund of Legal and Regulatory and Technical Documents. (In Russ.) URL: <https://docs.cntd.ru/document/1200093157> (accessed: 21.05.2025).

⁷ Ibid.

To do this, in the software environment of the Mathcad computer algebra system, the car power balance equation was solved at each DC point [18]. Figure 2 shows the selected DCs representing the dependence of speed of movement V on trip mileage S

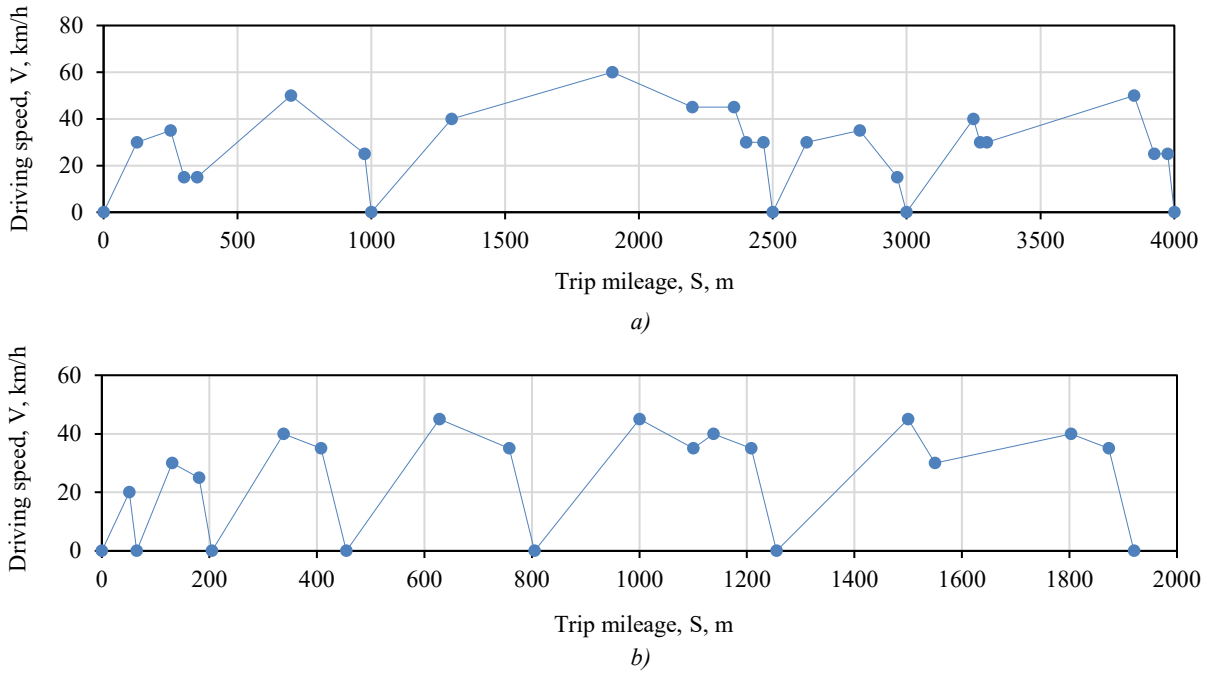


Fig. 2. Driving cycles selected for the research: *a* — urban cycle on the road for Class II M2 vehicles; *b* — urban cycle on the road for Class II M3 vehicles

These cycle variants were characterized by minimal accelerations, which was due to the low energy consumption of cars (Table 1) and the expected loss of maximum power developed by their engines when running on coal mine methane. The travel fuel consumption was determined as follows:

$$m = \frac{1}{S_{\text{EII}}} \left(\frac{1}{3,600} \int_0^{t_{\text{II}}} G(t) dt + t_0 \cdot G_{\text{XX}} \right), \text{ m}^3/\text{km} \text{ (kg/km)}, \quad (1)$$

where S_{EII} — DC distance (4 km for M₂ category and 1.92 km for M₃ category; t_{II} — DC duration (497 s for M₂ category and 288 s for M₃ category, excluding stops; $G(t)$ — function of hourly fuel consumption of travel time in a cycle, m³/h (kg/h); t_0 — total duration of stops, s; G_{XX} — часовой расход топлива двигателя в режиме hourly fuel consumption of the engine in the minimum stable idle rotation mode, m³/s (kg/s), $G_{\text{XX}} = 0.0007$ m³/s for gas ICEs and $G_{\text{XX}} = 0.005$ kg/s liquid-fueled ICEs [17]).

The bus range in DC conditions was calculated using formula (2) for gaseous fuels and formula (3) for liquid fuels:

$$S_A = \frac{V_3}{m} = \frac{n_B \cdot V_B}{m} = \frac{m_3}{m \cdot \rho_{1\Gamma}} = \frac{m_3}{m} \cdot \frac{R_{\Gamma} \cdot T_0}{P_0}, \text{ km}, \quad (2)$$

$$S_A = \frac{V_{\text{BT}} \cdot \rho_{\Gamma}}{m}, \text{ km}, \quad (3)$$

where V_3 — gas volume under normal conditions (NC) in the car; n_B — number of cylinders in the car; V_B — maximum gas volume with which one cylinder can be filled under NC; m_3 — filling mass of gas; $\rho_{1\Gamma}$ — gas density under NC; R_{Γ} — gas constant (Table 2); T_0 and P_0 — temperature and atmospheric pressure under NC, respectively; V_{BT} — fuel tank volume; $\rho_{1\Gamma}$ — liquid fuel density under NC.

CO₂ emissions under DC conditions were determined as follows:

– for gas-fueled internal combustion engines (including for gas-diesels):

$$q = n_{\text{CO}_2} \cdot \mu_{\text{CO}_2} = n_{\Gamma} \cdot M_{\text{CO}_2} \cdot \mu_{\text{CO}_2} = 10^3 \cdot m \cdot \rho_{1\Gamma} \cdot M_{\text{CO}_2} \cdot \frac{\mu_{\text{CO}_2}}{\mu_{\Gamma}}, \text{ g/km}, \quad (4)$$

where n_{CO_2} — amount of substance (CO₂) in the exhaust gases (EG), related to one kilometer, mol/km; μ_{CO_2} — CO₂ molecular weight, g/mol; n_{Γ} — number of moles of fuel consumed per kilometer, mol/km; M_{CO_2} — amount of CO₂, generated during the combustion of gaseous fuel, mol/mol, (6); μ_{Γ} — the molecular weight of the gas, g/mol (Table 2);

– for engines running on liquid fuel:

$$q = 10^3 \cdot m \cdot M_{\text{CO}_2} \cdot \mu_{\text{CO}_2}, \text{ g/km}, \quad (5)$$

where M_{CO_2} — amount of CO₂, produced during the combustion of liquid fuel, kmol/kg, (7).

For gas diesel, M_{CO_2} was determined by the formula:

$$M_{CO_2} = \sum n(C_n H_m O_r), \tag{6}$$

$$M_{CO_2} = C / 12, \tag{7}$$

$$M_{CO_2} = \sum n(C_n H_m O_r) + g_T \cdot C / 12, \tag{8}$$

where n, m, r — respectively, the number of carbon, hydrogen, and oxygen atoms in gas molecules of the gas mixture; $C_n H_m O_r$ — volume fraction of gas in the gas mixture, Table 2; C — mass fraction of carbon in the fuel (Table 2); g_T — mass of liquid fuel per 1 kmol of gas fuel, $g_T = 0.0084$ kg/kmol.

Results. We have obtained the following results:

- the component composition of laboratory gases selected from Donbass collieries has been determined (Table 2);
- for bus models commonly used on urban routes in Makeyevka, a thermal calculation of internal combustion engines has been performed when running on coal mine methane with different component compositions (Tables 3–5);
- numerical simulation of bus traffic has been carried out under urban DC conditions in accordance with GOST R 54810–2011⁸, and efficiency indicators for the use of coal mine methane as motor fuel have been determined (Table 6).

In Tables 2–6, the following designations were used for laboratory gas samples: gas No. 1 — Chaykino mine; gas No. 2 — natural gas used for refueling cars (from a gas filling compressor station); gas No. 3 — reference gas mixture according to GOST 31371.3–2008; gas No. 4 — Komsomolets Donbassa Mine, first WPS station; gas No. 5 — Komsomolets Donbass mine, second WPS.

Table 2

Component composition of laboratory gases (fuels)

Fuel component composition	Volume fractions					Mass fractions	
	Gas No. 1	Gas No. 2	Gas No. 3	Gas No. 4	Gas No. 5	Gasoline	Diesel
CO	0	0	0	0	0	–	–
H ₂	0	0	0	0	0.0000417	–	–
CH ₄	0.485	0.959	0.805	0.2745	0.445	–	–
C ₂ H ₆	0.00359	0.02253	0.04	0	0	–	–
C ₃ H ₈	0.00113	0.00694	0.005	0	0	–	–
C ₄ H ₁₀	0.005045	0.00201	0.005	0	0	–	–
C ₅ H ₁₂	0.000058	0.00031	0	0	0	–	–
O ₂	0.0158	0.00008	0	0.1686	0.11683	–	–
CO ₂	0.00137	0.00204	0.09	0.003	0.002583	–	–
N ₂	0.4878	0.00696	0.06	0.5538	0.435417	–	–
C ₆ H ₁₄	0	0.00012	0	0	0	–	–
He	–	–	0	0.0001	0.000075	–	–
C	–	–	–	–	–	0.855	0.860
H	–	–	–	–	–	0.145	0.126
O	–	–	–	–	–	0	0.014
Results of thermal calculation according to method [17]							
Specific gas constant, $R_T, J/(kg \cdot K)$	370.5	496	411	327	359	–	
Molecular weight, $\mu_T, g/mol$	22.4	16.76	20.23	25.43	23.16		
Lower heat of fuel combustion, gas (gasoline/diesel) MJ/m ³ , (MJ/kg)	18.256	18.257	33.5	32.3	9.8	(43.9)	(41.99)
Theoretically required amount of combustion air, kmol/kg, (kg/kg)	4.835	9.842	8.690	1.829	3.717	(14.95)	(14.3)
Heat of combustion of a combustible mixture, (gasoline/diesel) kJ/m ³ , (kJ/kg)	70086	70087	75011	74722	77598	(83555)	(52911)

⁸ GOST R 54810 2011. *Motor Vehicles. Fuel Economy. Test Methods*. Electronic Fund of Legal and Regulatory and Technical Documents. (In Russ.) URL: <https://docs.cntd.ru/document/1200093157> (accessed: 21.05.2025).

To assess the changes in the performance parameters (power output and fuel consumption) of selected models of internal combustion engines when running on coal mine methane compared to traditional liquid hydrocarbon and gas fuel, we performed a series of thermal calculations in accordance with methodology [17]. The results of these calculations are presented in Tables 3–5.

Table 3

Results of thermal calculation of the UMZ-A27460 EvoTech engine

Indicator/ parameter	Units	Gas No. 1	Gas No. 2	Gas No. 3	Gas No. 4	Gas No. 5	Gasoline
Excess air coefficient	–	1	1	1	1	1	1
Residual gases temperature	K	918	945	938	956	946	954
Final compression pressure	MPa	1.787	1.787	1.787	1.787	1.787	1.787
Final combustion pressure	MPa	6.135	6.342	6.342	6.432	6.360	6.962
Final combustion temperature	°C	2197	2303	2278	2342	2303	2505
Indicated mean pressure	MPa	0.91	0.96	0.95	0.98	0.96	1.1
Indicated efficiency	–	0.36	0.35	0.35	0.35	0.35	0.34
Mechanical efficiency	–	0.811	0.821	0.818	0.824	0.820	0.834
Effective efficiency	–	0.296	0.294	0.293	0.293	0.294	0.287
Mean effective pressure	MPa	0.739	0.791	0.779	0.807	0.788	0.869
Net torque	Nm	158	169	167	172	169	186
Engine output (nominal)	kW	66.3	71	70	72.4	70.7	78.5
Hourly gas consumption, <i>G</i> , (gasoline)	m ³ /h (kg/h)	44.1	23.7	26.5	90.9	54.5	(22.2)

Table 4

Results of thermal calculation of the ZMZ-5234 engine

Indicator/ parameter	Units	Gas No. 1	Gas No. 2	Gas No. 3	Gas No. 4	Gas No. 5	Gasoline
Excess air coefficient	–	1	1	1	1	1	1
Residual gases temperature	K	896.6	923.4	915.6	932.9	923.4	932.3
Final compression pressure	MPa	1.420	1.420	1.420	1.420	1.420	1.420
Final combustion pressure	MPa	4.875	5.039	5.039	5.110	5.054	5.740
Final combustion temperature	°C	2183.6	2287.5	2263.2	2325.3	2288.3	2384.1
Indicated mean pressure	MPa	0.762	0.807	0.796	0.821	0.806	0.874
Indicated efficiency	–	0.322	0.317	0.316	0.314	0.316	0.305
Mechanical efficiency	–	0.807	0.818	0.816	0.821	0.817	0.832
Effective efficiency	–	0.261	0.259	0.258	0.258	0.258	0.253
Mean effective pressure	MPa	0.615	0.660	0.649	0.674	0.657	0.727
Net torque	Nm	229.1	245.7	241.6	250.9	244.6	270.7
Engine output (nominal)	kW	81.5	87.5	86.1	89.3	87.1	96.1
Hourly gas consumption, <i>G</i> , (gasoline)	m ³ /h (kg/h)	61.8	33.2	37.2	127.4	76.4	31.2

Table 5

Results of thermal calculation of the CUMMINS ISF2.8S4R129 engine

Indicator/ parameter	Units	Gas No. 1	Gas No. 2	Gas No. 3	Gas No. 4	Gas No. 5	Diesel
Excess air coefficient for gas (for liquid fuel)	–	1.05	1.05	1.05	1.05	1.05	(1.6)
Residual gases temperature	K	850.4	874.1	867.5	879.6	882.8	792.4
Final compression pressure	MPa	6.735	6.735	6.735	6.735	6.735	6.720
Final combustion pressure	MPa	12.123	12.123	12.123	12.123	12.123	12.096
Final combustion temperature	°C	2239.5	2323.2	2301.1	2342.5	2359.5	1956.7
Indicated mean pressure	MPa	1.453	1.531	1.516	1.545	1.587	1.292

Indicated efficiency	–	0.432	0.423	0.423	0.412	0.414	0.491
Mechanical efficiency	–	0.848	0.856	0.854	0.857	0.861	0.822
Effective efficiency	–	0.366	0.362	0.362	0.353	0.356	0.404
Mean effective pressure	MPa	1.232	1.310	1.295	1.324	1.367	1.062
Net torque	Nm	272.3	289.4	285.9	292.5	301.8	234.6
Engine output	kW	102.7	109.1	107.8	110.3	113.8	88.4
Hourly gas consumption, G , (diesel)	m ³ /h (kg/h)	55.2	29.6	33.2	114.7	72.2	(18.8)

From the data given in Tables 3–4, it follows that for the spark ignition gas engines considered in the study:

– the maximum rated power developed when using gas No. 4 as a fuel, and amounted, respectively, to 72.4 kW for the UMZ–A27460 EvoTech with an hourly fuel consumption of 90.9 m³/h and 89.3 kW for the ZMZ–5234 with a consumption of 127.4 m³/h;

– the minimum gas consumption was when using gas No. 2: 23.7 m³/h for the UMZ–A27460 EvoTech and 33.2 m³/h for the ZMZ–5234; however, the rated power of the UMZ engine would be reduced to 71 kW, which was almost 8 kW less than its rated power on gasoline (78.5 kW), and the ZMZ engine is up to 87.5 kW at 96 kW on gasoline.

According to Table 5, the maximum effective power of a CUMMINS ISF2.8S4R129 turbocharged diesel engine converted to gas-diesel was 113.8 kW at nominal power and grew on gas sample No. 5, which exceeded by 28.7% the corresponding figure for diesel fuel, while the hourly consumption was 72.2 m³/h.

The traction and speed properties of cars depended on the values of the maximum engine power output.

The calculations performed allowed us to determine, using dependencies (1)–(8), to determine the operational properties of buses under DC conditions when their engines were running on the fuels under consideration. The results are summarized in Table 6.

Table 6

The results of numerical simulations of the bus movement process in urban driving cycles in accordance with GOST R 54810–2011⁹

Vehicle and operating conditions	Performance characteristics	Fuel					
		Gas No. 1	Gas No. 2	Gas No. 3	Gas No. 4	Gas No. 5	LF ¹
BAZ–2215 on Gazelle Business chassis with UMZ–A27460 EvoTech engine; urban driving cycle for M2 category vehicles according to GOST R 54810–2011 (Fig. 2 a)	Travel fuel consumption, m , m ³ /km (kg/km)	0.232	0.128	0.142	0.43	0.27	(0.11)
	Fuel distance under DC conditions, S_A , km	172.4	312.5	281.7	93	148.1	438.3
	CO ₂ emissions with EG, q , g/km	213.2	235.8	254.7	211.9	214.6	343.3
Gazelle Next Citiline with CUMMINS ISF2,8S4R129 engine; urban driving cycle for M2 category vehicles according to GOST R 54810–2011 (Fig. 2 a)	Travel fuel consumption, m , m ³ /km (kg/km)	0.251	0.14	0.156	0.486	0.309	(0.099)
	Fuel distance under DC conditions, S_A , km	159.4	285.7	256.4	82.3	129.4	553.9
	CO ₂ emissions with EG, q , g/km	230.9	258	280	240	245.9	313.4
PAZ 3203 with ZMZ–5234 engine; urban driving cycle for M3 category vehicles according to GOST R 54810–2011 (Fig. 2 b)	Travel fuel consumption, m , m ³ /km (kg/km)	0.544	0.291	0.326	0.994	0.624	(0.256)
	Fuel distance under DC conditions, S_A , km	110.3	206.2	184.01	60.4	96.2	278.3
	CO ₂ emissions with EG, q , g/km	499.9	536	584.7	489.9	496	802.5
¹ Liquid fuel (gasoline for UMZ–A27460 EvoTech, ZMZ–5234 internal combustion engines and diesel fuel for CUMMINS ISF2,8S4R129 internal combustion engines)							

⁹ GOST R 54810 2011. *Motor Vehicles. Fuel Economy. Test Methods*. Electronic Fund of Legal and Regulatory and Technical Documents. (In Russ.) URL: <https://docs.cntd.ru/document/1200093157> (accessed: 21.05.2025).

The minimum travel fuel consumption m (1) under different DC conditions was achieved on gas sample No. 2, and the maximum on sample No. 4. For BAZ–2215, the corresponding variation range was 3.36 at the lowest value of 0.128 m³/km, for the GAZELLE Next “Citiline” it was 3.47 at 0.14 m³/km, and for the PAZ 3203 — 3.42 at 0.291 m³/km.

Fuel distance SA (2) was inversely proportional to travel fuel consumption m and was equal to the fuel distance on gasoline: 21–71% for BAZ–2215, 15–91% for Gazelle Next Citiline and 22–74% for PAZ 3203. When calculating the fuel distance of gas-fueled vehicles of the M₂ category, the number of cylinders of the KPG-1 class with a volume of $V_B=0.05$ m³ and a maximum allowable internal pressure of 200 bar was assumed to be $n_B=4$, and for the M3 category $n_B=6$. The fuel tank capacity for the M₂ category was $V_{BT} = 0.064$ m³, and for M₃ $V_{BT} = V_B = 0.095$ m³.

Carbon dioxide emissions from gas-fueled buses significantly decreased in relation to liquid fuels: from 211.9 g/km for sample No. 4 to 254.7 g/km for BAZ-2215, which was 62% and 74% of the specific CO₂ emissions from gasoline; from 230.9 g/km for sample No. 1 to 280 g/km for Gazelle Next Citiline, which was 74% and 89% of the specific emissions when driving on diesel fuel, and from 496 g/km for sample No. 5 to 584.7 g/km for PAZ 3203, which was 62%–73% of gasoline emissions.

Discussion. The data obtained from laboratory studies on selected samples of mine methane (see Table 2) confirmed the variability in its component composition. Specifically, the volume fraction of CH₄ ranged from 0.275 at the Komsomolets Donbassa Mine to 0.485 at the Chaykino Mine, corresponding to 27% and 50% of natural gas used for car fuel, respectively, as well as 34% and 60% of the reference gas mixture according to GOST 31371.3–2008¹⁰. The impurity content of methane was up to 0.0098 in the sample from the Chaykino Mine. A significant portion of the gas sampled from the Komsomolets Donbassa Mine was air — 55% in volume for WPS No. 2 and 77% for WPS No. 1 — making these sources less preferable for the selection of gas engine fuel.

As a result of the analysis of the data obtained during the calculations and presented in Tables 3–5, we found that the maximum estimated power loss for internal combustion engines during their operation on the considered fuel samples for UMZ–A274–60 EvoTech and ZMZ–5234 spark engines was 15%. At the same time, for the CUMMINS ISF2.8S4R129 diesel engine converted to gas diesel, this indicator could be increased significantly due to a decrease in the excess air coefficient (Table 5) and the presence of pressure charging. However, without further studies on the detonation stability of this engine and the strength of its crank mechanism, gas supply should be limited.

It was established that the considered gas-fueled vehicles, when operated on all selected samples of coal mine methane, had sufficient traction and speed characteristics to be able to operate under the specified DC conditions according to GOST R 54810-2011¹¹. Additionally, the use of mine methane as fuel not only reduces the release of these harmful gases into the atmosphere, thereby minimizing their contribution to the greenhouse effect, but it also reduces CO₂ emissions from road transportation, thereby reducing the carbon footprint of vehicles.

A common challenge when using coal mine methane as a fuel is the variability in its composition and the presence of additional impurities in the form of air and inert gases, which can make up a significant volume fraction. Such motor fuel without prior enrichment with natural gas leads to the need to equip the internal combustion engine with power systems that will have increased capacity (almost three times) and feedback on the excess air coefficient in order to maintain the stoichiometric ratio of the fuel-air mixture. It is expected that the cost of such equipment will exceed the cost of a traditional automotive CNG storage and supply system by 50%. The power reserve values shown in Table 6 can be increased in proportion to the number of additional cylinders installed on the vehicle. However, with a mass of ≈ 65 kg in the refueled state (for example, CNG–1), the load capacity (and passenger capacity) of the car is also reduced. Accordingly, the results obtained in the work (Tables 3–6) made it possible to evaluate the fundamental possibility and energy efficiency of using coal mine methane as a gas engine fuel for commercial motor transport in the cities of Donbass. The economic feasibility of this is determined by a set of factors: the cost of degassing, the total cost of retrofitting cars, as well as the strategies adopted by enterprises for the implementation of the transport process.

¹⁰ GOST 31371.3–2008. *Natural Gas. Determination of Composition with Defined Uncertainty by Gas Chromatography Method*. Electronic Fund of Legal and Regulatory and Technical Documents. (In Russ.) URL: <https://docs.cntd.ru/document/1200068109> (accessed: 21.05.2025).

¹¹ GOST R 54810–2011. *Motor Vehicles. Fuel Economy. Test Methods*. Electronic Fund of Legal and Regulatory and Technical Documents. (In Russ.) URL: <https://docs.cntd.ru/document/1200093157> (accessed: 21.05.2025).

Conclusion. Thus, as a result of a theoretical analysis performed on the basis of laboratory research data, it was found that coal mine methane from Donbass coal deposits could be used as a gas engine fuel to power internal combustion engines of UMZ–A274–60 EvoTech, ZMZ–5234, CUMMINS ISF2.8S4R129 models used on commercial vehicles of BAZ–2215, PAZ 3203 and Gazelle Next Citiline models. The decrease in maximum effective power that occurred did not interfere with the movement of cars under urban DC conditions according to GOST R 54810-2011¹². However, it required equipping with an upgraded fuel-air mixture preparation system.

This work is a part of the scientific research conducted by the authors. In the future, we plan to explore the following areas:

1. Clarifying the effective performance of motor internal combustion engines when running on coal mine methane. For this purpose, motor tests are planned in the laboratory of the specialized scientific and technical center “Mechanization of Transport, Construction and Communal Works” of the Donbas National Academy of Civil Engineering and Architecture on the modernized stand KI–5543 of the GOSNITI. The tests will be carried out in both steady-state and non-steady-state modes using the device developed by the authors for sampling exhaust gases (RF patent RU 227257 U1)

2. Development of mathematical models of the speed characteristics of internal combustion engines and their environmental indicators for the subsequent assessment of the operational properties of vehicles.

3. Conducting a comprehensive assessment of the economic efficiency of converting commercial motor transport in Donbass to gas motor fuel.

4. Determination of the amount of prevented environmental damage.

References

1. Qingdong Qu, Hua Guo, Rao Balusu, Methane Emissions and Dynamics from Adjacent Coal Seams in a High Permeability Multi-Seam Mining Environment. *International Journal of Coal Geology*. 2022;253:103969. <https://doi.org/10.1016/j.coal.2022.103969>

2. Songling Jin, Wei Gao, Zichao Huang, Mingshu Bi, Haipeng Jiang, Rongjun Si, et al. Suppression Characteristics of Methane/Coal Dust Explosions by Active Explosion Suppression System in the Large Mining Tunnel. *Fire Safety Journal*. 2024;150(A):104251. <https://doi.org/10.1016/j.firesaf.2024.104251>

3. Pengfei Ji, Haifei Lin, Shugang Li, Xiangguo Kong, Xu Wang, Jingfei Zhang, et al. Technical System and Prospects for Precise Methane Extraction in the Entire Life Cycle of Coal Mining under the Goal of “Carbon Peak and Carbon Neutrality”. *Geoenergy Science and Engineering*. 2024;238:212855. <https://doi.org/10.1016/j.geoen.2024.212855>

4. Kuznetsov AN, Kolyada DA. The Use of Gas Fuel for Cars. In: *Proceedings of the International Scientific and Practical Conference of Young Scientists and Specialists Dedicated to the 110th Anniversary of Voronezh State Agrarian University Named after Emperor Peter I “Innovative Technologies and Technical Means for Agriculture”, Voronezh, November 10–11, 2022*. Voronezh: Voronezh State Agrarian University named after Emperor Peter the Great; 2022. P. 265–269. (In Russ.)

5. Ander Ruiz Zardoya, Inaki Lorono Lucena, Inigo Oregui Bengoetxea, Jose A Orosa, Research on the New Combustion Chamber Design to Operate with Low Methane Number Fuels in an Internal Combustion Engine with Pre-Chamber. *Energy*. 2023;275:127458. <https://doi.org/10.1016/j.energy.2023.127458>

6. Slavina YuA, Vozov DA. Application of Natural Gas as Fuel in Road Transport. In: *Proceedings of the XIV International Scientific and Technical Conference “Topical Issues of Organization of Road Transportation, Traffic Safety and Operation of Vehicles” Saratov, April 18, 2019*. Saratov: Saratov State Technical University named after Yuri Gagarin; 2019. P. 359–363. (In Russ.)

7. Pazyuchenko MA. Economic and Environmental Efficiency of Methane Extraction from Coal Seams. *Ekonomicheskie Sistemy*. 2023;16(2):173–181. (In Russ.) <https://doi.org/10.29030/2309-2076-2023-16-2-173-181>

8. Vigil DA, Johnson JrRL, Tauchnitz J. Improved Estimation Methods for Surface Coal Mine Methane Emissions for Reporting, Beneficial Use, and Emission Reduction Purposes and Relative to Australia's Safeguard Mechanisms. *Journal of Environmental Management*. 2025;376:124366. <https://doi.org/10.1016/j.jenvman.2025.124366>

¹² GOST R 54810 2011. *Motor Vehicles. Fuel Economy. Test Methods*. Electronic Fund of Legal and Regulatory and Technical Documents. (In Russ.) URL: <https://docs.cntd.ru/document/1200093157> (accessed: 21.05.2025).

9. Brodny J, Felka D, Tutak M. The Use of the Neuro–Fuzzy Model to Predict the Methane Hazard during the Underground Coal Mining Production Process. *Journal of Cleaner Production*. 2022;368:133258. <https://doi.org/10.1016/j.jclepro.2022.133258>
10. Shilov AA, Khrantsova AM. Utilization and Use of Mine Methane for Heat and Electricity Generation. *Mining Informational and Analytical Bulletin*. 2008;(S4):85–89. (In Russ.)
11. Nagaytsev I, Petrova T. Comparative Analysis of Promising Abatement Technologies Greenhouse Gas Emissions from Coal Mines. *Energy Policy*. 2024;(1(192)):38–57. (In Russ.) URL: <https://energypolicy.ru/wp-content/uploads/2024/02/ep-%E2%84%961192-1.pdf> (accessed: 27.06.2025).
12. Tailakov OV, Zastrelov DN, Utkaev EA, Sokolov SV, Kormin AN, Smyslov AI. Prospects of the Coal Mine Methane Utilization. *Bulletin of the Kuzbass State Technical University*. 2015;(6(112)):62–67. (In Russ.) URL: <https://vestnik.kuzstu.ru/index.php?page=article&id=2977> (accessed: 27.06.2025).
13. Konstantinova MS. Ways of Extraction and Industrial Use of Coal Mine Methane for Energy Purposes. *Vestnik Sovremennykh Issledovaniy*. 2019;(1.8(28)):95–99. (In Russ.)
14. Durnin MK. The Choice of Effective Technologies for the Utilization of Coal Mine Methane to Improve the Industrial Safety of Coal Mines. *Mining Informational and Analytical Bulletin*. 2007;(S13):415–429. (In Russ.)
15. Beloshitskii MV, Troitskii AA. The Use of Coal Mine Methane as an Energy Carrier. *Turbines & Diesels*. 2006;(6):2–9. (In Russ.) URL: <http://www.turbine-diesel.ru/rus/node/2108> (accessed: 27.06.2025).
16. Stokov AP, Levterov AM, Nechvolod PYu. Recycling of Mine Methane in Ecological Cogeneration Plant with Piston ICE. *Bulletin of Kharkov National Automobile and Highway University*. 2010;(48):89–93. (In Russ.)
17. Kuleshov AA. *Development of Calculation Methods and Optimization of Internal Combustion Engine Work Processes*. Dr. Sci. (Eng.) diss. Moscow; 2012. 235 p. (In Russ.)
18. Gorozhankin SA, Bumaga AD, Savenkov NV. Improving Car Fuel Efficiency by Optimising Transmission Parameters. *International Journal of Automotive and Mechanical Engineering*. 2019;16(3):7019–7033. <https://doi.org/10.15282/ijame.16.3.2019.14.0526>

About the Authors:

Nikita V. Savenkov, Cand. Sci. (Eng.), Associate Professor, Head of the Department of Automobile Transport, Service and Operation, Donbass National Academy of Civil Engineering and Architecture (2, Derzhavina St., Makeyevka, Donetsk People's Republic, 286128, Russian Federation), [SPIN-code](#), [ORCID](#), [ScopusID](#), [ResearcherID](#), n.v.savenkov@donnasa.ru

Ekaterina L. Golovatenko, Senior Lecturer of the Technosphere Safety Department, Donbass National Academy of Civil Engineering and Architecture (2, Derzhavina St., Makeyevka, Donetsk People's Republic, 286128, Russian Federation), [SPIN-code](#), [ORCID](#), e.l.golovatenko@donnasa.ru

Claimed Contributorship:

NV Savenkov: conceptualization, supervision.

EL Golovatenko: formal analysis, writing – original draft preparation, visualization.

Conflict of Interest Statement: the authors declare no conflict of interest.

All authors have read and approved the final manuscript.

Об авторах:

Никита Владимирович Савенков, кандидат технических наук, доцент, заведующий кафедрой «Автомобильный транспорт, сервис и эксплуатация» Донбасской национальной академии строительства и архитектуры (286128, Донецкая Народная Республика, г. Макеевка, ул. Державина, д. 2.), [SPIN-код](#), [ORCID](#), [ScopusID](#), [ResearcherID](#), n.v.savenkov@donnasa.ru

Екатерина Леонидовна Головатенко, старший преподаватель кафедры «Техносферная безопасность» Донбасской национальной академии строительства и архитектуры (286128, Донецкая Народная Республика, г. Макеевка, ул. Державина, д. 2.), [SPIN-код](#), [ORCID](#), e.l.golovatenko@donnasa.ru

Заявленный вклад авторов:

Н.В. Савенков: разработка концепции, научное руководство.

Е.Л. Головатенко: формальный анализ, написание черновика рукописи, визуализация.

Конфликт интересов: авторы заявляют об отсутствии конфликта интересов.

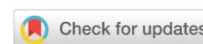
Все авторы прочитали и одобрили окончательный вариант рукописи.

Received / Поступила в редакцию 16.06.2025

Reviewed / Поступила после рецензирования 11.07.2025

Accepted / Принята к публикации 24.07.2025

CHEMICAL TECHNOLOGIES, MATERIALS SCIENCES, METALLURGY ХИМИЧЕСКИЕ ТЕХНОЛОГИИ, НАУКИ О МАТЕРИАЛАХ, МЕТАЛЛУРГИЯ



UDC 669.1

Original Empirical Research

<https://doi.org/10.23947/2541-9129-2025-9-3-221-229>

Surface Morphology Identification of Steel Natural Ferrite-Martensitic Composite Using ImageJ Software

 Valentina V. Duka , Lyudmila P. Aref'eva  

Don State Technical University, Rostov-on-Don, Russian Federation

✉ ludmilochka529@mail.ru

EDN: ZHEYTV

Abstract

Introduction. Modern materials require a deep understanding of their structure in order to predict their performance properties. However, the use of various imaging techniques and programs, such as optical and electron microscopy, is limited to two-dimensional images, making it difficult to fully analyze the morphology of materials. Despite research in this field, there is still a lack of knowledge about the three-dimensional organization of materials, leading to gaps in our understanding of how geometry affects the physical properties of composite materials. ImageJ was chosen for this study due to its versatility and ability to support multiple formats, simplifying the process of analysis. It also offers powerful tools for automated processing and allows users to extract three-dimensional information from two-dimensional images. This is crucial for accurately identifying structural components. The current study aims to fill in the missing information by analyzing the morphology of a steel ferrite-martensite composite. The aim of the work is to determine the 3D surface structure of the composite, which will improve understanding of its performance characteristics and confirm the significance of selecting appropriate visualization techniques.

Materials and Methods. An image of the microstructure of a steel natural ferrite-martensitic composite (NFMC), obtained using a Metam PB–22 optical microscope, was chosen as the starting material for analysis. The microstructure in question consists of two phases: the light phase being ferrite and the dark phase being martensite. The ImageJ program, which has been adapted to various formats of electron microscopic and metallographic images, was used to obtain a wide range of geometric characteristics of the surface.

Results. A study using ImageJ software on the microstructure of a steel ferrite-martensitic composite revealed a characteristic lineage structure consisting of a light phase (ferrite) and a dark phase (martensite). Image processing, including scaling and segmentation, led to the conversion to black and white format, allowing for clear visualization of the boundaries between the phases and the geometric shapes of the particles. The four-parameter Rodbard calibration function provided additional data on area, standard deviation, skewness, and kurtosis, making it difficult to analyze the structure. As a result, ferrite occupied 40.8% of the area, while martensite occupied 59.2%. The surface profile revealed an alternating pattern of misoriented crystals, and the quantitative information allowed for the creation of a clear 3D image of the composite surface.

Discussion. The thickness of grain boundaries in pixels was found to be thinner in this graphic editor than in others, which affected the area and, consequently, the amount of light phase. The change in the quantitative ratio of ferrite-martensite phases was due to the program's ability to suppress image “noise” and more clearly read the unrecognized gray phase, with some of it belonging to the light phase and some to the dark phase.

With the advancement of technology and the increasing demands for strength and wear resistance, understanding the microstructure of materials has become crucial for optimizing their properties. The selection of appropriate imaging techniques, such as the use of ImageJ software, not only allows for accurate data on phase distribution, but also contributes to a more in-depth analysis of mechanical properties such as hardness and corrosion resistance. These aspects are important in the context of the development of innovative technologies where reliability and durability are essential factors.

Conclusion. The use of the ImageJ software package for visualization in 2D and 3D graphics and qualitative and quantitative analysis of the surface morphology of heterogeneous structural states of materials is a convenient, effective and informative way to obtain geometric characteristics of particles of structural components. It is also possible to map the shape and size of particles. Automation of this process leads to time and resource savings, minimizing the influence of subjective factors on results at different stages of analysis. Identification of the 3D surface structure of composites helps to deepen our understanding of their operational characteristics, which is crucial in the context of modern technological demands. This knowledge allows us to develop new materials with improved properties such as strength, wear and corrosion resistance. Furthermore, it enables us to predict how materials will perform in actual conditions.

Keywords: ImageJ, composite, martensite, surface profile, pixel, microstructure, scale

Acknowledgments. The authors would like to thank the editors and reviewers for their attentive attitude to the article and comments that allowed them to improve its quality.

For citation. Duka VV, Aref'eva LP. Surface Morphology Identification of Steel Natural Ferrite-Martensitic Composite Using ImageJ Software. *Safety of Technogenic and Natural Systems*. 2025;9(3):221–229. <https://doi.org/10.23947/2541-9129-2025-9-3-221-229>

Оригинальное эмпирическое исследование

Идентификация морфологии поверхности стального естественного феррито-мартенситного композита с использованием программного обеспечения ImageJ

В.В. Дука , Л.П. Арефьева  

Донской государственный технический университет, г. Ростов-на-Дону, Российская Федерация

 ludmilochka529@mail.ru

Аннотация

Введение. Современные материалы требуют глубокого понимания их структуры для прогнозирования эксплуатационных свойств. Применение различных методик и программ для визуализации, таких как оптическая и электронная микроскопия, ограничено двумерными изображениями, что затрудняет детальный анализ морфологии. Несмотря на наличие исследований в этой области, существует недостаток в понимании трехмерной организационной структуры материалов, что создает пробелы в знании о влиянии геометрии на физические свойства композитов. Программа ImageJ была выбрана для данного исследования благодаря своей многофункциональности и поддержке множества форматов, что значительно упрощает анализ. Она также предлагает мощные инструменты для автоматизации процессов и позволяет извлекать 3D-информацию из двумерных изображений, что критично для точной идентификации структурных компонентов. Настоящее исследование направлено на устранение недостающей информации, фокусируясь на анализе морфологии стального феррито-мартенситного композита. Цель работы — идентификация 3D-структуры поверхности композита, что позволит улучшить понимание его эксплуатационных характеристик и подтвердить значимость выбора подходящих методов визуализации.

Материалы и методы. В качестве исходного материала для анализа было выбрано изображение микроструктуры стального естественного феррито-мартенситного композита (ЕФМК), полученное на оптическом микроскопе Метам РВ–22. Рассматриваемая микроструктура состоит из 2-х фаз, где светлой фазой является феррит, а темной — мартенсит. Использовалась программа ImageJ, адаптированная под различные форматы электронно-микроскопических и металлографических изображений и позволяющая получить широкий набор геометрических характеристик поверхности.

Результаты исследования. Исследование с использованием программного обеспечения ImageJ микроструктуры стального феррито-мартенситного композита выявило характерную строчечную структуру, состоящую из светлой фазы (феррита) и темной фазы (мартенсита). Обработка изображений, включая масштабирование и сегментацию, привела к преобразованию в черно-белый формат, что позволило четко визуализировать границы между фазами и геометрические формы частиц. Четырехпараметрическая калибровочная функция Родбарда обеспечила дополнительные данные о площади, стандартном отклонении, асимметрии и эксцессе, что затрудняет анализ структуры. В результате отмечено 40,8 % площади, занятый ферритом, и 59,2 % — мартенситом. Профиль поверхности показывает чередование слоев из разориентированных кристаллов, а количественная информация позволила создать четкое 3D-изображение поверхности композита.

Обсуждение. Измеряемая в пикселях толщина границ зерен оказывается тоньше, чем в других графических редакторах, за счёт чего изменяется площадь и соответственно количество светлой фазы. Изменение количественного

соотношения фаз «феррит-мартенсит» связано с тем, что в программе подавляется «шум» изображения и нераспознанная серая фаза прочитывается более чётко: часть её относится к светлой фазе, и часть — к тёмной.

В условиях современных технологий и высоких требований к прочности и износостойкости, понимание микроструктуры становится ключевым для оптимизации свойств материалов. Выбор подходящих методов визуализации, таких как применение программного обеспечения ImageJ, не только позволяет получить точные данные о распределении фаз, но также способствует более глубокому анализу механических свойств, таких как твердость и устойчивость к коррозии. Эти аспекты важны в контексте роста инновационных технологий, где надежность и долговечность материалов играют центральную роль.

Заключение. Применение программного комплекса ImageJ для визуализации в 2D и 3D графике и качественно-количественного анализа морфологии поверхности гетерогенных структурных состояний материалов является удобным, эффективным и информативным способом получения геометрических характеристик частиц структурных составляющих. Также возможно проведения картирования формы и размеров частиц. Автоматизация процесса приводит к экономии затрат времени и ресурсов, минимизирует влияние субъективных факторов на результат на разных этапах проведения анализа. Идентификация 3D-структуры поверхности композита помогает углубить знания о его эксплуатационных характеристиках, что крайне актуально в условиях современных технологических требований. Это понимание позволяет разрабатывать новые материалы, улучшать их характеристики, такие как прочность, износостойкость и устойчивость к коррозии, а также предсказывать, как материалы будут вести себя в реальных условиях.

Ключевые слова: ImageJ, композит, мартенсит, профиль поверхности, пиксель, микроструктура, масштаб

Благодарности. Авторы выражают благодарность редакции и рецензентам за внимательное отношение к статье и указанные замечания, которые позволили повысить ее качество.

Для цитирования. Дука В.В., Арефьева Л.П. Идентификация морфологии поверхности стального естественного феррито-мартенситного композита с использованием программного обеспечения ImageJ. *Безопасность техногенных и природных систем.* 2025;9(3):221–229. <https://doi.org/10.23947/2541-9129-2025-9-3-221-229>

Introduction. Currently, many techniques and specialized computer programs are actively used in the field of materials science, allowing for the expansion of visualization capabilities for material structures through increased resolution. This, in turn, increases the likelihood of predicting operational properties. The morphology of the surface, its chemical composition, and structural components are key indicators in the study of the structure of materials, as they directly influence material properties, behavior, and performance characteristics. Traditional methods for determining surface morphology include several techniques that allow for assessing topography, roughness, structure and defects of the surface. These include optical microscopy, scanning electron microscopy, transmission electron microscopy, profilometry, and others. However, all these methods, despite their widespread use, only allow for the acquisition of two-dimensional images. This limits the information that can be obtained about the surface relief formed by the phase composition of the material. Additionally, these methods are typically destructive in nature. At the same time, the use of software algorithms based on modern digital technologies allows for the extraction of three-dimensional (3D) information from two-dimensional images of structures without losing resolution. This also enables efficient storage and quick interpretation of 3D images at both micro- and nano-levels. Electronic 3D structural images enhance the reliability of morphological organization of the material due to precision detail. This allows for precise estimation of geometric dimensions of structural components and local determination of their physical and mechanical properties, minimizing errors. When selecting programs for visualizing 3D images, it is essential to consider the goals and objectives of the study, as well as the convenience of working with the interface and its functionality. Currently, there is a wide range of image processing applications with a diverse set of capabilities. Among the available software packages such as Adobe Photoshop [1], Gimp [2], CellProfiler [3], Huygen [4], Leica QWin [5], Gwyddion, ImageJ stands out for its versatility, support for multiple formats, flexibility, performance and automation capabilities. These qualities make it especially in demand when working with images [6]. The digital image processing method for analyzing the surface relief using the ImageJ program allows extracting 3D information from 2D images obtained through optical microscopy without losing resolution [7]. This is particularly important for identifying the morphology of composite structural components and then interpreting its properties as a whole. In this study, we use the ImageJ software for the first time to study a natural ferrite-martensitic composite [8]. The aim of the work is to identify the surface morphology of natural steel ferrite-martensitic composite using ImageJ software.

Materials and Methods. The object of the study was an image of the microstructure of a natural ferrite-martensitic composite obtained using a Metam PB–22 optical microscope [9].

To obtain additional information about the structural state of NFMC, the ImageJ program was used. It was adapted to various formats of electron microscopic and metallographic images [10]. The program allows you to calculate the area, length, volume, perimeter, and angular dimensions of the surface of structural components, including statistical indicators both in pixel values and in the SI system [11]. In this case, the geometric characteristics were determined as a result of sequential mapping of the structure (Fig. 1) with subsequent integration of the entire image area [12].

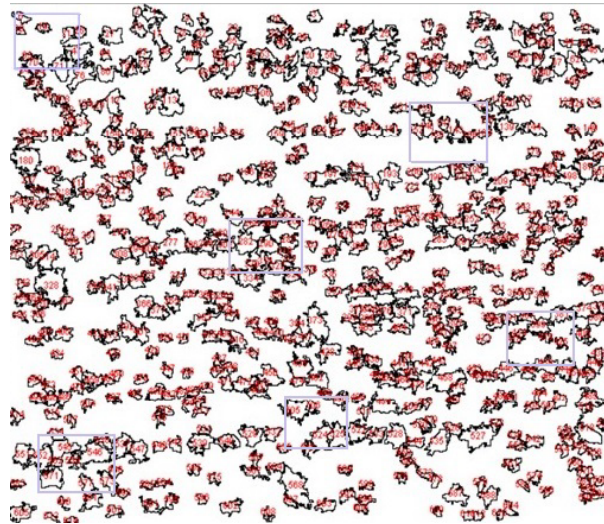


Fig. 1. Sequential mapping of the NFMC structure

The “Set Measurements” option of the program allows users to calculate both total and relative area of particles in structural components, as well as their average size [9–12, 13]. The four-parameter Rodbard calibration function, according to Equation 1, accurately identifies the shades of black and white by analyzing the pixel intensity along a line inside the image and converts a 2D surface into a 3D image [13, 14].

$$y = d + \frac{a - b}{1 + \left(\frac{x}{c}\right)^b}, \quad (1)$$

where y — function value; x — independent variable; d — maximum function value (upper asymptote); a — minimum function value (lower asymptote); b — parameter that determines the slope (steepness) of the curve; c — value at which the function takes a value equal to the midpoint between a and d .

NFMC is a composite material based on hot-rolled pre-eutectoid 14G2 structural steel with an initial ferrite-pearlite lineage structure. After quenching from the inter-critical temperature range (ITR), the structure of such a composite consists of alternating layers of ferrite and martensite, which act as a reinforcing component. This structure makes it possible to obtain an unusual ratio of high plasticity, viscosity, and strength.

It is known that in NFMC, the main indicators of mechanical, physical and operational properties are determined by the chemical composition and the quantitative phase ratio. The ratio of the volume fractions of ferrite and martensite as well as the microhardness of the hardening phase depend on the ITR tempering temperature. It was found that when quenched at a temperature of 730°C the volume fraction of the martensitic component did not exceed 25–30%, and its microhardness was 735–740 MPa. When quenched at a higher temperature of 780°C, a martensite structure was formed with a higher volume fraction of 55–60%, but with a lower microhardness of 450–455 MPa. The decrease in microhardness was due to the fact that with an increase in the quenching temperature in the ITR, the amount of carbon in martensite decreased [15].

Results. Figure 2 *a*, obtained using a Metam PB–22 optical microscope, shows the characteristic lineage structure of NFMC, which consists of layers of a light phase — ferrite, and a dark phase — martensite. However, it was difficult to detail the structural components. After preprocessing the image by sequentially scaling, segmentation, and extraction of geometric characteristics, ImageJ converted the image to a black-and-white 8-bit format (Fig. 2 *b*), where each pixel was a single byte value in the range from 0 to 255, indicating brightness. This increased the contrast of the image, making the geometric shapes of the particles and boundaries between phase layers more visible. This significantly expanded the possibilities for structural analysis of 2D images of the heterogeneous morphology of natural ferrite-martensitic composite [16].

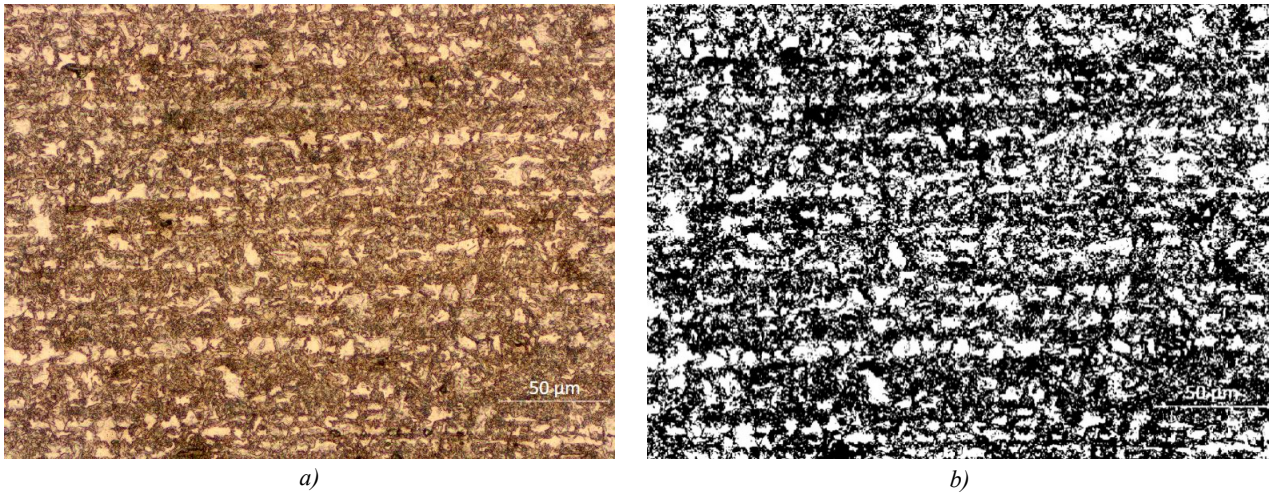


Fig. 2. NFMC microstructure after hardening from ITR (light area — ferrite, dark area — martensite):

a — NFMC microstructure before processing in the ImageJ program;

b — NFMC microstructure after conversion to black-and-white graphics using the ImageJ computer program

The use of a four-parameter Rodbard calibration function (Fig. 3) made it possible to extract additional information on the structural components parameters set in the “Set Measurements” option — the total study area, standard deviation, asymmetry, and kurtosis of the pixel image, the fraction of the area and the perimeter of the analyzed phases. The values of these parameters, after scaling, are presented in Table 1.

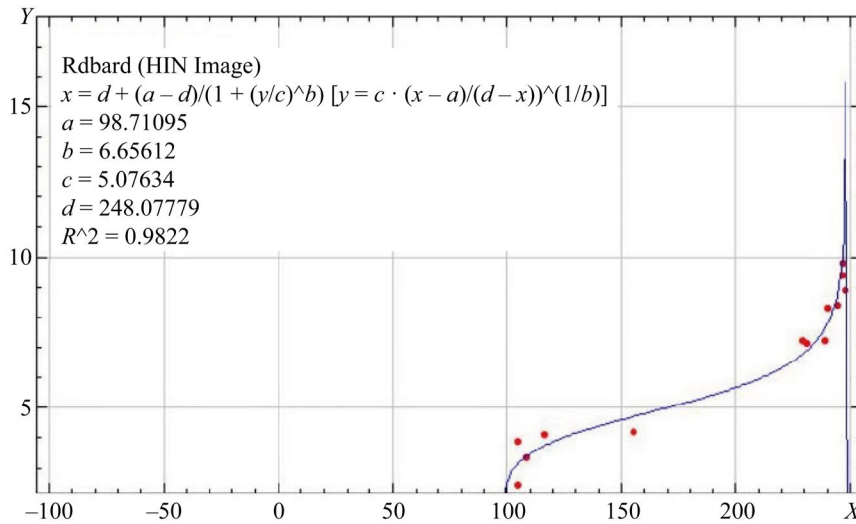


Fig. 3. Rodbard's four-parameter calibration function, on the X-axis — distance along the line, on the Y-axis — pixel intensity

Table 1

The results of the specified measurements in the “Set Measurements” dialog box

Parameter	Meaning
Area (pxl)/(μm ²)	313,908 / 66,789
Standard deviation	124.7
Skewness	0.4
Area fraction of the light phase — ferrite (%)	40.8
Area fraction of the dark phase — martensite (%)	59.2
Mean gray value	101.0
Perimeter(px1)/(μm)	2,248 / 478.3
Kurtosis	-1.8

Based on the data obtained, a two-dimensional graph of the profile was constructed (Fig. 4). From this graph, it was concluded that a lineage structure was formed on the NFMC surface, the distinctive feature of which was the presence of alternating layers of martensite and ferrite consisting of crystals disoriented in space. This could be seen by the local maxima and minima in the profile.

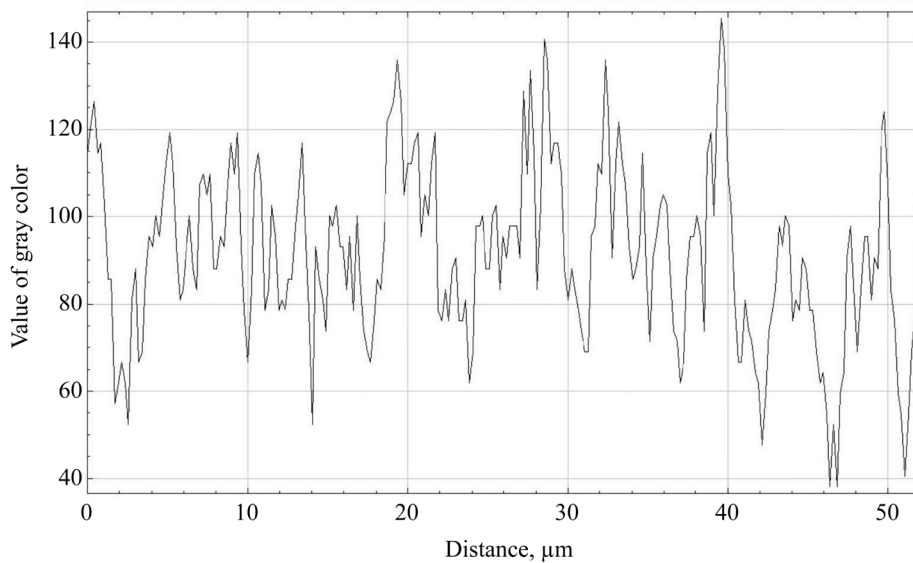


Fig. 4. NFMC surface profile

The use of the “Analyze Particles” function, which was built into the “Set Measurements” option, allowed objects to be filtered by size and shape. This made it possible to determine the total and relative areas of the structural components in question, as well as their average size. Thus, the total number of dark and light phase particles over the entire image area was 1,088, of which 27,316 μm^2 or 40.8% of the total area of 66,789 μm^2 was occupied by a light ferritic component with an average size of 4.72 μm , and the remaining proportion of 39,473 μm^2 or 59.2% was occupied by a dark martensite phase with an average size of 5.29 μm . Quantitative information about the location and intensity of pixels allowed us to obtain a clear 3D image of the NFMC surface profile (Fig. 5)

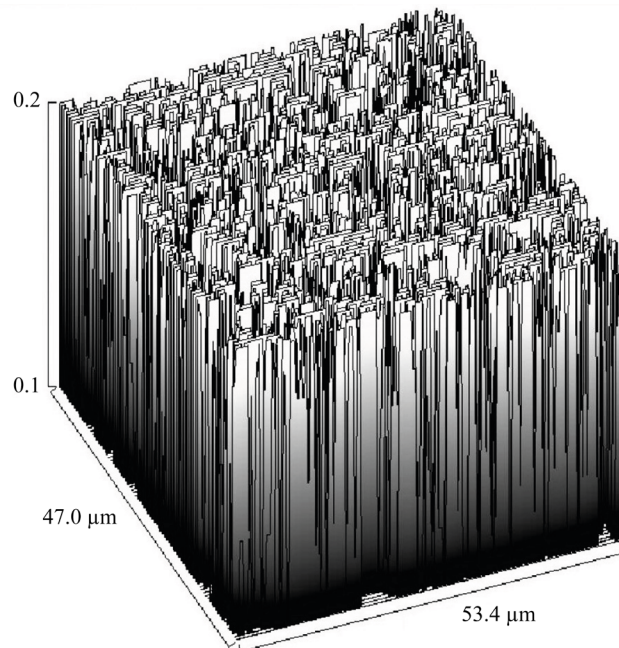


Fig. 5. 3D image of the NFMC surface profile

Discussion. It is known from [17, 18] that the percentage ratio of ferrite and martensite phases after quenching at 790–800°C averages 35/65–30/70. The quantitative ratio of ferrite and martensite in the image studied in the ImageJ program turned out to be, respectively, ~ 40/60. The deviation of the data obtained from the results of [17, 18] is explained by the fact that the ImageJ program processes images based on peak intensity, which makes it possible to view grain boundaries more accurately. The thickness of the grain boundaries, measured in pixels, turns out to be thinner than in other graphic editors, which, in turn, changes the area and the corresponding amount of light phase. The change in the quantitative ratio of the ferrite-martensite phases is due to the fact that the “noise” of the image is suppressed in the program, and the unrecognized gray phase is read more clearly: part of it belongs to the light phase, and part to the dark one. The results obtained make it possible to more accurately quantify the degree of heterogeneity and the location of ferrite and martensite in the studied image. The results are in good agreement with the work data and generally correspond to the visual images obtained.

Conclusion. The ImageJ program offers convenient tools for visualizing and documenting the results of studies on heterogeneous structural states of materials with various functional purposes. It allows users to create reports with visual illustrations in 2D and 3D graphics formats. A wide range of built-in options enables users to evaluate various geometric parameters of particle morphology and, based on this, analyze shape, size, location, quantity, and even perform mapping. The use of this software package to study the NFMC surface morphology by processing photographs of the microstructure significantly increases the efficiency, accuracy and objectivity of the study. Automating the process significantly saves time and human resources, as well as minimizes data variability associated with manual processing. The use of such tools is especially beneficial when combined with traditional data collection methods, as it allows for a more comprehensive and reliable understanding of the properties and structure of materials.

References

1. Tim Gräning, Lizhen Tan, Ishtiaque Robin, Yutai Katoh, Ying Yang. A Novel Design of Transitional Layer Structure between Reduced Activation Ferritic Martensitic Steels and Tungsten for Plasma Facing Materials. *Journal of Materials Research and Technology*. 2023;24:4285–4299. <https://doi.org/10.1016/j.jmrt.2023.04.019>
2. Garcia JuM, Accioly Monteiro AC, Barcelos Casanova AM, Checca Huaman NR, Monteiro SN, Brandao LP. Microstructural Analysis of Phase Precipitation during High Temperature Creep in AISI 310 Stainless Steel. *Journal of Materials Research and Technology*. 2023;23:5953–5966. <https://doi.org/10.1016/j.jmrt.2023.02.175>
3. Karin P, Chammana P, Oungpakornkaew P, Rungsritanapaisan P, Amornprapa W, Charoenphonphanich C, et al. Impact of Soot Nanoparticle Size and Quantity on Four-Ball Steel Wear Characteristics Using EDS, XRD and Electron Microscopy Image Analysis. *Journal of Materials Research and Technology*. 2022;16:1781–1791. <https://doi.org/10.1016/j.jmrt.2021.12.111>
4. Setareh Medghalchi, Ehsan Karimi, Sang-Hyeok Lee, Benjamin Berkels, Ulrich Kerzel, Sandra Korte-Kerzel. Three-Dimensional Characterisation of Deformation-Induced Damage in Dual Phase Steel Using Deep Learning *Journal Materials & Design*. 2023;232:112108. <https://doi.org/10.1016/j.matdes.2023.112108>
5. Starovoitov VV, Golub YuI. *Digital Images. From Receipt to Processing*. Minsk: UIIP NAS of Belarus; 2014. 202 p. (In Russ.)
6. Pustovoit VN, Dolgachev YuV, Dombrovskii YuM, Duka VV. The Structure and Properties of a Natural Steel Ferritic-Martensitic Composite. *Metallovedenie i Termicheskaya Obrabotka Metallov*. 2020;(6(780)):15–21. (In Russ.) URL: <https://mitom.folium.ru/index.php/mitom/article/view/251> (accessed: 01.06.2025).
7. Vernezi NL, Rusakov VA. On the Control of Metal Strength of Structural Elements of Floating Cranes. *Safety of Technogenic and Natural Systems*. 2022;(3):50–51. <https://doi.org/10.23947/2541-9129-2022-3-48-53>
8. Pustovoit VN, Dolgachev YuV, Dombrovskii YuM. Ballistic Resistance of Steel with the Structure of a Natural Ferrite-Martensitic Composite. *Safety of Technogenic and Natural Systems*. 2022;(3):54–59. <https://doi.org/10.23947/2541-9129-2022-3-54-59>
9. Zilbergleit MA, Temruk VI. Package ImageJ. Application for Image Processing Obtained Scanning Electronic Microscopy (Paper Analysis). *Polymer Materials and Technologies*. 2017;3(1):71–74. (In Russ.)
10. Ioffe AI. Method for Estimation of a Given Area Relief Roughness. *Earth Research from Space*. 2013;(3):92–94. (In Russ.) <https://doi.org/10.7868/S0205961413020048>

11. Burger W, Burge MJ. *Digital Image Processing. An Algorithmic Introduction Using Java. Second Edition.* London: Springer; 2016. 811 p.
12. Atroshenko SA, Maier SS, Smirnov VI. Structural Phase State of the Metal of a Rail with an Internal Crack after Long-Term Operation. *Zhurnal Tekhnicheskoi Fiziki.* 2021;91(9):1363–1368. (In Russ.) <https://doi.org/10.21883/JTF.2021.09.51215.72-21>
13. Torres AL, Bidarra SJ, Pinto MT, Aguiar PC, Silva EA, Barrias CC. Guiding Morphogenesis in Cell-Instructive Microgels for Therapeutic Angiogenesis. *Biomaterials.* 2018;154:34–47. <https://doi.org/10.1016/j.biomaterials.2017.10.051>
14. Rueden CT, Schindelin J, Hiner MC, DeZonia BE, Walter AE, Arena ET. ImageJ2: ImageJ for the Next Generation of Scientific Image Data. *BMC Bioinformatics.* 2017;18(1):529. <https://doi.org/10.1186/s12859-017-1934-z>
15. Duka VV, Pustovoi VN, Ostapenko DA, Aref'eva LP, Dombrovskij YuM. The Use of the Atomic Force Microscopy to Investigate the Structure of Steel 14G2. *IOP Conference Series: Materials Science and Engineering.* 2019;680:012023. <https://doi.org/10.1088/1757-899X/680/1/012023>
16. Duka VV, Aref'eva LP, Pustovoi VN, Kiseleva DA. Study of the Lineage Structure of Building Steel by Atomic Force Microscopy. *Letters on Materials.* 2020;10(4(40)):445–450. (In Russ.) <https://doi.org/10.22226/2410-3535-2020-4-445-450>
17. Aref'eva LP, Duka VV, Zabayaka IY. Relationship between the Structural-Phase Composition and the Fracture Mechanism of High-Strength Construction Steel. *Technical Physics Letters.* 2022;48(8):39–42. (In Russ.) <https://doi.org/10.21883/PJTF.2022.08.52366.19093>
18. Duka VV, Aref'eva LP, Mitrin BI, Pustovoi VN. Investigation of the Fracture Structure of a Composite Material after Bending Test by Atomic Force Microscopy. *IOP Conference Series: Materials Science and Engineering.* 2021;1029:012059. <https://doi.org/10.1088/1757-899X/1029/1/012059>

About the Authors:

Valentina V. Duka, Senior Lecturer of the Department of Materials Science and Technology of Metals, Don State Technical University (1, Gagarin Sq., Rostov-on-Don, 344003, Russian Federation), [SPIN-code](#), [ORCID](#), [ScopusID](#), valentina.duka.92@mail.ru

Lyudmila P. Aref'eva, Dr. Sci. (Phys.-Math.), Associate Professor, Associate Professor of the Department of Materials Science and Technology of Metals, Don State Technical University (1, Gagarin Sq., Rostov-on-Don, 344003, Russian Federation), [SPIN-code](#), [ORCID](#), [ScopusID](#), [ResearcherID](#), ludmilochka529@mail.ru

Claimed Contributorship:

VV Duka: conceptualization, formal analysis, investigation, validation, visualization, writing – original draft preparation.

LP Aref'eva: conceptualization, data curation, methodology, resources, supervision, writing – review & editing.

Conflict of Interest Statement: the authors declare no conflict of interest.

All authors have read and approved the final manuscript.

Об авторах

Валентина Владимировна Дука, старший преподаватель, кафедры «Материаловедение и технологии металлов» Донского государственного технического университета (344003, Российская Федерация, г. Ростов-на-Дону, пл. Гагарина, 1), [SPIN-код](#), [ORCID](#), [ScopusID](#), valentina.duka.92@mail.ru

Людмила Павловна Арефьева, доктор физико-математических наук, доцент, доцент, кафедры «Материаловедение и технологии металлов» Донского государственного технического университета (344003, Российская Федерация, г. Ростов-на-Дону, пл. Гагарина, 1), [SPIN-код](#), [ORCID](#), [ScopusID](#), [ResearcherID](#), ludmilochka529@mail.ru

Заявленный вклад авторов

В.В. Дука: разработка концепции, формальный анализ, проведение исследований, валидация результатов, визуализация, написание черновика рукописи.

Л.П. Арефьева: разработка концепции, курирование данных, разработка методологии, предоставление ресурсов, научное руководство, написание рукописи — внесение замечаний и исправлений.

Конфликт интересов: авторы заявляют об отсутствии конфликта интересов.

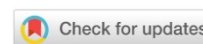
Все авторы прочитали и одобрили окончательный вариант рукописи.

Received / Поступила в редакцию 10.06.2025

Reviewed / Поступила после рецензирования 30.06.2025

Accepted / Принята к публикации 14.07.2025

CHEMICAL TECHNOLOGIES, MATERIALS SCIENCES, METALLURGY ХИМИЧЕСКИЕ ТЕХНОЛОГИИ, НАУКИ О МАТЕРИАЛАХ, МЕТАЛЛУРГИЯ



UDC 621.762: 621.7 016.2

Original Empirical Research

<https://doi.org/10.23947/2541-9129-2025-9-3-230-241>

Influence of the Production Method and the Structure of Chromium-Nickel Corrosion Resistant Steels on the Kinetics of the Formation of the Outer Cage of Spherical Joints



EDN: OHKNMX

Nikolai A. Konko ✉, Badrudin G. Gasanov ✉

Platov South-Russian State Polytechnic University (NPI), Novocheerkassk, Russian Federation

✉ konko2013@mail.ru

Abstract

Introduction. Investigating the issues of wear resistance of joints, the authors of this paper have previously studied how the features of chromium-nickel corrosion resistant steels affect the shaping of the outer cage of spherical hinges. They sintered compacts made of 12Kh18N10T, VP 304.200.30 and 304L-AW-100 at 1,200°C in vacuum for 3 hours. However, in practice, it is necessary to test different steels in different conditions. This paper describes 10Kh18N9 rolled stainless steel. Powder VP 304.200.30 was sintered at 1,150°C for 2 hours. The aim of the research is to demonstrate how the production method and the metal structure affect the kinetics of the outer cage formation and, consequently, the strength of the product.

Materials and Methods. Samples made of 10Kh18N9¹ and VP 304.200.30 were radially compressed according to GOST 26529–85² and stretched³ on an UMM-5⁴ testing machine. Hardness was measured using a Rockwell TP 5006⁵ instrument, and microhardness was measured according to Vickers on an HVS-1000⁶ instrument. X-ray phase analysis was performed on an XRD-6100 diffractometer. Microscopes *Tescan VEGA II LMU* (for electron probe studies), *Quanta 200* and *Altami MET-1M* (for studying microstructure and metallography) were used. Cold stamping of the outer cage with a spherical hinge flange was modeled in *QForm*.

Results. The strength and yield strength of VP 304.200.30 were comparable to those of some chromium-nickel austenitic steels, but were inferior in terms of ductility. A comparison between 10Kh18N9 and VP 304.200.30 revealed differences in their deformation mechanisms. The critical limitation for powder steel was not the oxide phase, but the localization of oxides at particle boundaries, which provoked brittle fracture under tension. Due to the chemical heterogeneity in the particles and residual porosity, powder steel had a 6-fold lower elongation compared to rolled steel. However, under compression conditions, sintered material could reach a hardness of 195 HV, making it suitable for use in the outer cage of spherical hinges.

Discussion. An analysis of the deformation characteristics of sintered and rolled steels confirmed the suitability of the proposed methodology for assessing the deformation state of samples during cold stamping of the outer cage of spherical hinges.

Conclusion. The findings from this study allow us to predict the locations of macrodefects and optimize the manufacturing process for spherical hinges.

¹ GOST 5632–2014. *Stainless Steels and Corrosion Resisting, Heat-Resisting and Creep Resisting Alloys. Grades.* Electronic Fund of Legal and Regulatory and Technical Documents. (In Russ.) URL: <https://docs.cntd.ru/document/1200113778> (accessed: 21.06.2025).

² GOST 26529–85. *Powder Materials. Radial Crushing Test Method.* Electronic Fund of Legal and Regulatory and Technical Documents. (In Russ.) URL: <https://docs.cntd.ru/document/1200011117> (accessed: 21.06.2025).

³ GOST 1497–84. *Metals. Methods of Tension Test.* Electronic Fund of Legal and Regulatory and Technical Documents. (In Russ.) URL: <https://docs.cntd.ru/document/1200004888> (accessed: 21.06.2025).

⁴ GOST 28840–90. *Machines for Tension, Compression and Bending Testing of Materials. General Technical Requirements.* Electronic Fund of Legal and Regulatory and Technical Documents. (In Russ.) URL: <https://docs.cntd.ru/document/1200023577> (accessed: 21.06.2025).

⁵ GOST 9013–59. *Metals. Method of Measuring Rockwell Hardness.* Electronic Fund of Legal and Regulatory and Technical Documents. (In Russ.) URL: <https://docs.cntd.ru/document/1200004663> (accessed: 21.06.2025).

⁶ GOST 9450–76. *Measurements Microhardness by Diamond Instruments Indentation.* Electronic Fund of Legal and Regulatory and Technical Documents. (In Russ.) URL: <https://docs.cntd.ru/document/1200012869> (accessed: 21.06.2025).

Keywords: 10Kh18N9 rolled steel, VP 304.200.30 powder steel, outer race of spherical joint, microcracks in chromium-nickel steel

Acknowledgements. The authors would like to thank the Editorial board and the reviewers for their attentive attitude to the article and for the specified comments that improved the quality of the article.

For citation. Konko NA, Gasanov BG. Influence of the Production Method and the Structure of Chromium-Nickel Corrosion Resistant Steels on the Kinetics of the Formation of the Outer Cage of Spherical Joints. *Safety of Technogenic and Natural Systems*. 2025;9(3):230–241. <https://doi.org/10.23947/2541-9129-2025-9-3-230-241>

Оригинальное эмпирическое исследование

Влияние способа получения и структуры хромоникелевых коррозионноустойчивых сталей на кинетику формирования наружной обоймы сферических шарниров

Н.А. Конько  , Б.Г. Гасанов 

Южно-Российский государственный политехнический университет (НПИ) имени М.И. Платова,
г. Новочеркасск, Российская Федерация

 konko2013@mail.ru

Аннотация

Введение. Исследуя вопросы износостойкости шарниров, авторы представленной работы ранее выяснили, как особенности хромоникелевых коррозионно-стойких сталей влияют на формирование наружной обоймы сферических шарниров. Прессовки из 12X18H10T, ВП 304.200.30 и 304L-AW-100 спекали 3 ч в вакууме при 1 200 °С. Однако практика требует испытаний разных сталей при разных условиях. В данной статье описана катаная нержавеющая сталь 10X18H9. Порошковую ВП 304.200.30 спекали 2 ч при 1 150 °С. Цель работы — показать, как способ получения и структура металла определяют кинетику формирования наружной обоймы сферических шарниров и в итоге — прочность изделия.

Материалы и методы. Образцы из 10X18H9 и ВП 304.200.30 радиально сжимали по ГОСТ 26529–85, растягивали на испытательной машине УММ-5. Твердость измеряли на приборе Роквелла ТР 5006, микротвердость — по Виккерсу на приборе HVS-1000. Рентгенофазовый анализ проводили на дифрактометре XRD-6100. Использовали микроскопы *Tescan VEGA II LMU* (для электронно-зондовых исследований), *Quanta 200* и *Altami MET-1M* (для изучения микроструктуры и металлографии). Холодную штамповку наружной обоймы с фланцем сферического шарнира моделировали в *QForm*.

Результаты исследования. Предел прочности и текучести ВП 304.200.30 соизмерим с показателями некоторых хромоникелевых аустенитных сталей, но уступает им по пластичности. Сопоставление 10X18H9 и ВП 304.200.30 выявило различия в механизмах деформации. Критическое ограничение для порошковой стали — не оксидная фаза, а локализация оксидов на границах частиц, что провоцирует хрупкое разрушение при растяжении. Из-за химической неоднородности частиц и остаточной пористости относительное удлинение порошковой стали в 6 раз меньше, чем катаной. Но в условиях сжатия спеченный материал упрочняется до 195 HV, то есть подходит для производства наружной обоймы сферических шарниров.

Обсуждение. Анализ особенностей деформаций спеченных и катаных сталей подтвердил адекватность предложенной методики оценки деформированного состояния образцов при холодной штамповке наружной обоймы сферических шарниров.

Заключение. Результаты исследования позволяют прогнозировать очаги зарождения макродефектов и оптимизировать производство сферических шарниров.

Ключевые слова: катаная сталь 10X18H9, порошковая сталь ВП 304.200.30, наружная обойма сферического шарнира, микротрещины хромоникелевой стали

Благодарности. Авторы выражают благодарность редакции и рецензентам за внимательное отношение к статье и замечания, которые позволили повысить ее качество.

Для цитирования. Конько Н.А., Гасанов Б.Г. Влияние способа получения и структуры хромоникелевых коррозионноустойчивых сталей на кинетику формирования наружной обоймы сферических шарниров. *Безопасность техногенных и природных систем*. 2025;9(3):230–241. <https://doi.org/10.23947/2541-9129-2025-9-3-230-241>

Introduction. Due to the economic and technical significance of the task of extending the operational lifespan of hinge joints, which are components of many machines and mechanisms, it is essential to continuously research materials and manufacturing techniques. For instance, spherical hinge joints, which effectively absorb shock loads, are widely employed in vehicle suspensions [1]. At the same time, they are made of chromium-nickel corrosion-resistant steels, which have low wear resistance [2]. The choice of this metal for manufacturing spherical hinge parts is based on its performance characteristics during prolonged contact with aggressive media (salt solutions, moisture, and wear products). Powder metallurgy methods [4] are used to improve the tribotechnical properties of friction units made of chromium-nickel steels [3]. However, the production technology depends on the chemical composition of the material [5], the operating conditions of the machinery, the design of the friction units, and other factors [6]. Cold stamping is one option for forming the outer cage parts of spherical hinges [7] from sintered cylindrical blanks, with the inner surface coated with a solid lubricant [8] (Fig. 1).

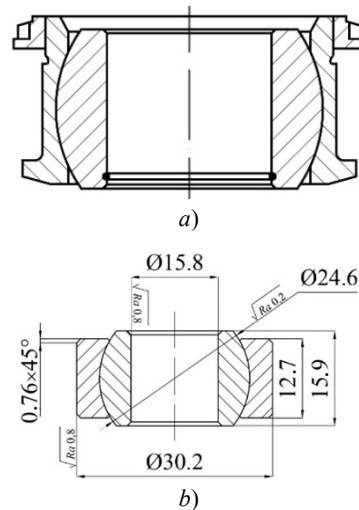


Fig. 1. The design of spherical hinge assemblies: *a* — outer cage with flange; *b* — outer cage without flange [1]

There is currently no publicly available information regarding the manufacturing process for the outer cage of spherical hinges made of sintered, corrosion-resistant steel and the estimated lifespan of these components. This has been confirmed through an analysis of recent Russian scientific literature and patents. Therefore, the following tasks are relevant:

- ensuring the required properties and quality of spherical hinges [9];
- reduction of the production costs;
- improvement of the reliability of tooling and technological equipment [10].

The team of authors of this article has already conducted scientific research in this area. Experiments with 12Kh18N10T, 304L-AW-100 and VP 304.200.30 powder steels have been described in [11]. Compacts were sintered for 3 hours in vacuum at 1,200°C. However, this is not enough. Production and operational practices are much more complex. Therefore, it is necessary to test different corrosion-resistant steels under various conditions. In this context, the following are considered:

- rolled corrosion-resistant chromium-nickel steel 10Kh18N9;
- powder steel VP 304.200.30, which was sintered for 2 hours at 1,150°C.

The aim of this research is to investigate how the production method and structure of 10Kh18N9 and VP 304.200.30 influence the kinetics of forming the outer cage of spherical hinges. The development of this approach, both theoretically and practically, opens up the potential to use data on the production method of chromium-nickel steel blanks to predict their structural formation, as well as their technological, tribological, and mechanical properties of the outer cage of spherical hinges.

Materials and Methods. Previously, studies have been conducted using corrosion-resistant chromium-nickel powder steels, such as VP 304.200.30, 304L-AW-100, and 12Kh18N10T [11]. This study focuses on the comparative analysis of VP 304.200.30 powder steel manufactured by Severstal (Russia) and its counterpart, 10Kh18N9 steel. The comparison is expected to establish a correlation between the production technology and the physical, mechanical, and operational properties of the samples.

Ring samples were made of 10Kh18N9 rolled steel (GOST 5632–2014⁷) and powder corrosion-resistant chromium-nickel VP 304.200.30 steel [11]. Geometric dimensions of the ring samples, mm:

- outer diameter of the sleeve (D_H) — 25;
- inner diameter of the sleeve (d_B) — 19.5;
- height of the sleeve (H) — 15.

The samples were obtained through the machining of 10Kh18N9 round rolled products and the static cold pressing of VP 304.200.30 powder using an HPM-60L hydraulic press in a cylindrical mold [11]. The compacting pressure varied in the range of 600–800 MPa. Powder molds were sintered in a VSI-16-22-U vacuum electric furnace at a temperature of 1150°C for two hours. The porosity of the blanks after sintering was 14–22%. Prior to cold stamping, solid lubricants were applied to the inner surface of the cylindrical sleeve: molybdenum disulfide (MoS_2) (TU 48–19–133–90⁸), pencil graphite (GOST 23463–79⁹) and polytetrafluoroethylene (PTFE, GOST 10007–80¹⁰) [11].

To assess the critical values of deformations during cold stamping, the ring samples, turned out of the rod and sintered, were tested for radial compression (Fig. 2) according to the procedure described in GOST 26529–85¹¹.

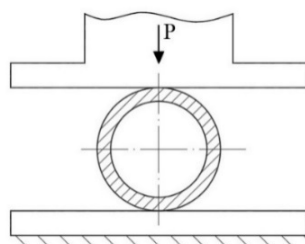


Fig. 2. Schematic of the ring sample testing for radial compression

According to the procedure described in GOST 1497–84¹², prismatic samples were produced for stretching experiments on the universal testing machine UMM-5 (GOST 28840–90¹³).

A Rockwell instrument TR 5006 (GOST 9013–59¹⁴) was used to determine the hardness of the samples. The microhardness was measured using the Vickers method (GOST 9450–76¹⁵) on an *HVS-1000* device.

The microstructure was studied using an *Altami MET-1M* metallographic microscope and a *Quanta 200* scanning electron microscope. Electron probe surveys were performed using a *Tescan VEGA II LMU* scanning electron microscope. X-ray phase analysis was performed on an XRD-6100 X-ray diffractometer with a θ -2 θ vertical goniometer.

The origin and development of cracks is caused by exceeding the deformation limits [12], therefore, its value during cold stamping of powder blanks is critically important and requires control at each stage of shaping [13]. Specialized software [14], calculation schemes, and simulation modeling in the *QForm* program were used to analyze the deformed state of products.

Results. The deformed state of the material of the ring samples affected their hardness after radial deformation (ϵ_R). To assess the relative degree of deformation, hardness was measured using the Vickers method in different sections of the ring samples (Fig. 3 a).

⁷ GOST 5632–2014. *Stainless Steels and Corrosion Resisting, Heat-Resisting and Creep Resisting Alloys. Grades*. Electronic Fund of Legal and Regulatory and Technical Documents. (In Russ.) URL: <https://docs.cntd.ru/document/1200113778?ysclid=mdohk7rxu9621196527> (accessed: 21.06.2025).

⁸ TU 48–19–133–90. *Molybdenum Disulfide. Technical Specifications*. (In Russ.) URL: <https://gostrf.com/normadata/1/4293788/4293788422.pdf> (accessed: 21.06.2025).

⁹ GOST 23463–79. *High-Purity Powdery Graphite. Specifications*. Electronic Fund of Legal and Regulatory and Technical Documents. (In Russ.) URL: <https://docs.cntd.ru/document/1200014916> (accessed: 21.06.2025).

¹⁰ GOST 10007–80. *Polytetrafluoroethylene. Specifications*. Electronic Fund of Legal and Regulatory and Technical Documents. (In Russ.) URL: <https://docs.cntd.ru/document/1200020654> (accessed: 21.06.2025).

¹¹ GOST 26529–85. *Powder Materials. Radial Crushing Test Method*. Electronic Fund of Legal and Regulatory and Technical Documents. (In Russ.) URL: <https://docs.cntd.ru/document/1200011117?ysclid=mdoi2gfjlh811854453> (accessed: 21.06.2025).

¹² GOST 1497–84. *Metals. Methods of Tension Test. Specifications*. Electronic Fund of Legal and Regulatory and Technical Documents. (In Russ.) URL: <https://docs.cntd.ru/document/1200004888> (accessed: 21.06.2025).

¹³ GOST 28840–90. *Machines for Tension, Compression and Bending Testing of Materials. General Technical Requirements*. Electronic Fund of Legal and Regulatory and Technical Documents. (In Russ.) URL: <https://docs.cntd.ru/document/1200023577> (accessed: 21.06.2025).

¹⁴ GOST 9013–59. *Metals. Method of Measuring Rockwell Hardness*. Electronic Fund of Legal and Regulatory and Technical Documents. (In Russ.) URL: <https://docs.cntd.ru/document/1200004663?ysclid=mdpkinhrw605168957> (accessed: 21.06.2025).

¹⁵ GOST 9450–76. *Measurements Microhardness by Diamond Instruments Indentation*. Electronic Fund of Legal and Regulatory and Technical Documents. (In Russ.) URL: <https://docs.cntd.ru/document/1200012869?ysclid=mdpkn680t1373636400> (accessed: 21.06.2025).

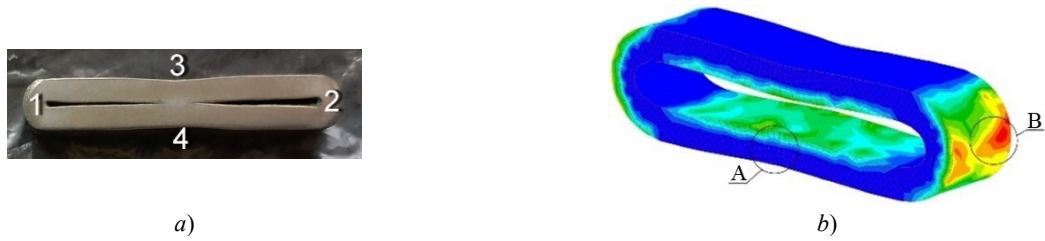


Fig. 3. Radial upsetting of annular samples:

a — 10Kh18N9 rolled steel; *b* — simulation of radial upsetting from dispersed VP 304.200.30 powder

The hardness in different zones of the ring samples differed significantly. For example, in tension zones 1 and 2 for ring samples made of 10Kh18N9 steel, the hardness varied from 190 HV to 205 HV. The indicator for VP 304.200.30 sintered steel was 130–140 HV. In compression zones 3 and 4, the hardness was slightly higher: 210–230 HV for 10Kh18N9 and 185–195 HV for VP 304.200.30.

This could be explained by the fact that the stress-strain state of the material depended on the configuration of the workpieces before and after radial upsetting. In zone A (3 and 4), the material strengthened better as a result of plastic deformation (work hardening) than in tension zones B (1 and 2) (Fig. 3 *b*).

It is known from [11] that when upsetting sintered ring samples with an austenitic structure and porosity of 18–20% (Fig. 4 *a*), cracks appear at the interparticle boundaries with increased concentrations of Cr₂O₃, CrO₂ (Fig. 4 *b*). The analysis of the results from mapping the crack mouth showed that microcracks were developing:

- along interparticle boundaries with a higher concentration of O;
- in areas with heterogeneous chemical composition (Fig. 4 *c*).

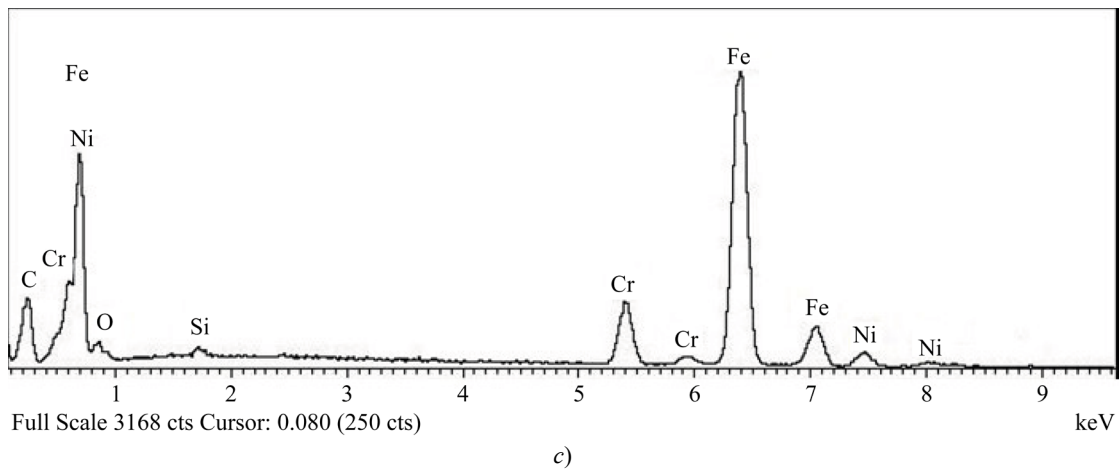
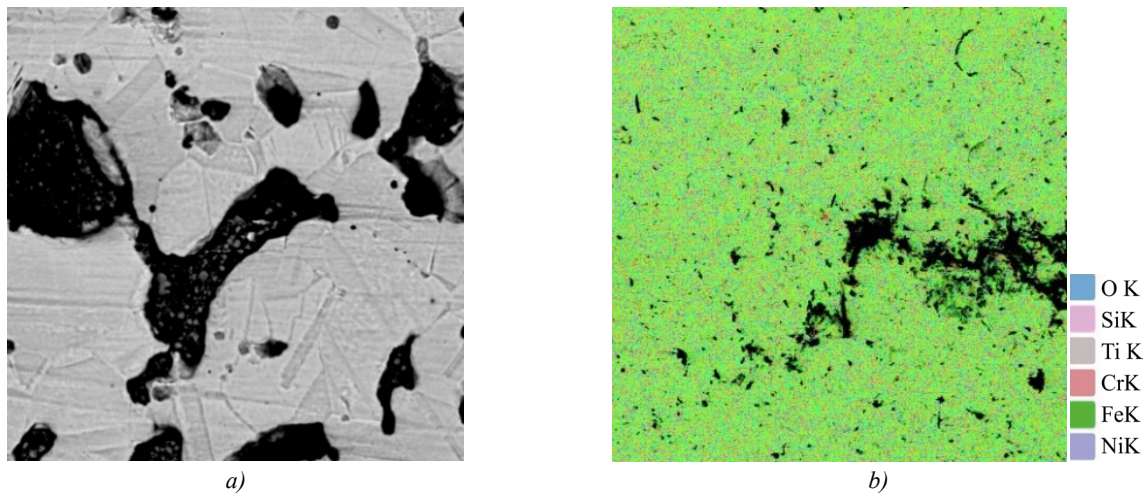


Fig. 4. Mapping of a sintered ring sample made of VP powder 304.200.30 (Si — 0.7, Cr — 12.2, Fe — 75.5, Ni — 7.90, O — 3.7): *a* — microstructure before testing; *b, c* — distribution of chemical elements in the crack mouth after radial deformation

Plastic properties of sintered steels were particularly strongly influenced by the distribution of chromium oxides and carbides in areas of intense plastic deformation. This was confirmed by the mapping of microsection sites at the crack mouth (Fig. 5).

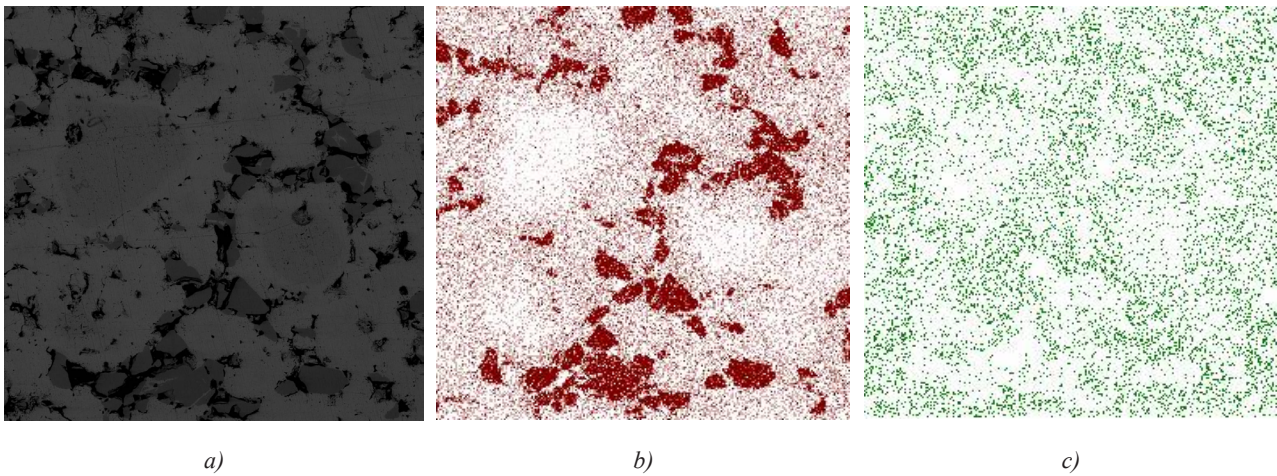


Fig. 5. Mapping of sintered VP 304.200.30 chromium-nickel steel:
a — microstructure; *b, c* — distribution of Cr and Ni

In the 10Kh18N9 rolled steel samples, the steel structure was more homogeneous in chromium and nickel (Fig. 6 *a*). The content of foreign inclusions was significantly less than in sintered steel from dispersed powders with similar compositions (Fig. 6 *b, c*).

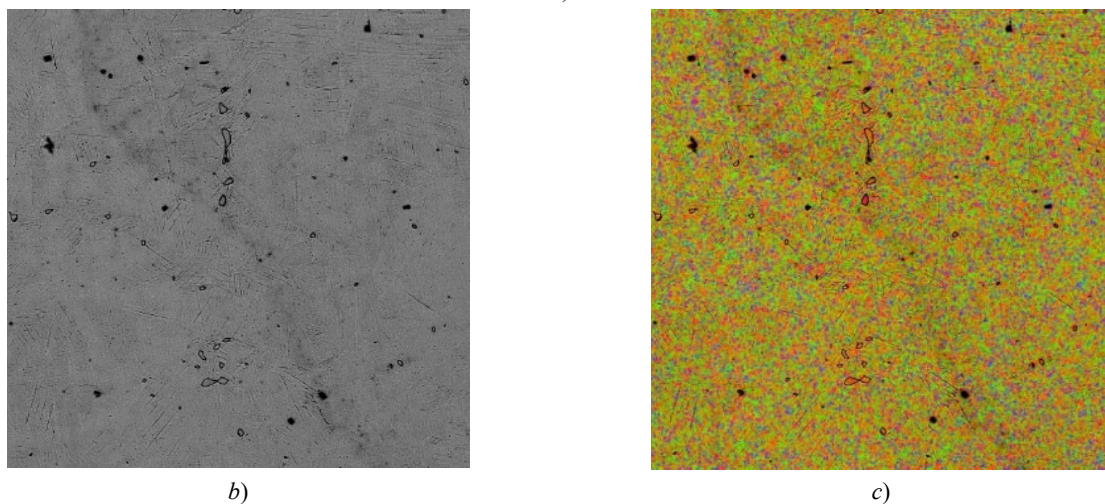
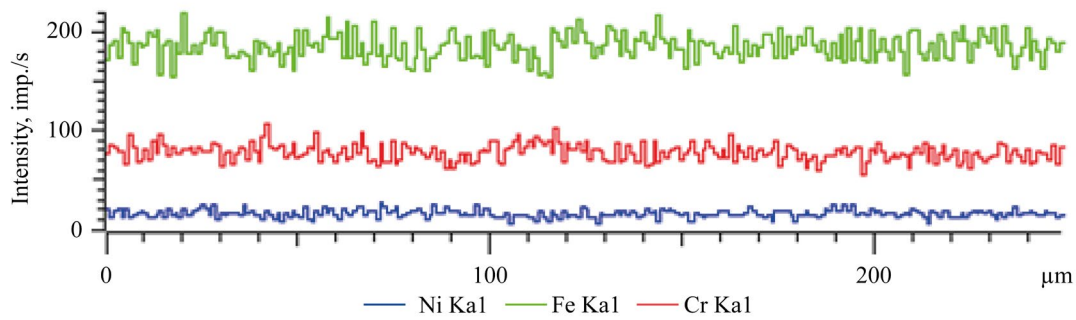


Fig. 6. Mapping of 10Kh18N9 steel:
a — distribution of Cr and Ni; *b, c* — microstructure

When ring samples were upset, the shear deformation of the material was provided by various mechanisms. Their contribution was determined by the scheme and degree, size, grain shape and porosity of the workpieces before deformation, chemical and phase composition of the material (Fig. 7 *a*), properties and size of excess phases and other conditions.

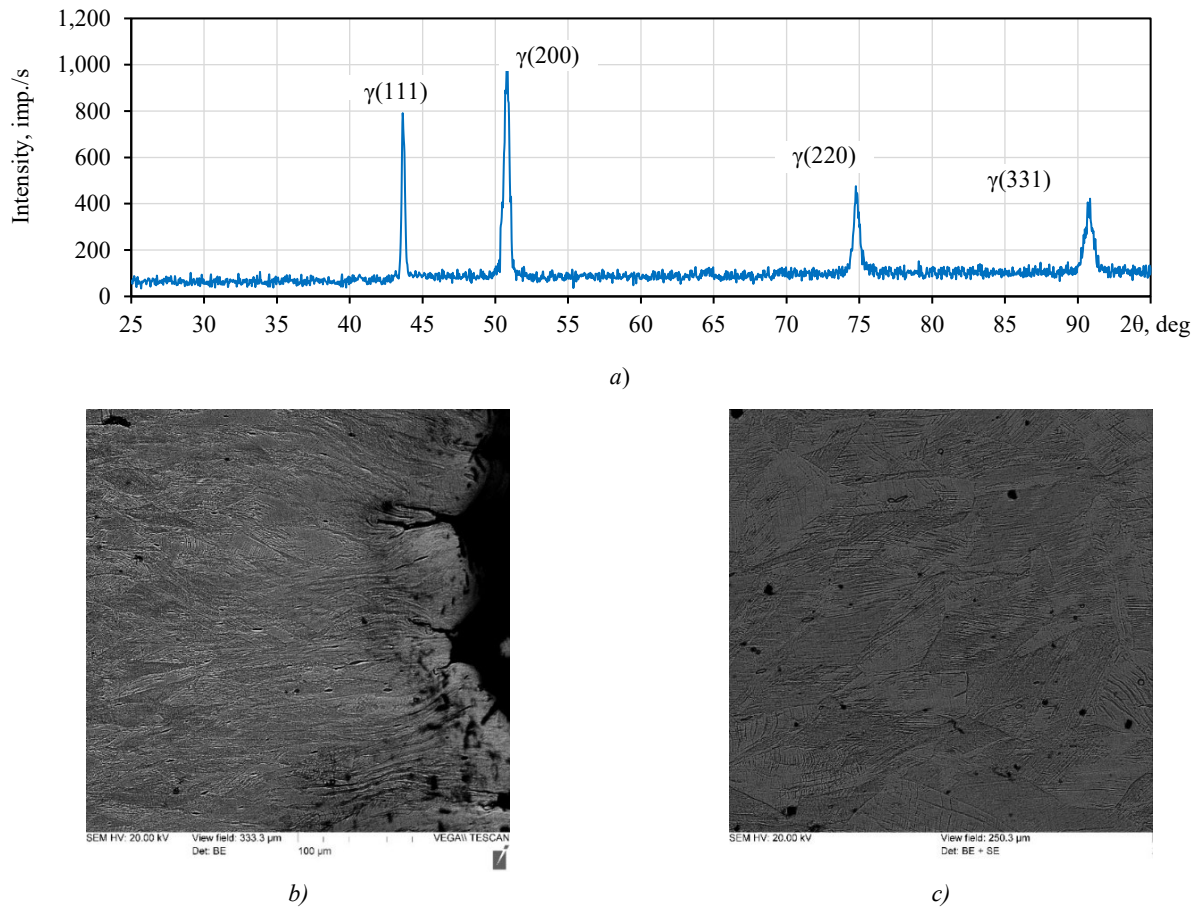


Fig. 7. Phase analysis and microstructure of 10Kh18N9 rolled steel:
a — diffractogram after radial compression; *b* — microstructure of rings in the compression zone;
c — microstructure in the stretching zone after upsetting $\epsilon_R = 63\%$

Therefore, lineage structure in certain sections, characteristic of rolled chromium-nickel steels of the austenitic class (Fig. 7 *a*), not only reduced their plastic properties, but also affected the kinetics of microstructure formation after cold stamping. Inhomogeneous deformation in different parts of the sample was the cause of twinning, deformation bands, and transition bands (Fig. 7 *b, c*).

The mechanical properties of sintered blanks made of VP 304.200.30 chromium-nickel steel powders were influenced by several factors:

- the initial microstructure and the presence of foreign inclusions;
- the microstructure and chemical composition of the particles formed during the melt sputtering and cooling of the powder particles.

Apparently, upon rapid cooling, stable α -phase nuclei with an increased concentration of iron were formed in liquid melt droplets (Fig. 8 *a*). In particular, such spherical particles (Table 1, Fig. 8, Spectrum 3) contained about 91% (at.) of iron, while nuclei of other particles (Table 1, Fig. 8, Spectrum 2) contained about 80%. In other areas of the same particles, the Cr content reached 74% (at., Table 1, Fig. 8, Spectrum 1). This was several times higher than its average concentration in steel powders. In this case, the word “spectrum” refers to the place and order of spike on the examined microsection.

Table 1

Distribution of chemical elements in sintered steel of VP 304.200.30 powder on various sections of particles in samples before cold stamping

Spectrum	Si	Cr	Mn	Fe	Ni	Total
1	0.07	74.63	0.70	24.29	0.31	100
2	2.24	10.25	0.31	80.22	6.99	100
3	1.03	6.12	0.09	91.28	1.49	100

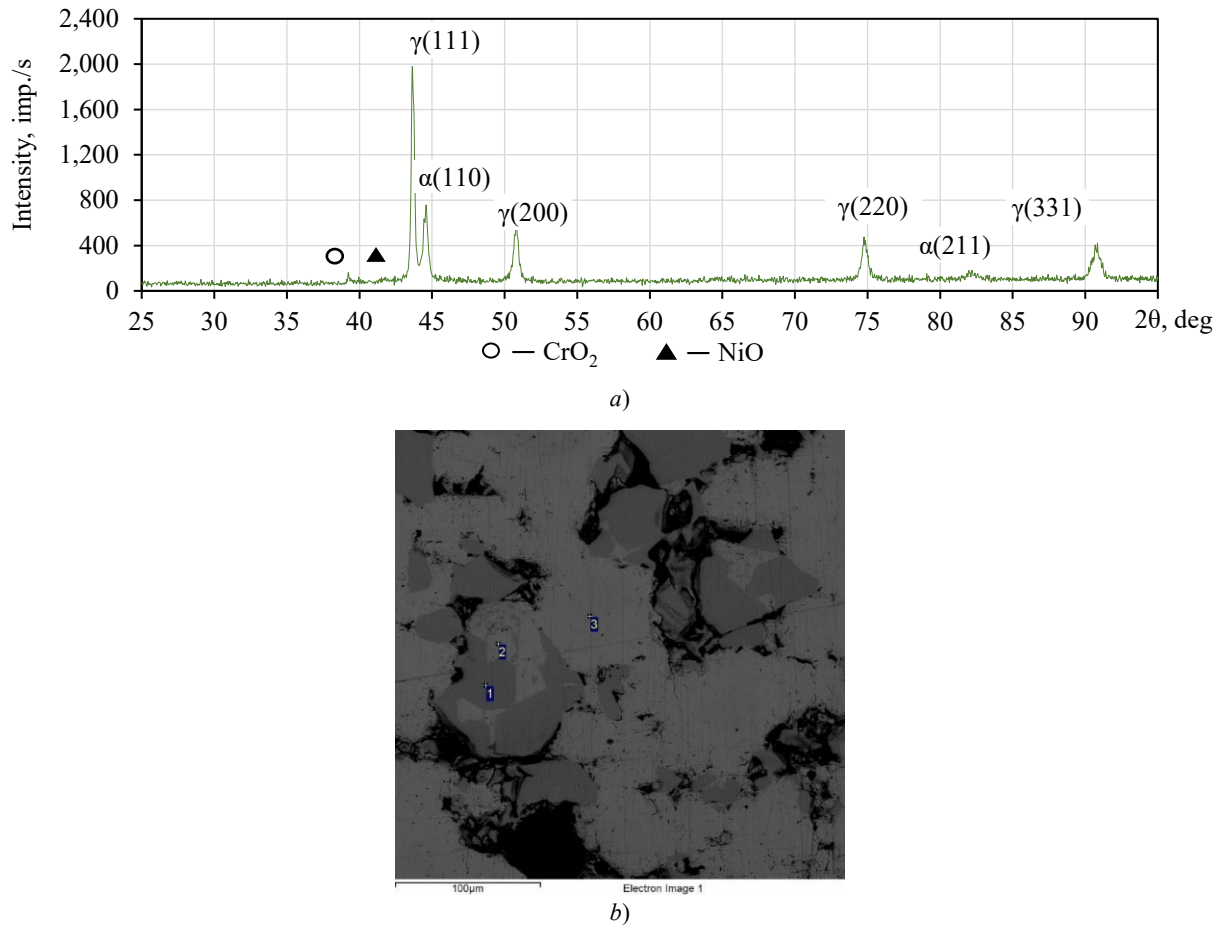


Fig. 8. Phase composition and microstructure of samples before cold stamping in sintered steel of VP powder 304.200.30: *a* — diffractogram; *b* — distribution of chromium, nickel and other elements

During sintering of the samples from dispersed VP 304.200.30 powder at a temperature of 1150–1180°C for 2 hours, diffusion homogenization occurred. Chromium, nickel, and iron were mutually dissolved and distributed more evenly over the volume (Fig. 9), which generally affected the ductility of the blanks sintered in vacuum.

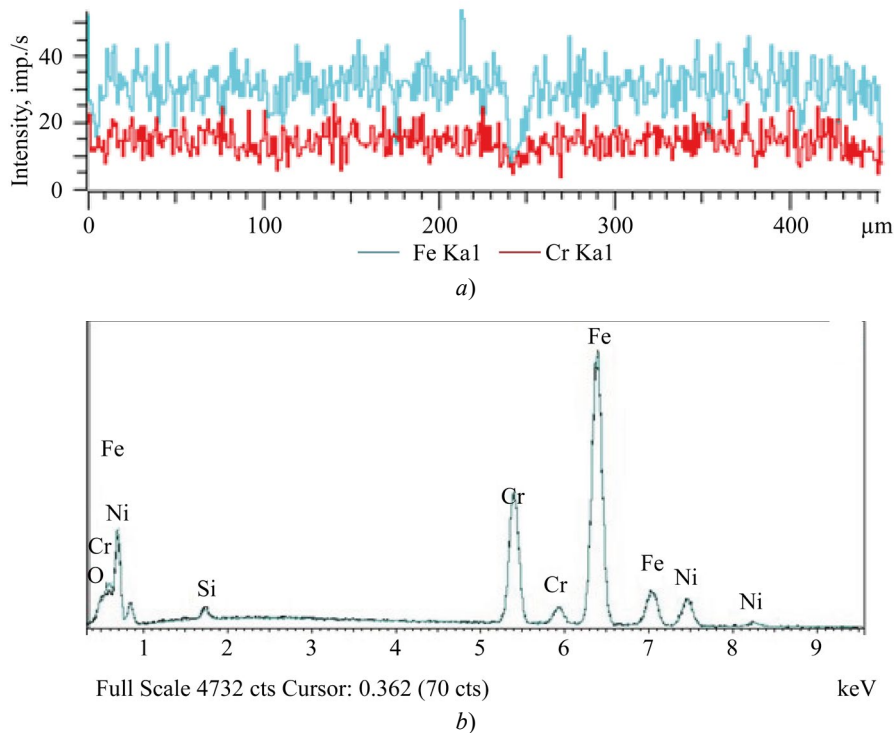


Fig. 9. Distribution of chemical elements in sintered steel of VP 304.200.30 powder: *a* — linear distribution of Cr and Fe; *b* — spectral analysis of Cr, Ni and other elements

The larger the pore in the interparticle boundaries, the greater the difference in particle deformation, especially with small medium deformations of the material. Therefore, the microstructure of sintered steel after upsetting and, consequently, the microhardness differed markedly in different areas of the same zone (Fig. 10).

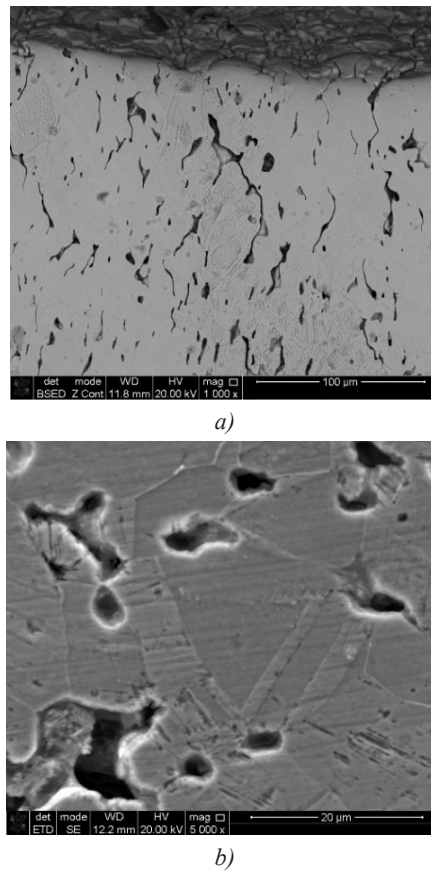


Fig. 10. Microstructure of sintered VP 304.200.30 steel:
a — compression zone (A); *b* — stretching zone (B) after upsetting $\epsilon_R \approx 0.5$

The tensile strength of vacuum-sintered steels made of VP 304.200.30 powder was comparable to the strength and yield strength of some austenitic chromium-nickel steels, but inferior to them in terms of ductility (Table 2).

Table 2

Physical-mechanical properties of chromium-nickel corrosion-resistant steels

Material	Properties					
	σ_s , MPa	δ , %	Ψ , %	Π , %	ρ , g/cubic cm	Hardness
10Kh18N9	195.00	45.00	55.00	–	7.90	29 HRC
VP 304.200.30	180.63	7.67	8.08	19.05	6.65	45 HRB

Thus, an analysis of the fracture mechanism during upsetting of rings made of stainless chromium-nickel steels revealed that the strength and ductility of sintered steel in the tensile zone depended not only on the stress-strain state of the material. In this case, two more factors were important:

- the quality of the contact between the particles;
- the presence of foreign inclusions on the surface of the dispersed powders.

Modeling of the cold stamping process of an outer cage with a spherical hinge flange in the *QForm* program (Fig. 11) gave an idea of the kinetics of shaping [15]. Sintered cylindrical blanks made of VP 304.200.30 powder were used. The zone highlighted in dark green had a minimum plasticity resource. This was where macro- and micro-cracks could originate.

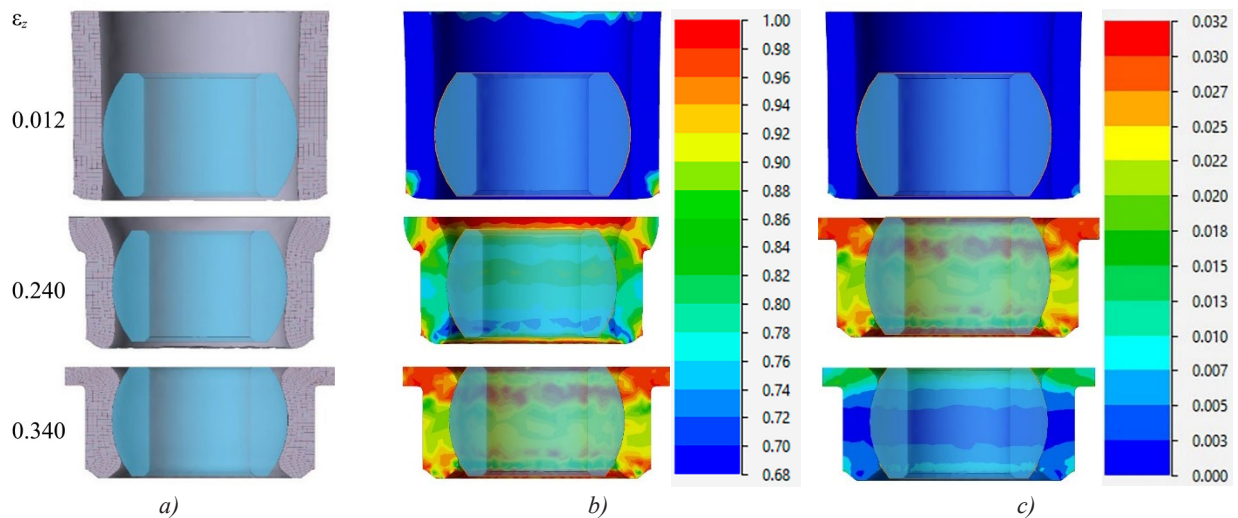


Fig. 11. Simulation modeling of the kinetics of forming an outer cage with a flange of a porous blank in the *QForm* program: *a* — change in the coordinate grid; *b* — volume distribution of relative density; *c* — plasticity resource

In Figure 11 ε_z is a dimensionless quantity. This is a relative degree of deformation, that is, the ratio of the absolute deformation (change in size) to the original length of the body. During the modeling process, a coordinate grid was applied to the sample, and during deformation, the material was distorted, as can be seen in Figure 11. The figure shows the direction in which the material moved during deformation.

A comparison of 10Kh18N9 rolled steel and VP 304.200.30 powder steel revealed fundamental differences in the deformation mechanisms. For powder steel, the critical limitation was not the oxide phase, but the localization of oxides at the particle boundaries, which provoked brittle fracture under tension. The chemical heterogeneity of the particles and the residual porosity exacerbated the problem: in comparison with rolled steel, the elongation decreased by 6 times (see the indicator δ in Table 2). At the same time, under compression conditions, the sintered material hardened to 195 HV, and this indicated the possibility of its use in the manufacture of external spherical hinges.

Discussion. To conclude, during the deformation of sintered workpieces, the intensity of stress fields in the contact zones of powder particles and on the pore surfaces differed significantly from the average values. According to [11], the critical value of the strain intensity during radial upsetting of ring samples made of VP 304.200.30 powder was 0.195. This caused inhomogeneity of deformations, and also prevented the determination of the deformed state by the plasticity condition (if the stress state is known). The patterns of the main deformations determined the uneven and anisotropic nature of changes in the mechanical properties of the sintered parts during cold stamping. Therefore, the plasticity resource was affected not only by the porosity, but also by the deformed state of the material. This has been confirmed experimentally.

The analysis of the deformation behavior of sintered and rolled steels, as described in the article, confirmed the validity of the proposed method for assessing the deformed state of cylindrical blanks during cold stamping of the outer cages of spherical hinges. Practical application of the results from this study will enhance the efficiency of chromium-nickel steel manufacturing processes. Based on the findings of the scientific research presented in the article, it appears that this material would be an ideal choice for spherical hinges.

Conclusion. The revealed mechanism of sintered chromium-nickel steel destruction during cold stamping allows us to estimate the critical strain intensity values and the effect of steel structure on its tensile ductility in this zone.

We have established that the plasticity resource of sintered chromium-nickel stainless steels depends not only on the stress-strain state of the material, but also on the initial structure, the presence of impurities, as well as the quality of interparticle contacts and grain boundaries.

Our research focused on the qualitative features of spherical hinges used in vehicle suspensions. Experimental and simulation studies have revealed the technological aspects of their production through cold stamping of sintered workpieces.

References

1. Mikhailov AN, Matvienko SA, Strel'nik YuN, Lukichev AV. Functionally-Oriented Analysis of the Operating Conditions and Production Technologies of Transport Vehicles Spherical Swivel Connections. In: *Proceedings of the International Scientific and technical conference "Technical operation of Water Transport: Problems and Ways of Development" Petropavlovsk-Kamchatsky, 17–19 October, 2018*. Petropavlovsk-Kamchatsky: Kamchatka State Technical University; 2019. P. 112–115. (In Russ.)

2. Haidorov AD, Yunusov FA. Vacuum Heat Treatment of high Alloy Corrosion-Resistant Steels. *St. Petersburg Polytechnic University Journal of Engineering Sciences and Technology*. 2017;23(1):226–235. (In Russ.) <http://doi.org/10.18721/JEST.230123>
3. Woodhead J, Truman CE, Booker JD. Modelling of Dynamic Friction in the Cold Forming of Plain Spherical Bearings. *Surface and Contact Mechanics Including Tribology XII*. 2015;91:141–152. <http://doi.org/10.2495/SECM150131>
4. Ilyuschenko AF. Current Developments in Powder Metallurgy for Mechanical Engineering. *Mechanics of Machines, Mechanisms and Materials*. 2012;(3(20)–4(21)):113–120. (In Russ.) URL: https://mmmm.by/pdf/ru/2012/3_4_2012/11.pdf (accessed: 02.06.2025).
5. Hojati M, Danninger H, Gierl-Mayer Ch. Mechanical and Physical Properties of Differently Alloyed Sintered Steels as a Function of the Sintering Temperature. *Metals*. 2022;12(1):13–20. <https://doi.org/10.3390/met12010013>
6. Bram M, de Freitas Daudt N, Balzer H. Porous Metals from Powder Metallurgy Techniques. *Encyclopedia of Materials: Metals and Alloys*. 2022;3:427–437. <https://doi.org/10.1016/B978-0-12-819726-4.00093-4>
7. Lingzhu Gong, Xiaoxiang Yang, Kaibin Kong, Shuncong Zhong. Optimal Design for Outer Rings of Self-Lubricating Spherical Plain Bearings Based on Virtual Orthogonal Experiments. *Advances in Mechanical Engineering*. 2018;10(6):1–11. <https://doi.org/10.1177/1687814018783402>
8. Gasanov BG, Konko NA, Baev SS. Study of the Kinetics of Forming of Spherical Sliding Bearing Parts Made of Corrosion-Resistant Steels by Die Forging of Porous Blanks. *Metal Working and Material Science*. 2024;26(2):127–142. (In Russ.) <http://doi.org/10.17212/1994-6309-2024-26.2-127-142>
9. Rozenberg OA, Mikhailov OV, Shtern MB. Strain Hardening of Porous Bushings by Multiple Mandreling: Numerical Simulation. *Powder Metallurgy and Metal Ceramics*. 2012;51:379–384. <http://doi.org/10.1007/s11106-012-9445-y>
10. Kondo H, Hegedus M. Current Trends and Challenges in the Global Aviation Industry. *Acta Metallurgica Slovaca*. 2020;26(4):141–143. <https://doi.org/10.36547/ams.26.4.763>
11. Gasanov BG, Konko NA, Baev SS. The Effect of the Method for Producing Chromium-Nickel Stainless Steel Powders on the Strain State and Properties of the Outer Cage of a Spherical Hinge Joint. *Diagnostics, Resource and Mechanics of Materials and Structures*. 2024;5:138–158. (In Russ.) <https://doi.org/10.17804/2410-9908.2024.5.138-158>
12. Kovalchenko MS. Deformation Hardening of a Powder Body during Pressing. *Powder Metallurgy*. 2009;(3/4):13–27. (In Russ.)
13. Egorov MS, Egorova RV, Pustovoi VN, Atrokhov AA. Mechanical Properties of Powder Materials after Hot Forging. *Metallurg*. 2020;3:92–96. (In Russ.)
14. Burlakov IA, Zabelyan DM, Bondarenko AK, Gladkov YuA, Leonidov AN. Efficient Utilization of the Plasticity Resource at Cold Forming of Sheet Workpieces Based on the Cockroft and Kolmogorov Criteria. *Forging and Stamping Production. Material Working by Pressure*. 2016;(12):3–8. (In Russ.)
15. Baglyuk GA, Kurikhin VS, Khomenko AI, Kozachenko IS. Improving Methods for Studying the Strain Distribution in Powders During Compaction. *Powder Metallurgy and Metal Ceramics*. 2015;54:129–135. (In Russ.) <https://doi.org/10.1007/s11106-015-9689-4>

About the Authors:

Nikolai A. Konko, Assistant Professor of the Department of General Engineering Disciplines, Platov South Russian State Polytechnic University (NPI) (132, Prosveshcheniya Str., Novochoerkassk, 346428, Russian Federation), [SPIN-code](#), [ORCID](#), [ResearcherID](#), konko2013@mail.ru

Badrudin G. Gasanov, Dr. Sci. (Eng.), Professor of the Department of International Logistics Systems and Complexes, Platov South Russian State Polytechnic University (NPI) (132, Prosveshcheniya Str., Novochoerkassk, 346428, Russian Federation), [SPIN-code](#), [ORCID](#), [ScopusID](#), gasanov.bg@gmail.com

Claimed Contributorship:

NA Konko: formal analysis, research, methodology, validation, visualization, writing – original draft preparation.

BG Gasanov: conceptualization, data curation, supervision.

Conflict of Interest Statement: the authors declare no conflict of interest.

All authors have read and approved the final manuscript.

Об авторах:

Николай Андреевич Конько, ассистент кафедры «Общественные дисциплины», Южно-Российского государственного политехнического университета (НПИ) имени М.И. Платова (346428, Российская Федерация, г. Новочеркасск, ул. Просвещения, 132), [SPIN-код](#), [ORCID](#), [ResearcherID](#), konko2013@mail.ru

Бадрудин Гасанович Гасанов, доктор технических наук, профессор кафедры «Международные логистические системы и комплексы» Южно-Российского государственного политехнического университета (НПИ) имени М.И. Платова (346428, Российская Федерация, г. Новочеркасск, ул. Просвещения, 132), [SPIN-код](#), [ORCID](#), [ScopusID](#), gasanov.bg@gmail.com

Заявленный вклад авторов:

Н.А. Конько: формальный анализ, проведение исследования, разработка методологии, валидация результатов, визуализация, написание черновика рукописи.

Б.Г. Гасанов: создание концепции, курирование работы с данными, научное руководство.

Конфликт интересов: авторы заявляют об отсутствии конфликта интересов.

Авторы прочитали и одобрили окончательный вариант рукописи.

Received / Поступила в редакцию 30.06.2025

Reviewed / Поступила после рецензирования 14.07.2025

Accepted / Принята к публикации 25.07.2025

**CHEMICAL TECHNOLOGIES,
MATERIALS SCIENCES, METALLURGY
ХИМИЧЕСКИЕ ТЕХНОЛОГИИ,
НАУКИ О МАТЕРИАЛАХ, МЕТАЛЛУРГИЯ**



UDC 669.1:66.04

Original Empirical Research

<https://doi.org/10.23947/2541-9129-2025-9-3-242-249>

Influence of the Magnetic Field on the Behavior of Cracks in Steel after Heat Treatment to a High-Strength State

Viktor N. Pustovoyt , Yuri V. Dolgachev  

Don State Technical University, Rostov-on-Don, Russian Federation

 ydolgachev@donstu.ru



EDN: OIJHCO

Abstract

Introduction. Fatigue failure develops at stresses below the ultimate strength and is characterized by its suddenness and catastrophic consequences. Statistical data indicate that failure under cyclic loading is one of the common types of damage to materials and their performance is largely determined by their resistance to crack growth. In addition to well-known methods for achieving high-strength states, it has been proposed to use heat treatment in the magnetic field (HTMF). However, the mechanisms of crack behavior changes after such treatment and factors affecting crack resistance remain poorly understood. In this regard, this study aims to assess the effect of the structure after HTMF on the kinetic features of fatigue crack growth and the effectiveness of structural barriers formed during HTMF, preventing the destruction of steel.

Materials and Methods. The kinetics of fatigue crack development was studied during cyclic testing of prismatic samples using an original setup with a special stabilizer of oscillation amplitude. The occurrence and subsequent development of a crack was recorded by the method of electric potentials. The studies were conducted on steels that had been heat-treated to achieve a high-strength state: 18Kh2N4VA steel after quenching in air with a martensite structure and 30KhGSA steel after isothermal quenching at 380°C to a lower bainite structure. A magnetic field of 1.6 MA/m was obtained in the magnetic gap of the FL-1 electromagnet.

Results. It was found that heat treatment of 30KhGSA and 18Kh2N4VA steels in a magnetic field of 1.6 MA/m led to a noticeable decrease in the rate of fatigue crack propagation. An increase in the threshold stress values for the delamination of the main crack by the tear-off mechanism was noted, which indicated an increase in durability. When analyzing the crack trajectories, an increase in their branching indicators was revealed: an increase in the standard deviation of crack inclination angles, as well as a decrease in the correlation interval of the crack bend inclination relative to the average position by 0.5 μm. These changes were due to the effect of the magnetic field on the microstructure of martensite, the formation of a greater number of effective barriers on the path of crack movement, which ultimately affected the resistance to fatigue failure of steels and their mechanical properties.

Discussion. Analysis of the obtained results, based on modern theories of strength and fracture, revealed that the mechanism of viscous destruction, which was typical for the steels under study, worked by the origin, growth and coalescence of pores. Under the influence of normal stresses, vacancies settled on the surface of micropores and as a result, the pore gradually transformed into a crack. Observations of cracks in foils showed that the change in the crack trajectory did not depend on the type of heat treatment and was a random process.

Conclusion. The statistical data obtained in this study allow us to conclude that after HTMF, a structure is formed that leads to an increase in the micro-tortuosity of cracks, with a steeper trajectory of bends due to frequent structural barriers. These features of crack behavior suggest that HTMF is a practical method for achieving a high-strength state in steels, which can be applied to a wide range of steel grades without requiring significant changes to their heat treatment processes. By increasing the crack resistance of steels, we can improve the safety of various devices and man-made systems, as well as reduce their costs and maintenance requirements.

Keywords: steel, high-strength condition, magnetic field, fatigue failure, cracks

Acknowledgments. The authors would like to thank the editorial board of the journal for their insightful comments and to the staff of the Department of Materials Science and Technology of Metals for their assistance in obtaining and reviewing the results.


For Citation. Pustovoyt VN, Dolgachev YuV. Influence of the Magnetic Field on the Behavior of Cracks in Steel after Heat Treatment to a High-Strength State. *Safety of Technogenic and Natural Systems*. 2025;9(3):242–249. <https://doi.org/10.23947/2541-9129-2025-9-3-242-249>

Оригинальное эмпирическое исследование

Влияние магнитного поля на особенности поведения трещин в стали после термической обработки на высокопрочное состояние

В.Н. Пустовойт , Ю.В. Долгачев  

Донской государственный технический университет, г. Ростов-на-Дону, Российская Федерация

 ydolgachev@donstu.ru

Аннотация

Введение. Усталостное разрушение происходит при напряжениях ниже предела прочности, характеризуясь внезапностью и катастрофическими последствиями. Статистические данные свидетельствуют о том, что разрушение при циклическом нагружении является одним из наиболее распространённых видов повреждений материалов, а их работоспособность во многом определяется сопротивлением росту трещин. Кроме уже известных методов достижения высокопрочного состояния, предлагается использовать термическую обработку в магнитном поле (ТОМП). Тем не менее, механизмы изменения поведения трещин после такой обработки и факторы, влияющие на трещиностойкость, всё ещё недостаточно изучены. В связи с этим поставлена цель оценить влияние структуры после ТОМП на кинетические особенности роста усталостных трещин и эффективность образуемых в процессе ТОМП структурных барьеров, препятствующих разрушению стали.

Материалы и методы. Кинетику развития усталостной трещины исследовали при циклических испытаниях призматических образцов на оригинальной установке со специальным стабилизатором амплитуды колебаний. Возникновение и последующее развитие трещины регистрировали методом электропотенциалов. Исследования проводили на сталях, термически обработанных на высокопрочное состояние: сталь 18Х2Н4ВА после закалки на воздухе со структурой мартенсита и сталь 30ХГСА после изотермической закалки при 380 °С на структуру нижнего бейнита. Магнитное поле напряженностью 1,6 МА/м получали в магнитном зазоре электромагнита ФЛ–1.

Результаты исследования. Установлено, что термическая обработка сталей 30ХГСА и 18Х2Н4ВА в магнитном поле напряженностью 1,6 МА/м приводит к заметному снижению скорости распространения усталостных трещин. Отмечено повышение пороговых значений напряжений для расслоения магистральной трещины по отрывному механизму, что свидетельствует о повышении долговечности. При анализе траекторий трещин был выявлен рост показателей их ветвления — увеличение стандартного отклонения углов наклона трещин, а также уменьшение интервала корреляции наклона изгибов трещины относительно среднего положения на 0,5 мкм. Эти изменения обусловлены влиянием магнитного поля на микроструктуру мартенсита, формированием большего числа эффективных барьеров на пути движения трещин, что в итоге сказывается на устойчивости к усталостному разрушению сталей и их механических свойствах.

Обсуждение. Анализ полученных результатов на основе современных теорий прочности и разрушения показал, что механизм вязкого разрушения, который характерен для исследуемых сталей, работает путём зарождения, роста и коалесценции пор. Под действием нормальных напряжений на поверхности микропор оседают вакансии и в результате этого пора постепенно трансформируется в трещину. Наблюдения за трещинами в фольгах показали, что изменение траектории трещины не зависит от вида термической обработки и является случайным процессом.

Заключение. Статистическая обработка опытных данных, полученных в этой работе, позволяет сделать вывод, что после ТОМП формируется структура, обеспечивающая увеличение микроизвилистости трещины с повышенной крутизной изгибов траектории из-за часто встречающихся структурных барьеров. Выявленные особенности поведения трещин положительно характеризуют ТОМП как практический способ создания высокопрочного состояния сталей, применимый для широкого ассортимента марок и не требующий кардинальных изменений в технологии их термической обработки. Повышение трещиностойкости сталей способствует улучшению безопасности различных устройств и техногенных систем, а также снижению их себестоимости и затрат на обслуживание.

Ключевые слова: сталь, высокопрочное состояние, магнитное поле, усталостное разрушение, трещины

Благодарности. Авторы благодарят редакцию журнала за ценные замечания и сотрудников кафедры «Материаловедение и технологии металлов» за помощь в получении и обсуждении результатов.

Для цитирования. Пустовойт В.Н., Долгачев Ю.В. Влияние магнитного поля на особенности поведения трещин в стали после термической обработки на высокопрочное состояние. *Безопасность техногенных и природных систем.* 2025;9(3):242–249. <https://doi.org/10.23947/2541-9129-2025-9-3-242-249>

Introduction. Destruction under cyclic loading is one of the most common types of damage to materials. The performance of these materials is largely determined by their resistance to crack growth. The problem is that cyclic loads can cause fatigue failure even at stresses below the ultimate strength of the material. Although the growth of a fatigue crack occurs gradually, the fracture itself can occur suddenly, leading to catastrophic consequences. There are extensive statistics [1] on railway and plane crashes, bridge collapses, and man-made accidents caused by the development of such defects. According to ASM International [2], up to 90% of mechanical failures in mechanical engineering are due to fatigue. In the oil and gas industry, billions of dollars are lost annually due to fatigue cracks in pipelines and drilling rigs. To address this issue, non-destructive defect control methods are introduced. These methods can account for up to 30% of maintenance costs in the aerospace industry. To ensure safe and long-term operation of machine parts and devices, it is essential to achieve their high-strength state with increased crack resistance.

Known methods of achieving a high-strength state [1, 2] involve combining a specific alloy composition with heat treatment methods, minimizing the presence of non-metal inclusions, creating a heterogeneous microstructure, and using surface hardening techniques. Previously, researchers have proposed a technology of heat treatment in a magnetic field (HTMF) [3], which allows for the creation of a high-strength state in steels under certain conditions. A feature of the proposed technology is an increase in strength characteristics without reducing viscosity. At the same time, widely used grades of alloy steels are subjected to almost traditional heat treatment modes, but with the application of permanent magnetic field energy.

Existing methods for increasing crack resistance [1, 2] operate by the following mechanisms: increasing the area of plastic deformation at the crack tip; branching the crack trajectory (increasing its path); creating compressive stresses to slow down crack growth; local hardening along the crack path; reducing the number and size of stress concentrators; creating microstructural barriers. However, there is still not enough information about how cracks behave in steels that have been treated with permanent magnetic fields. Therefore, the aim of this research is to investigate how the resistance to cracks and the rate of crack growth change after HTMF.

Materials and Methods. The features of crack development over time were studied using an installation that creates cyclic oscillations with stabilized amplitude. The design of this installation was described in [4]. The method of electric potentials [5, 6] made it possible to record the moment of origin and the stages of development of fatigue cracks. The data obtained in this way was transferred into real values using a calibration diagram that had known data on crack length and prismatic sample size.

The research results are presented in the form of dependencies with $dl/dN - lg\Delta K$ axes [2, 7], characterizing the development of fatigue failure. The value of dl/dN ratio determines the exponential rate of crack propagation over a certain number of load cycles. Parameter ΔK demonstrates the range of variation of the stress intensity coefficient (SIC) under cyclic loads and is calculated as the difference between the highest and lowest SIC values:

$$\Delta K = K_{lcmax}^II - K_{lcmin}^II. \quad (1)$$

K_{lc}^II values were calculated in terms of the maximum stresses (σ), that occur during cyclic bending of a prismatic sample with a crack of length l , according to the formula:

$$K_{lc}^II = \sigma \sqrt{\pi \cdot l}. \quad (2)$$

Studies were conducted on prismatic samples of 18Kh2N4VA, 30KhGSA steels, which were heat-treated (18Kh2N4VA — air hardening for martensite; 30KhGSA — isothermal quenching at 38°C for lower bainite) for high-strength condition. A magnetic field with strength of 1.6 MA/m was in the magnetic gap of the FL – 1 electromagnet.

An Emma – 4 transmission electron microscope and a ZEISS CrossBeam 340 scanning electron microscope (SEM) were used to study the fine structure

Results. Figure 1 illustrates the dependence of the fatigue crack length on the number of test cycles after various treatments for the studied steels.

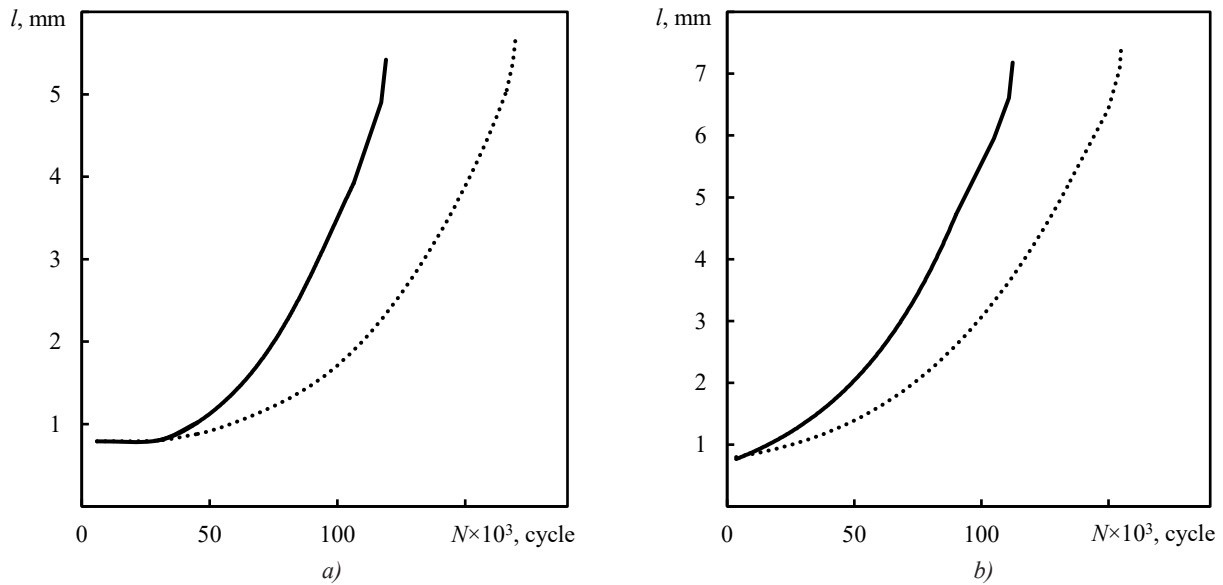


Fig. 1. Dependence of fatigue crack growth on the number of cycles of alternating bending of steels: *a* — 30KhGSA; *b* — 18Kh2N4VA; solid line — processing without a field; dotted line — in a 1.6 MA/m magnetic field.

Diagrams of the development of fatigue cracks over time are presented in Figure 2. Their appearance illustrates the three stages of crack development. At each of these stages, the crack has a certain propagation velocity: 1st stage — slow growth; 2nd stage — stable growth, and 3rd stage — accelerated or unstable growth [1]. Each of the stages is characterized by its own features of the fracture surface relief [2], which are well detected on the sample fracture after the cyclic bending test.

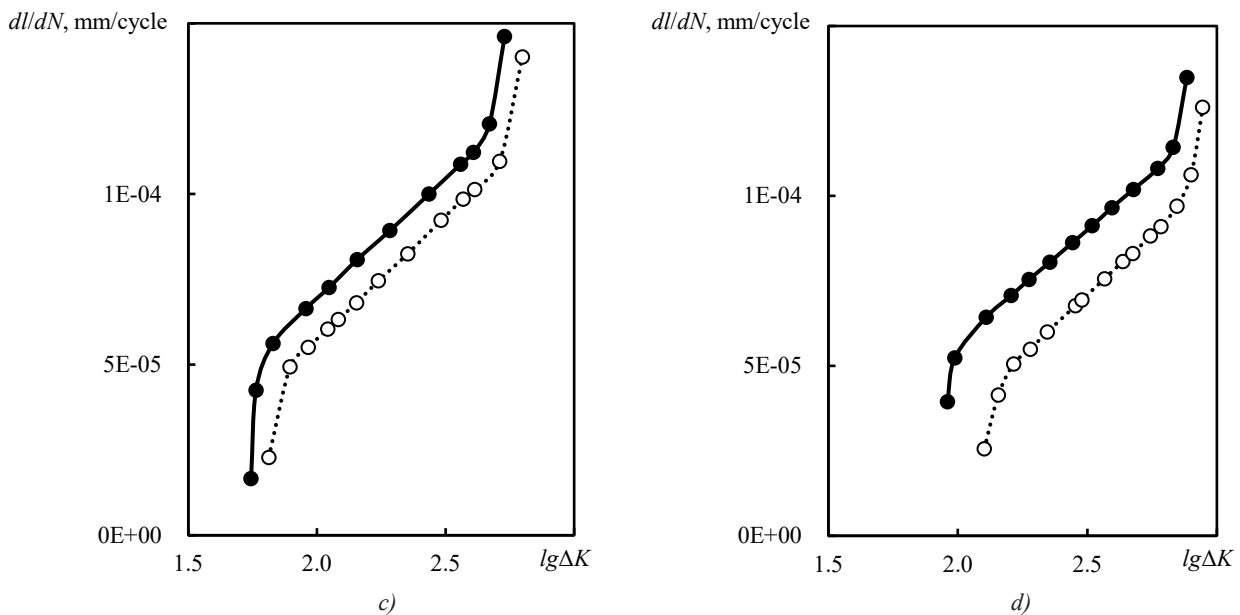


Fig. 2. Kinetic diagrams of fatigue crack development in steels: *a* — 30KhGSA; *b* — 18Kh2N4VA; solid line — processing without a field; dotted line — in a 1.6 MA/m magnetic field

It can be seen (Fig. 2) that the crack propagation rate significantly decreases after HTMF compared to the treatment without a field, while the range of SIC ΔK values remains commensurate. The fracture of the sample occurs with a longer cyclic crack length and a larger K_{Ic}^{II} value, as shown in Table 1. The numerator contains data for processing without a field, and the denominator contains data for processing in a field with a voltage of 1.6 MA/m. Confidence intervals are indicated with a confidence probability of $P = 0.95$ and the number of measurements $n = 5$.

Table 1

Parameters characterizing the viscosity during cyclic fracture

Steel	K_{lc}^{II}	K_0^{II}	l_{kp}, MM	Number of cycles before destruction $N \times 10^3$
	MH/m ^{3/2}			
18Kh2N4VA	70.1 ± 1.0	8.3 ± 0.4	6.74 ± 0.05	109 ± 10
	81.5 ± 1.0	9.9 ± 0.4	7.11 ± 0.05	153 ± 10
30KhGSA	51.1 ± 1.0	5.1 ± 0.3	4.92 ± 0.05	115 ± 10
	60.3 ± 1.0	6.3 ± 0.3	5.16 ± 0.05	168 ± 10

Figure 3 *a* illustrates the mechanism of viscous fracture by nucleation, growth, and coalescence of pores, which is typical for steels a18Kh2N4VA and 30KhGSA. Figure 3 *b* shows the result of how a crack forms from the pores under the influence of normal stresses.

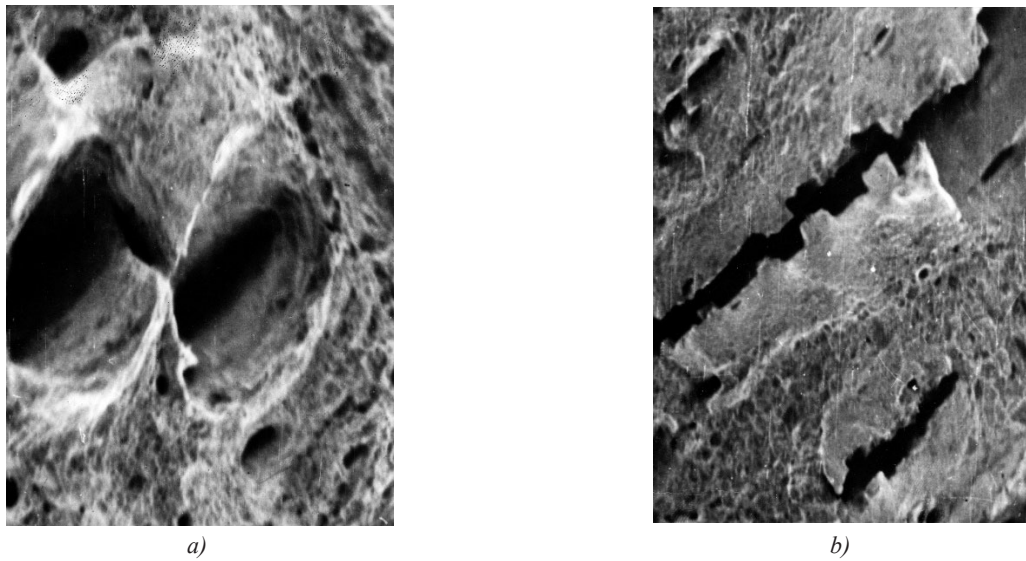


Fig. 3. The mechanism of crack formation in 30KhGSA steel (SEM):
a — fracture with pores ($\times 1,200$); *b* — transformation of pores into a crack ($\times 500$)

Figure 4 demonstrates the fragments of cracks under heat treatment conditions in a magnetic field and without a field. An analysis of such data was conducted to identify the dependence of the change in the crack trajectory on the type of heat treatment.

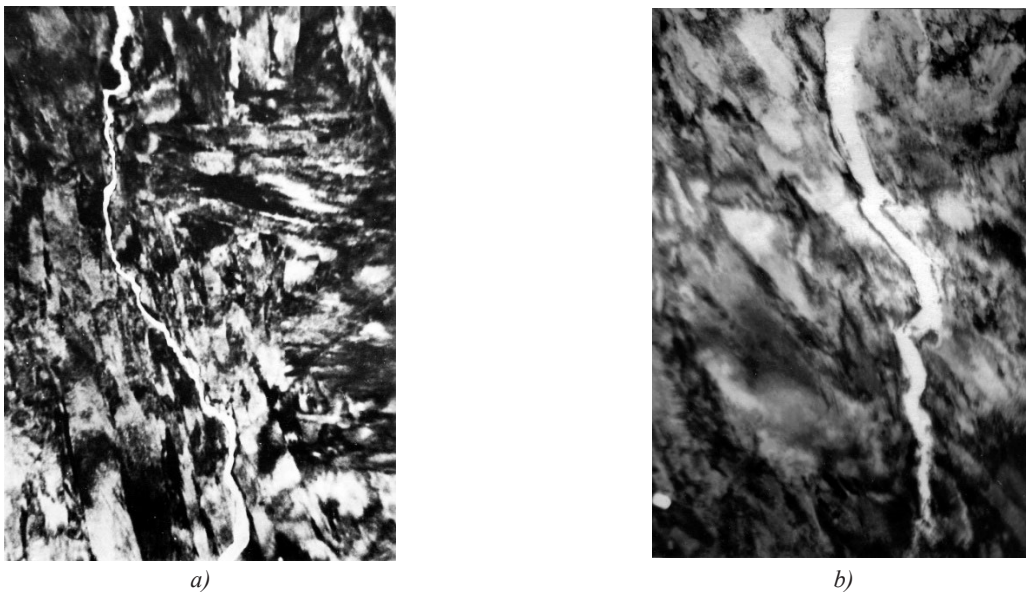


Fig. 4. Crack in the foil of 30KhGSA steel after quenching in oil ($\times 10,000$):
a — in a magnetic field; *b* — without a field

Discussion. The data in Figure 1 indicate that in the case of heat treatment in a magnetic field, the kinetics of crack propagation is more suppressed compared to treatment without a field, and the last stage of destruction occurs with a larger number of test cycles. Kinetic diagrams of fatigue crack development (Fig. 2) also demonstrate a significant decrease in the crack development rate under magnetic field treatment conditions while maintaining the SIC ΔK range. There are suggestions [8, 9] that in cyclic tests it is more expedient to characterize the viscosity by the initial (threshold) value of SIC K_0^{II} , corresponding to the beginning of the separation of the main crack by a tear-off mechanism (with a given degree of constraint on plastic deformation), rather than by the maximum value of SIC corresponding to the limiting state. As can be seen from Table 1, the value K_0^{II} increases after the HTMF. It is reasonable to anticipate an increase in the durability and operability of mechanical engineering products after heat treatment in a magnetic field [10, 11], which is also indicated by the results of previous studies on the effect of HTMF on mechanical properties [12, 13].

Monograph [3] summarizes the data that during processing to a high-strength state (the structure of upper martensite or lower bainite [14, 15]), the influence of a magnetic field manifests itself in significant fragmentation of the structure, increased dispersion of individual crystals of the ferromagnetic α -phase and their ensembles (packages), an increase in the specific surface area of the sub-boundaries that impede movement dislocations during loading. Local overstress at the tip of the dislocation cluster can relax through the formation of a crack nucleus, the development of which depends on the nature of the steel structure. Depending on the loading conditions and the initial state of the martensite [16, 17], the growth of a microscopic crack can occur by various mechanisms that determine the appearance of the fracture surface. It should be noted that for the 30KhGSA and 18Kh2N4VA steels under consideration, viscous fracture occurs when pores appear, grow, and combine (Fig. 3 a). Alternating loads lead to fatigue failure by forming a large number of excess vacancies (for example, as a result of inter-dislocation interactions and sliding with the formation of jogs [2, 18]), which can combine to form a pore. Normal stresses acting on the surface of the pore nuclei contribute to the vacancies sink, which leads to the transformation of the pores into a crack (Fig. 3 b).

The formed crack progress depends on the presence of obstacles in its path, which is determined by the features of the existing structure of the material. In this regard, the parameters of the crack propagation trajectory in thin foils were studied using electron microscopy, since they are very dependent on the structure [1]. The results of the fine structure analysis allow us to conclude that the use of HTMF technology does not affect the mechanism of changing the crack trajectory, i.e. the trajectory changes randomly (Fig. 4) when encountering various structural elements (carbides, phase boundaries, etc.) and does not depend on the method of heat treatment.

The autocorrelation functions analysis (AFA) [19, 20] linking the deviation of the crack line from its average position and the 1st derivative of its propagation trajectory (Fig. 5), which characterizes the angular parameters of the change in the trajectory of crack propagation in the foil, allows us to evaluate the effectiveness of the structural barriers caused by HTMF on the path of crack development. AFA allowed us to estimate the effect of HTMF on the statistical parameters of cracks: $K_x(0)$ — standard deviation of the crack line; $K'_x(0)$ — standard spread of the tangent of the trajectory angle (tortuosity index); $\tau_x(0)$ и $\tau'_x(0)$ — ranges of interdependence of the linear spread functions and slope tangents, respectively (they characterize an increase in crack length as a result of a single factor). The statistical parameters of cracks $K_x(0)$; $\tau_x(0)$; $K'_x(0)$; $\tau'_x(0)$ for 30KhGSA steel are shown in Table 2. It shows the standard deviations of the experimental data.

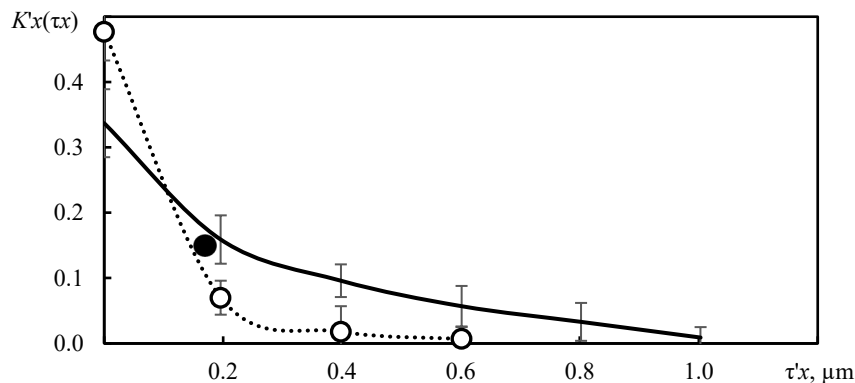


Fig. 5. Graphs of autocorrelation functions of the slope of the bends of the crack line relative to the average position: solid line — processing without a field; dotted line — processing in a magnetic field with a strength of 1,6 MA/m

Table 2

Effect of heat treatment modes on the propagation parameters of a crack with a length of $l = 6 \mu\text{m}$

Magnitude of the magnetic field strength, MA/m	$\sqrt{K_x(0)}$	$\tau_x(0)$	$\sqrt{K'_x(0)}$	$\tau'_x(0)$
0.0	0.156 ± 0.03	0.5 ± 0.20	0.58 ± 0.04	1.1 ± 0.3
1.6	0.144 ± 0.03	1.1 ± 0.15	0.66 ± 0.03	0.6 ± 0.2

According to the data in Table 2, it can be noted that HTMF affects all the listed statistical characteristics of cracks. Standard tangent spread of the slope angles of the fracture line sections ($\sqrt{K'_x(0)}$) after HTMF increases by 0.12, which corresponds to an increase in the average slope modulus of the crack trajectory by $\sim 6^\circ$ (from 29 to 35°). At the same time, correlation interval ($\tau'_x(0)$) decreases by $0.5 \mu\text{m}$.

Conclusion. The main result of this work is the identification of changes in the kinetics of fatigue crack development and the identification of mechanisms that contribute to increased crack resistance after HTMF. Based on the data obtained, it can be concluded that the technology of heat treatment in a magnetic field contributes to the formation of a structure that ensures an increase in the curvature of cracks. There is an increase in the steepness of the bending trajectory due to a greater number of effective barriers (an increase in the dispersion of martensite) in its path. In this respect, the nature of the HTMF's structure organization has much in common with the process of high-temperature thermomechanical treatment. This leads to the development of a new practical method for creating a high-strength state that can be applied to a wide range of steel grades without requiring significant changes to their heat treatment process. In turn, increasing the crack resistance of steels makes it possible to ensure greater safety of various devices and man-made systems, as well as reduce their cost and maintenance costs.

References

- Gdoutos EE. *Fracture Mechanics: An Introduction*. Springer Nature Switzerland AG; 2020. 477 p.
- Yukitaka Murakami. *Metal Fatigue: Effects of Small Defects and Nonmetallic Inclusions*. Academic Press; 2019. 758 p.
- Pustovoit VN, Dolgachev YuV. *Magnetic Heterogeneity of Austenite and Transformations in Steels*. Monograph. Rostov-on-Don: Don State Technical University; 2021. 198 p. (In Russ.)
- Pustovoit VN, Grishin SA, Duka VV, Fedosov VV. Setup for Studying the Kinetics of Crack Growth in Cyclic Bending Tests. *Industrial Laboratory. Diagnostics of Materials*. 2020;86(7):59–64. (In Russ.) <https://doi.org/10.26896/1028-6861-2020-86-7-59-64>
- Si Y, Rouse JP, Hyde CJ. Potential Difference Methods for Measuring Crack Growth: A Review. *International Journal of Fatigue*. 2020;136:105624. <https://doi.org/10.1016/j.ijfatigue.2020.105624>
- Tarnowski KM, Dean DW, Nikbin KM, Davies CM. Predicting the Influence of Strain on Crack Length Measurements Performed Using the Potential Drop Method. *Engineering Fracture Mechanics*. 2017;182:635–657. <https://doi.org/10.1016/j.engfracmech.2017.06.008>
- Zerbst U, Madia M, Vormwald M, Beier HTh. Fatigue Strength and Fracture Mechanics – A General Perspective. *Engineering Fracture Mechanics*. 2018;198:2–23. <https://doi.org/10.1016/j.engfracmech.2017.04.030>
- Pineau A, McDowell DL, Busso EP, Antolovich SD. Failure of Metals II: Fatigue. *Acta Materialia*. 2016;107:484–507. <https://doi.org/10.1016/j.actamat.2015.05.050>
- Tatsuo Sakai, Akiyoshi Nakagawa, Noriyasu Oguma, Yuki Nakamura, Akira Ueno, Shoichi Kikuchiet, et al. A review on fatigue fracture modes of structural metallic materials in very high cycle regime. *International Journal of Fatigue*. 2016;93(2):339–351. <https://doi.org/10.1016/j.ijfatigue.2016.05.029>
- Schastlivtsev VM, Kaletina YuV, Fokina EA, Mirzaev DA. Effect of External Actions and a Magnetic Field on Martensitic Transformation in Steels and Alloys. *Metal Science and Heat Treatment*. 2016;58:247–253. <https://doi.org/10.1007/s11041-016-9997-4>
- Yan Wang, Zhiguo Xing, Yanfei Huang, Weiling Guo, Jiajie Kang, Haidou Wang, et al. Effect of Pulse Magnetic Field Treatment on the Hardness of 20Cr2Ni4A Steel. *Journal of Magnetism and Magnetic Materials*. 2021;538:168248. <https://doi.org/10.1016/j.jmmm.2021.168248>
- Pustovoyt VN, Dolgachev YuI. Structural State of Martensite and Retained Austenite in Carbon Steels after Quenching in Magnetic Field. *Metallovedenie i Termicheskaya Obrabotka Metallov*. 2022;(12(810)):10–14. (In Russ.) <https://doi.org/10.30906/mitom.2022.12.10-14>
- Pustovoit VN, Dolgachev YV. Formation of Residual Stress Diagram after Quenching in a Magnetic Field. *Safety of Technogenic and Natural Systems*. 2024;8(4):54–61. <https://doi.org/10.23947/2541-9129-2024-8-4-54-61>
- Bhadeshia HKDH, Honeycombe RWK. *Steels: Structure, Properties, and Design*. Elsevier; 2024. 550 p.

15. Fultz B. *Phase Transitions in Materials*. Cambridge University Press; 2020. 604 p.

16. Jinliang Wang, Xiaohui Xi, Yong Li, Chenchong Wang, Wei Xu. New Insights on Nucleation and Transformation Process in Temperature-Induced Martensitic Transformation. *Materials Characterization*. 2019;151:267–272. <https://doi.org/10.1016/j.matchar.2019.03.023>

17. Wang JL, Huang MH, Xi XH, Wang CC, Xu W. Characteristics of Nucleation and transformation sequence in Deformation-Induced Martensitic Transformation. *Materials Characterization*. 2020;163:110234. <https://doi.org/10.1016/j.matchar.2020.110234>

18. Anderson PM, Hirth JP, Lothe J. *Theory of Dislocations*. Cambridge University Press; 2017. 699 p.

19. Webster JG, Eren H (eds.). *Measurement, Instrumentation, and Sensors Handbook: Two-Volume Set*. CRC press; 2018. 3559 p.

20. Whitehouse DJ. *Handbook of Surface Metrology*. CRC press; 2023. 350 p.

About the Authors:

Viktor N. Pustovoyt, Dr. Sci. (Eng.), Professor, Professor of the Materials Science and Metal Technology Department, Don State Technical University, (1, Gagarin Sq., Rostov-on-Don, 344003, Russian Federation), [SPIN-code](#), [ORCID](#), [ScopusID](#), pustovoyt45@gmail.com

Yuri V. Dolgachev, Dr. Sci. (Eng.), Associate Professor of the Materials Science and Metal Technology Department, Don State Technical University, (1, Gagarin Sq., Rostov-on-Don, 344003, Russian Federation), [SPIN-code](#), [ORCID](#), [ScopusID](#), [ResearcherID](#), ydolgachev@donstu.ru

Claimed Contributorship:

VN Pustovoyt: formulation of the basic concept, goals and objectives of the research, academic advising, text revision, conclusions correction.

YuV Dolgachev: obtaining experimental data, calculations, research results analysis, text preparation, conclusions formulation.

Conflict of Interest Statement: the authors declare no conflict of interest.

All authors have read and approved the final manuscript.

Об авторах:

Виктор Николаевич Пустовойт, доктор технических наук, профессор, профессор кафедры «Материаловедение и технологии металлов» Донского государственного технического университета (344003, Российская Федерация, г. Ростов-на-Дону, пл. Гагарина, 1), [SPIN-код](#), [ORCID](#), [ScopusID](#), pustovoyt45@gmail.com

Юрий Вячеславович Долгачев, доктор технических наук, доцент кафедры «Материаловедение и технология металлов» Донского государственного технического университета (344003, Российская Федерация, г. Ростов-на-Дону, пл. Гагарина, 1), [SPIN-код](#), [ORCID](#), [ScopusID](#), [ResearcherID](#), ydolgachev@donstu.ru

Заявленный вклад авторов:

В.Н. Пустовойт: формирование основной концепции, цели и задач исследования, научное руководство, доработка текста, корректировка выводов.

Ю.В. Долгачев: получение экспериментальных данных, расчеты, анализ результатов исследований, подготовка текста, формулирование выводов.

Конфликт интересов: авторы заявляют об отсутствии конфликта интересов.

Все авторы прочитали и одобрили окончательный вариант рукописи.

Received / Поступила в редакцию 06.06.2025

Reviewed / Поступила после рецензирования 02.07.2025

Accepted / Принята к публикации 10.07.2025

CHEMICAL TECHNOLOGIES, MATERIALS SCIENCES, METALLURGY ХИМИЧЕСКИЕ ТЕХНОЛОГИИ, НАУКИ О МАТЕРИАЛАХ, МЕТАЛЛУРГИЯ



UDC 621.793

Original Empirical Research

<https://doi.org/10.23947/2541-9129-2025-9-3-250-256>

Fine Steel Structure after Microarc Molybdenum Steel Saturation

 Makar S. Stepanov , Yurii M. Dombrovskii 

Don State Technical University, Rostov-on-Don, Russian Federation

✉ stepanovms@yandex.ru

EDN: BECKGZ

Abstract

Introduction. In modern production, it is important to increase reliability and durability of steel products. One way to achieve this is by creating high-hardness, wear-resistant coatings on their surface. These coatings can be formed using the method of diffusion saturation, which involves the introduction of carbide-forming elements into the metal. Traditional methods for creating these coatings are time-consuming, taking up to 8 hours or more. To accelerate this process, researchers have proposed using high-energy methods such as laser and plasma treatments. However, these methods require specialized equipment that can be expensive. In this paper, we consider a method for creating a high-hardness molybdenum-based coating by microarc alloying. This method involves exposing a processed steel product immersed in coal powder to multiplicative microarc discharges that occur between the metal surface and the surrounding powder medium. The discharges are generated when an electric current is passed through them. This method allows for a significant increase in the process of diffusive surface saturation. It is characterized by simplicity and low energy consumption. The properties of the resulting coatings are primarily determined by their fine structure. Therefore, studying this structure is a crucial task. The aim of this research was to investigate the features of the fine structure of the steel surface layer after microarc molybdenum plating.

Materials and Methods. A coating containing finely dispersed ammonium molybdate powder and an electrically conductive gel as a binder in a volume ratio of 1:1 was used as a source of molybdenum for diffusion saturation. The coating was applied to the surface of cylindrical samples made of 20 steel with a diameter of 12 mm and a length of 35 mm. Then they were immersed in a metal container with a carbon powder with a particle size 0.4–0.6 mm. An electric current was passed through this powder for 6 minutes, with a surface current density of 0.53 A/cm². A Neophot-21 microscope, an ARL X'TRA-435 diffractometer, a ZEISS CrossBeam 340 scanning electron microscope with an X-ray microanalyzer, and a NanoEducator scanning probe microscope were used to study the fine structure of steel.

Results. After microarc molybdenum saturation of steel samples, a coating with a multilayer structure and a complex phase composition was formed. On the surface of the material, there was a slightly etched layer with a thickness of 50–55 μm, under which there was a carbonized layer with eutectoid structure and a thickness of approximately 200 μm, and the original ferrite-pearlite structure was preserved lower. The base of the slightly etched layer was a dispersed ferrite-carbide mixture containing about 47% wt. % of Mo and having a microhardness of 8–9 GPa. This layer contained carbide inclusions up to 5 μm in size, containing 94 wt. % of Mo and having microhardness up to 21 GPa. The surface relief was characterized by the presence of carbide inclusions of 3–5 μm in size, as well as multiple nanoscale inclusions protruding above the surface to a height of 10 to 150–200 nm.

Discussion. The results of the study, obtained using metallographic analysis, scanning electron microscopy, X-ray phase analysis and atomic force microscopy, showed that during microarc molybdenum steel saturation, a diffusion layer was formed containing nanoscale particles of the carbide phase. These particles reached a volume fraction of up to 70% and were located at the base of the layer. This layer was a ferrite-carbide eutectoid mixture. A quantitative assessment of the strengthening effect of these particles confirmed that the presence of such particles, characterized by high microhardness, determines the high hardness of the resulting coating.

Conclusion. Microarc molybdenum steel saturation is an effective method for creating coatings with exceptional performance characteristics. These coatings are characterized not only by their high hardness, due to the presence of nanoscale carbide particles located in a ferrite-carbide base, but also by their improved mechanical properties. This makes them promising for use in various industries where high wear resistance and durability of products are required. The research findings indicate that microarc molybdenum steel saturation significantly reduces processing time and avoids the use of expensive equipment, which makes it more affordable for industrial implementation.

Keywords: modification of the steel surface, creation of a molybdenum coating, formation of a diffusion layer

Acknowledgements. The authors would like to thank the Editorial board of the journal and the reviewers for their attentive attitude to the article and the comments that improved its quality.


For Citation. Stepanov MS, Dombrovskii YuM. Fine Steel Structure after Microarc Molybdenum Steel Saturation. *Safety of Technogenic and Natural Systems*. 2025;9(3):250–256. <https://doi.org/10.23947/2541-9129-2025-9-3-250-256>

Оригинальное эмпирическое исследование

Тонкая структура стали после микродугового молибденирования

М.С. Степанов  , Ю.М. Домбровский 

Донской государственный технический университет, г. Ростов-на-Дону, Российская Федерация

 stepanovms@yandex.ru

Аннотация

Введение. В условиях современного производства важной задачей является повышение надежности и долговечности стальных изделий. Для решения этой проблемы целесообразно создавать на их поверхности высокопрочные износостойкие покрытия, формируемые методом диффузионного насыщения металла карбидообразующими элементами. Традиционные способы получения таких покрытий отличаются значительной продолжительностью — до 8 и более часов. Для ускорения процесса формирования в литературе предложены различные методы, основанные на применении высокоэнергетического воздействия на материал (лазерного, плазменного и т.д.), однако они требуют использования сложного и дорогостоящего оборудования. В настоящей работе рассмотрен способ получения высокотвердого покрытия на основе молибдена методом микродугового легирования, который заключается в воздействии на обрабатываемое стальное изделие, погруженное в угольный порошок, мультипликативных микродуговых разрядов, возникающих между поверхностью металла и окружающей порошковой средой при пропускании электрического тока. Этот метод позволяет значительно интенсифицировать процесс диффузионного поверхностного насыщения, отличается простотой и низкой энергоемкостью. Свойства получаемых покрытий в основном определяются их тонкой структурой, поэтому исследование этой структуры представляет собой актуальную задачу. Таким образом, целью работы было изучение особенностей тонкой структуры поверхностного слоя стали после микродугового молибденирования.

Материалы и методы. В качестве источника молибдена для диффузионного насыщения использовали обмазку, содержащую мелкодисперсный порошок молибдата аммония и электропроводный гель в качестве связующего в объемном соотношении 1:1. Обмазку наносили на поверхность цилиндрических образцов диаметром 12 мм и длиной 35 мм, изготовленных из стали 20, после чего их погружали в металлический контейнер с угольным порошком с размером частиц 0,4–0,6 мм. Через данный порошок пропускали электрический ток в течение 6 минут, при этом поверхностная плотность тока составляла 0,53 А/см². Для исследований тонкой структуры стали использовали микроскоп Neophot-21, дифрактометр ARL X'TRA-435, сканирующий электронный микроскоп ZEISS CrossBeam 340 с рентгеновским микроанализатором и сканирующий зондовый микроскоп NanoEducator.

Результаты исследования. После микродугового молибденирования стальных образцов образуется покрытие, обладающее многослойным строением и сложным фазовым составом. На поверхности материала обнаруживается слаботравящийся слой толщиной 50–55 мкм, под которым расположен науглероженный слой с эвтектоидной структурой толщиной около 200 мкм, а еще ниже сохраняется исходная феррито-перлитная структура. Основа слаботравящегося слоя представляет собой дисперсную феррито-карбидную смесь, содержащую около 47 мас. % Мо и имеющую микротвердость 8–9 ГПа. В этом слое расположены карбидные включения размером до 5 мкм, содержащие 94 мас. % Мо и обладающие микротвердостью до 21 ГПа. Рельеф поверхности характеризуется наличием карбидных включений размером 3–5 мкм, а также множественными наноразмерными включениями, выступающими над поверхностью шлифа на высоту от 10 до 150–200 нм.

Обсуждение. Результаты исследования, полученные с использованием металлографического анализа, сканирующей электронной микроскопии, рентгеновского фазового анализа и атомно-силовой микроскопии, показали, что при микродуговом молибденировании стали формируется диффузионный слой, содержащий наноразмерные частицы карбидной фазы, достигающие объёмной доли до 70 %, расположенные в основе слоя, представляющего собой феррито-карбидную эвтектоидную смесь. Количественная оценка упрочняющего влияния этих частиц подтвердила, что наличие таких частиц, характеризующихся высокой микротвердостью, и обуславливает высокую твердость образующегося покрытия.

Заключение. Микродуговое молибденирование стали представляет собой эффективный метод получения покрытий, обладающих выдающимися эксплуатационными характеристиками. Полученные вследствие этого покрытия не только отличались высокой твердостью за счет наноразмерных карбидных частиц, расположенных в феррито-карбидной основе, но и демонстрировали улучшенные механические свойства. Это делает их перспективными для применения в различных отраслях, где требуются высокая износостойкость и долговечность изделий. Результаты исследований показывают, что использование данного метода значительно сокращает время обработки и позволяет избежать применения дорогостоящего оборудования, что делает его более доступным для промышленного внедрения.

Ключевые слова: модифицирование поверхности стали, создание молибденированного покрытия, формирование диффузионного слоя

Благодарности. Авторы благодарят сотрудников редакции и рецензентов за внимание, проявленное к публикации и ценные замечания, которые позволили улучшить ее содержание.

Для цитирования. Степанов М.С., Домбровский Ю.М. Тонкая структура стали после микродугового молибденирования. *Безопасность техногенных и природных систем.* 2025;9(3):250–256. <https://doi.org/10.23947/2541-9129-2025-9-3-250-256>

Introduction. In modern production, the requirements for reliability and durability of steel products are constantly increasing, particularly those that operate under difficult operating conditions. To address this issue, traditional methods involve forming diffusion coatings on the surfaces of these products with increased hardness and wear resistance [1, 2]. This includes carbide-type coatings obtained by diffusion saturation of steel with chromium [3], tungsten [4], molybdenum and other carbide-forming elements [5]. A significant disadvantage of this technology is that it is time-consuming, taking more than 8 hours to complete. However, it is possible to accelerate diffusion saturation by applying high-energy effects on the material, for example, plasma [6], ion plasma [7], laser [8, 9], electric spark [10], as well as heating using thermionic effects [11]. These technologies are effective, but require complex and expensive equipment. In this regard, the method of microarc surface alloying [12] has an undeniable advantage. In this process, heating and diffusion saturation of steel products occur in a metal container filled with coal powder. Heating is caused by microarcs that result from the passage of an electric current through the circuit: power source – container – coal powder – steel product. Acceleration of the diffusion saturation process is achieved by exposing the material to microarc discharges that occur between the surface of the product and the coal powder. The obvious simplicity of this technology, combined with its low energy consumption, does not require additional evidence of its advantages.

Carbide-type coatings containing molybdenum are widely used in mechanical engineering. The process of molybdenum steel saturation involves heating of chemical compounds based on molybdenum or ferromolybdenum in powders, as well as in a gaseous medium of molybdenum halides, or in melts based on sodium molybdate. This process is conducted at temperatures ranging from 1000 to 1200°C for at least six to seven hours. The use of the microarc alloying method to obtain such coatings can significantly reduce time required for this process, making it an urgent area of research [13, 14]. The main factor that determines the properties of these coatings is the presence of carbide phase particles in their structure. In this study, we aimed to investigate the features of the fine structure of the surface layer of steel after microarc molybdenum steel saturation.

Materials and Methods. Microarc molybdenum steel saturation was performed using a coating of ammonium molybdate $(\text{NH}_4)_2\text{MoO}_4$ powder in an electrically conductive gel, in a volume ratio of 1:1. The coating was applied to the surface of steel 20 samples, each with a diameter of 12 mm and length of 35 mm. These samples were then immersed in a metal container containing carbon powder with a dispersion of 0.4–0.6 mm, and an electric current was passed through the source – container – coal powder – sample chain for six minutes. To achieve the desired temperature for the molybdenum plating process, a current density of 0.53 A/cm² was maintained on the surface of the samples.

After diffusion saturation, a transverse microplate was created by pouring epoxy resin into cylindrical mandrels, ensuring strict perpendicularity of the sample's surface to its longitudinal axis. The samples were then ground on abrasive papers with grain sizes ranging from P480 to P2500 and polished first with Cr₂O₃ oxide grade OXA-0 according to GOST 2912–79, and finally with AM diamond paste with a 3/2 powder grain size according to GOST 25593–83. After removing any remaining paste residue with ethyl alcohol, chemical etching was performed using Rzheshotarsky reagent (a 4% solution of nitric acid in ethyl alcohol).

The microstructure was studied on a Neophot-21 microscope with a TouPCam Xcam0720P-H HDMI digital console. X-ray phase analysis was performed on an ARL X'TRA-435 diffractometer in Cu-K α radiation. The hardness of the diffusion layer was measured with a PMT-3 microhardness meter at loads of 0.490 and 0.196 N. The molybdenum content in the layer was determined using a ZEISS CrossBeam 340 scanning electron microscope with an Oxford Instruments X-max 80 X-ray microanalyzer. The relief of the transverse section of the diffusion layer was studied on an atomic force microscope (AFM) NanoEducator in constant force mode.

Results. Metallographic analysis revealed a weakly etching coating with a thickness of 50–55 μm on the surface of the samples after microarc molybdenum steel saturation. A carbonized layer with a pearlitic structure about 200 μm thick was found under it, followed by the initial structure. The coating consisted of a dispersed ferrite-carbide mixture containing carbide inclusions up to 5 μm in size. The microhardness of the base layer was 8–9 GPa, and the carbide inclusions were up to 21 GPa (Fig. 1).

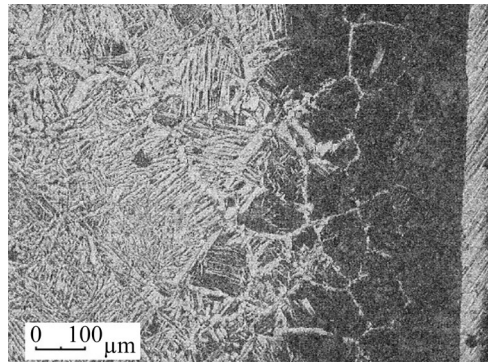


Fig. 1. Microstructure of the surface layer of steel 20 after microarc molybdenum plating

The results of measuring the mass fraction of molybdenum (Fig. 2) are presented in Table 1. From the data obtained, it could be seen that the molybdenum content at different points of the coating differed, and the coating itself had a heterogeneous composition.

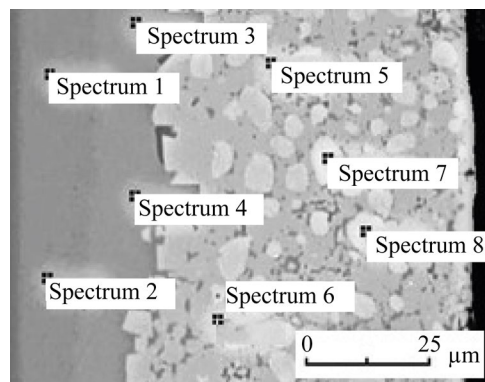


Fig. 2. Structure of the molybdenum coating in backscattered electrons

Table 1

Concentration of C diffusant at individual coating points

No.	1	2	3	4	5	6	7	8
C, weight %	–	–	3.1	3.3	46.8	47.0	93.9	94.1

There was no molybdenum in points 1 and 2. Next, a transition zone of a solid molybdenum solution was formed, containing about 3% Mo. The thickness of the diffusion layer was 50–55 μm . It consisted of a base (spectra 5, 6) with rounded inclusions located in it (spectra 7, 8). As can be seen from Table 1, the base contained approximately 47% Mo, and therefore it could be an intermetallic Fe_3Mo_2 or carbides $(\text{Fe},\text{Mo})_3\text{C}$ [15, 16]. The inclusions (spectra 7, 8) contained approximately 94% Mo, which corresponded to the carbide phase Mo_2C [16, 17].

The formation of such carbides in the surface layer was confirmed by X-ray phase analysis (Fig. 3).

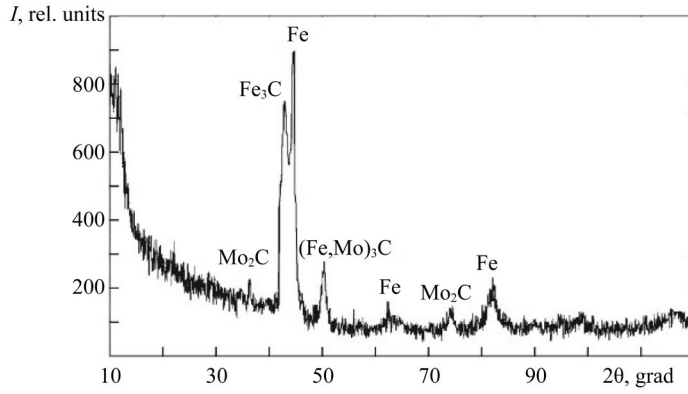


Fig. 3. Diffractogram of the molybdenum coating

High microhardness of the coating base could be explained by the formation of nanoscale carbide particles in it, which was confirmed by the results of atomic force microscopy (AFM) (Fig. 4, 5).

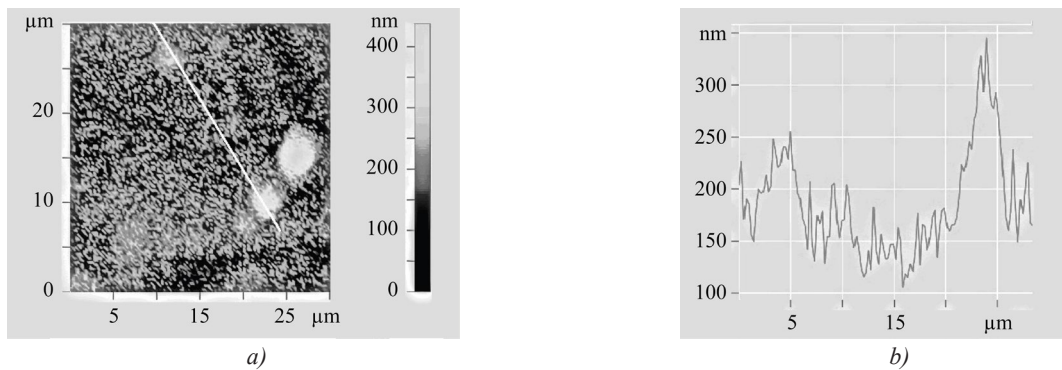


Fig. 4. Relief of the sample surface:

a — section in direction 1; *b* — profile corresponding to this section

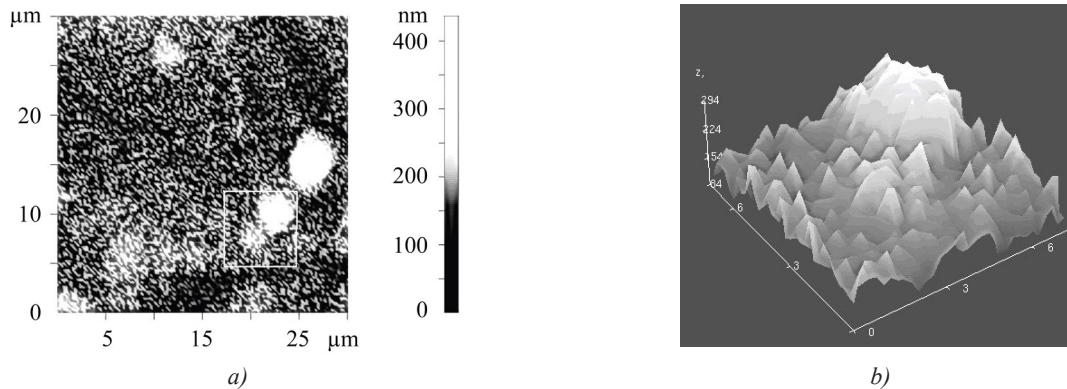


Fig. 5. Image of the steel surface obtained by the AFM method:

a — 2D image; *b* — 3D image

Thus, the coating structure contained carbide inclusions up to 5 μm in size, as well as multiple nanoscale inclusions that protruded above the surface plane of the sample. Such inclusions had a higher hardness compared to other structural components.

To quantify the strengthening effect of these particles, it was advisable to use the hardness additivity rule, according to which H_{AB} hardness of a two-phase alloy could be represented as the sum of the hardness H_A and H_B of the constituent phases A and B, taken in their volume fractions V_A and V_B :

$$H_{AB} = H_A \cdot V_A + H_B \cdot V_B. \quad (1)$$

The dispersed ferrite-carbide mixture acted as phase *A*, the base of the diffusion layer, and nanoscale carbide inclusions acted as phase *B*. For the calculation according to formula (1), the following initial data were used: $H_A = 3,000$ MPa, $H_B = 23$ GPa, the values of V_A and V_B were determined according to method [18] and assumed to be equal to: $V_A = 0.73$; $H_B = 0.27$. From where it was obtained: $H_{AB} = 8,400$ MPa, which is consistent with the measurement results of the integral microhardness of the diffusion layer.

Discussion. The data obtained confirmed the possibility of accelerated production of a high-hardness molybdenum coating on steel using the microarc surface alloying method. With a total coating thickness of 50–55 μm , it has a complex structure in depth and consists of a dispersed ferritocarbide mixture with a microhardness of 8–9 GPa, with inclusions of relatively large particles of the carbide phase up to 5 μm in size (microhardness up to 21 GPa), and multiple nanoscale inclusions. This is followed by a carbonized layer with a pearlitic structure about 200 μm thick, which transforms into the initial structure of steel 20. A calculated assessment of the strengthening effect of such nanoscale inclusions confirmed that their presence determines the high microhardness of the coating base. It should be noted that the obtained value of the microhardness of the coating base exceeds its value, which is achieved using traditional molybdenum plating methods. It can be assumed that the formation of nanoscale inclusions of the carbide phase during microarc molybdatation occurs under the influence of numerous microarc discharges that occur between the surface of the steel and the adjacent coal powder during passage of electric current. However, the physical processes taking place under such conditions require separate consideration and could be one of the areas for future research.

Conclusion. Microarc surface alloying can be used to create high-hardness coatings on steel using the method of molybdenum plating. Investigation of the fine structure of the coating has shown that it has a complex phase composition: a dispersed ferritic-carbide mixture with numerous small and nanoscale carbide inclusions, which gives the coating high microhardness. Underneath this, there is a carbonized layer with a pearlitic structure, followed by the original steel structure. The results obtained from these studies can be useful for the development of technologies to harden the surfaces of steel products such as tools and machine parts that operate in difficult conditions.

References

- Mittemeijer EJ, Somers MAJ (eds.). *Thermochemical Surface Engineering of Steels*. Woodhead Publishing; 2015. 827 p.
- Wang RJ, Qian YY, Liu J. Structural and Interfacial Analysis of WC92–Co8 Coating Deposited on Titanium Alloy by Electrospark Deposition. *Applied Surface Science*. 2024;228(1–4):405–409. <https://doi.org/10.1016/j.apsusc.2004.01.043>
- Guryev MA, Guryev AM, Ivanov SG, Chernykh EV. Influence of the Chemical Composition of Steel on the Structure and Properties of Diffusion Coatings Obtained by Simultaneous Saturation of Structural Steels with Boron, Chromium, and Titanium. *Physics of the Solid State*. 2023;65(1):62–65. <https://doi.org/10.1134/S1063783423700014>
- Stepanov MS, Dombrovskiy YuM. Deposition of Carbide-Type Coatings during Micro-Arc Thermomdiffusion Tungstening of Steel. *Materialovedenie*. 2018;(1):20–25. (In Russ.)
- Yu-Hsien Liao, Fan-Bean Wu. Microstructure Evolution and Mechanical Properties of Refractory Molybdenum-Tungsten Nitride Coatings. *Surface and Coatings Technology*. 2024;476:130154. <https://doi.org/10.1016/j.surfcoat.2023.130154>
- Kalita VI, Komlev DI, Radyuk AA, Mikhailova AB, Demin KYu, Rummyantsev BA. Investigation of the Structure and Microhardness of Plasma Coatings Made of Austenitic Steel after Friction Treatment. *Metally*. 2024;(3):32–42. (In Russ.)
- Kudryakov OV, Varavka VN, Zabiya IYu, Yadrets EA, Karavaev VP. Morphology and Genealogy of Structural Defects in Vacuum Ion-Plasma Coatings. *Advanced Engineering Research (Rostov-on-Don)*. 2020;20(3):269–279 <https://doi.org/10.23947/2687-1653-2020-20-3-269-279>
- Shaburova NA, Pashkeev KYu, Myasoedov VA. Comparative Analysis of Structure and Properties of Chromocobalt Coating Applied by Diffusion Saturation and Laser Surfacing. *Materialovedenie*. 2024;(6):12–20. (In Russ.) <https://doi.org/10.31044/1684-579X-2024-0-6-12-20>
- Liexin Wu, Li Meng, Yueyue Wang, Shuhuan Zhang, Wuxia Bai, Taoyuan Ouyang, et al. Effects of Laser Surface Modification on the Adhesion Strength and Fracture Mechanism of Electroless-Plated Coatings. *Surface And Coatings Technology*. 2022;429:127927. <https://doi.org/10.1016/j.surfcoat.2021.127927>
- Khimukhin SN, Eremina KP, Khe VK. Structure of Combined Intermetallide Electrospark Coatings on Steel 45. *Metallovedenie i Termicheskaya Obrabotka Metallov*. 2024;(11):20–27. (In Russ.) <https://doi.org/10.30906/mitom.2024.11.20-27>
- Shaburova NA. Chromium Plating of Steel Parts Using the Thermoemission Field. *Materials Physics and Mechanics*. 2024;52(3):154–160. https://doi.org/10.18149/MPM.5232024_14
- Stepanov MS, Dombrovskii YuM, Pustovoi VN. Microarc Diffusion Saturation of Steel with Carbon and Carbide-Forming Elements. *Metallovedenie i Termicheskaya Obrabotka Metallov* 2017;(5(743)):45–49. (In Russ.)
- Stepanov MS, Dombrovskii YuM. Thermodynamic Analysis of Carbide Layer Formation in Steel with Microarc Saturation by Molybdenum. *Steel in Translation*. 2016;46(2):79–82. <https://doi.org/10.3103/S0967091216020169>
- Stepanov MS, Dombrovskii YM. Microarc Molybdenum Steel Saturation Using Ammonium Molybdate. *Safety of Technogenic and Natural Systems*. 2024;8(4):47–53. <https://doi.org/10.23947/2541-9129-2024-8-4-47-53>
- Kalin BA, Platonov PA, Tuzov YuV, Chernov II, Strombakh YaI. Structural Materials of Nuclear Engineering. In: *Physical Materials Science*, vol. 6. Moscow: National Research Nuclear University MEPhI; 2021. 736 p. (In Russ.)
- Kobernik NV, Pankratov AS, Mikheev RS, Orlik AG, Sorokin SP, Petrova VV, et al. Application of Chromium Carbides in Surfacing Materials Intended for Obtaining of Abrasion Resistant Coatings. *Vestnik Mashinostroeniya*. 2020;(9):64–68. <https://doi.org/10.36652/0042-4633-2020-9-64-68>

17. Aleshin NP, Kobernik NV, Pankratov AS, Petrova VV. Thermodynamic Modeling of the Formation of Chromium Carbides in the Surfaced Metal. *Vestnik Mashinostroeniya*. 2020;(7):67–71. (In Russ.) <https://doi.org/10.36652/0042-4633-2020-7-67-71>
18. Volkov NV, Skrytny VI, Filippov VP, Yaltsev VN. Methods for Studying the Structural and Phase State of Materials. In: *Physical Materials Science*, vol. 3. Moscow: National Research Nuclear University MEPhI; 2021. 800 p. (In Russ.)

About the Authors:

Makar S. Stepanov, Dr. Sci. (Eng.), Professor of the Department of Quality Management, Don State Technical University (1, Gagarin Sq., Rostov-on-Don, 344003, Russian Federation), [SPIN-code](#), [ORCID](#), [ScopusID](#), [ResearcherID](#), stepanovms@yandex.ru

Yurii M. Dombrovskii, Dr. Sci. (Eng.), Professor of the Materials Science and Technology of Metals Department, Don State Technical University (1, Gagarin Sq., Rostov-on-Don, 344003, Russian Federation), [SPIN-code](#), [ORCID](#), [ScopusID](#), yurimd@mail.ru

Claimed Contributorship:

MS Stepanov: conceptualization, writing – original draft preparation, visualization.

YuM Dombrovskii: investigation, experiments.

Conflict of Interest Statement: the authors declare no conflict of interest.

All authors have read and approved the final manuscript.

Об авторах:

Макар Степанович Степанов, доктор технических наук, профессор кафедры «Управление качеством» Донского государственного технического университета (344003, Российская Федерация, г. Ростов-на-Дону, пл. Гагарина, 1), [SPIN-код](#), [ORCID](#), [ScopusID](#), [ResearcherID](#), stepanovms@yandex.ru

Юрий Маркович Домбровский, доктор технических наук, профессор кафедры «Материаловедение и технологии металлов» Донского государственного технического университета (344003, Российская Федерация, г. Ростов-на-Дону, пл. Гагарина, 1), [SPIN-код](#), [ORCID](#), [ScopusID](#), yurimd@mail.ru

Заявленный вклад авторов:

М.С. Степанов: разработка концепции, создание и подготовка рукописи, визуализация результатов исследования и полученных данных.

Ю.М. Домбровский: осуществление научно-исследовательского процесса, включая выполнение экспериментов.

Конфликт интересов: авторы заявляют об отсутствии конфликта интересов.

Все авторы прочитали и одобрили окончательный вариант рукописи

Received / Поступила в редакцию / 03.06.2025

Reviewed / Поступила после рецензирования / 30.06.2025

Accepted / Принята к публикации / 06.07.2025